Combined Author's Response

Table of Contents:

Response to **Reviewer #1**

Thank you for the review.

Chen et al. provide an overview of VOC budgets as observed in a set of aircraft campaigns and as modeled by GEOS-Chem. The model shows a dominance of biogenic VOC emissions in terms of magnitude and reactivity, and anthropogenic VOCs in terms of VOC loading. Model skill is variable, and the authors highlight the importance of discrepancies caused by a small subset of VOCs. They show discrepancies in the FT are linked to an underestimate of BL ventilation. Overall, the paper is well written and the results are suitable for publication in ACP. I have only a few remarks, below:

Thank you for the positive comments. We have prepared a point by point response to the reviewer's comments below.

Major and Minor Comments:

Comment 1: A predictable concern is that a single model year (2013) is directly compared to C1 observations spanning from 2010 to 2014. This may disproportionately influence anthropogenic VOCs comparisons, as California is largely sampled in 2010, and DC is sampled in 2011. It needs to be shown that interannual variability in emissions and meteorology is unlikely to affect the overall magnitude and spatial pattern in biases shown here.

Reply to Comment 1: Thank you for the suggestion. To address this concern, we conducted a set of one-month (June) high-resolution (0.25˚×0.3125˚) simulations spanning multiple years (2012-2016) to assess the potential impact of interannual variability. This approach provides a compromise between sufficient temporal coverage and tractable computational burden (running the full set of simulated months for all years would not be feasible). While the utilized aircraft campaigns span 2010-2014, we use the 2012-2016 timeframe to assess variability over 5 years based on the availability of the GEOS-FP meteorological product. June was chosen based on the temporal overlap of two campaigns (SENEX and CalNex) sampling very different regions. Each of the five monthly simulations was initialized after a ~1-week nested spin-up of regridded concentration fields from a 1-year global spin-up.

As the reviewer notes, factors driving interannual variability include both emissions and meteorology. In our simulations, biogenic emissions are computed in each model grid square and temporal step based on GEOS-FP meteorological data for that location and time, while pyrogenic emissions are from the GFED4s database which likewise includes interannual variability. Anthropogenic emission over North America employ NEI 2011 with year-specific scale factors applied, with the default GEOS-Chem configuration used here employing 2013 scale factors also for later years. The latest EPA trends information (Table below) indicates that total US anthropogenic VOC emissions for each year in 2010-2014 (the years encompassed by all the aircraft campaigns used in this study) differ by less than 4% from those of 2013 (the year of our simulations). Inventory changes in the transportation sector are somewhat larger but still less than 15%. As a result, even if we were to carry out model simulations spanning the entire time range of the aircraft studies and using year-specific EPA emissions, the modeled anthropogenic VOC flux would only differ by a few percent compared to the values used for 2013. Therefore, changing meteorology, biogenic emissions, and pyrogenic emissions are the main factors expected to drive differences in the model results for total-VOC quantities between years.

Figure S7 below shows the resulting multi-year variability in modeled VOC-carbon and reactivity profiles when sampling the model in different years along the June SENEX and CalNex flight tracks. The observed total VOC-carbon and reactivity is higher during SENEX than CalNex due to elevated VOC

emissions in the US Southeast plus a more extensive instrument payload. These differences in VOC-carbon and reactivity between the two regions are well-captured by the model regardless of the simulation year.

The modeled CalNex VOC-C and reactivity profiles show only modest interannual variability in both the planetary boundary layer (PBL) and free troposphere (FT). The simulated SENEX profiles likewise show very little interannual variability in the FT. We see a higher degree of variability for SENEX in the PBL and in the PBL-FT transition region, but for both VOC-C and reactivity the general pattern of model-measurement difference remains robust between 2013 (the simulation year used in the paper) and the other four years : specifically, a model underestimate near-surface, an overly-flat vertical profile within the PBL, and a strong FT underestimate.

We have added this new figure to the paper (as Fig. S7) and now state in Sect. 5.3 that "Given the range in measurement years spanned by the aircraft measurements, we performed a set of one-month simulations spanning multiple years to assess the potential impact of interannual variability on these findings. Results (see Supplement) suggest that the key features of the model-measurement comparisons discussed here are robust across years."

The following text (plus Fig. S7 below) have been added to the Supplement: "Given the range in measurement years spanned by the aircraft measurements, we performed a set of one-month simulations spanning 5 different years (June for 2012-2016) to assess the potential impact of interannual variability on these findings. Results are shown in Fig. S7 for the CalNex and SENEX flight tracks. In both cases the model-measurement VOC-C differences are highly consistent across years. We see a higher degree of interannual variability for VOC-reactivity over the SENEX domain, reflecting year-to-year differences in biogenic VOC emissions over this region. However, the key features of the comparison (a model underestimate near-surface, overly-flat vertical profile within the PBL, and strong FT underestimate) are consistent between our simulation year (2013) and the other four years."

Comment 2: Observed VOC-loading is operationally defined by aircraft payload (section 5.1). The authors note that this is typically more comprehensive in the summer-time, BVOCcentric campaigns. Are there any biases that are expected to persist in a certain dataset? This information may be extractable from Table S1, but it should be directly stated. Similarly, are there any points where VOC loading as measured by each aircraft can be compared?

Reply to Comment 2: We wish to clarify here that the model is sampled according to the specific VOC payload for each campaign, so that the model-measurement analyses are comparing consistent quantities in each case. For example, 25 observed VOCs were summed to derive the total-VOC quantities during SEAC^{4}RS (Fig. S19), and those same 25 VOCs as simulated by GEOS-Chem were then summed to derive the corresponding total-VOC quantities for the model. Analogously, both the modeled and observed total-VOC quantities for DISCOVER-AQ DC are based on the same set of 9 VOCs (Fig. S12). Only those VOCs that are present in both the GEOS-Chem model and in the measurement payload for a given campaign are included in these comparisons. As a result we do not expect any payload differences between campaigns to affect the conclusions of the model-measurement comparisons.

Based on the same reasoning, we feel that the model-measurement comparisons are more informative than a measurement-measurement total-VOC comparison between campaigns with inherently different payloads.

Comment 3: What are the BOVOC/AOVOC tracer sources (section 7)? Are they formed from the oxidation of some VOC precursor with a specific lifetime? A more detailed explanation of the model setup is needed.

Reply to Comment 3: We have modified the wording in Section 7 slightly to make this point more clear: "a unique pair of biogenic ($\mathcal{B}_{OVOC}$) and anthropogenic ($\mathcal{A}_{OVOC}$) source tracers was developed for each OVOC based on the mixing ratio difference along the flight track for that species between the model base-case and simulations with either i) all biogenic VOC emissions perturbed by 10%, or ii) all anthropogenic VOC emissions perturbed by 10% (see Section 4.3)."

These tracers are thus derived based on the three model simulations described in Sect. 4.3: R1) base case; R2) all biogenic VOC emissions decreased by 10%; R3) all anthropogenic VOC emissions decreased by 10%. For a given OVOC, $\mathcal{B}_{OVOC}$ would be derived as the modeled mixing ratio difference along the aircraft flight track between simulations R1 and R2, and $\mathcal{A}_{OVOC}$ as the R1 – R3 difference. Analogous tracer pairs were derived for each of the OVOC in our analysis.

Comment 4: Yu et al. (2018) also diagnose weak PBL ventilation – this cited in the conclusions but perhaps should be specifically discussed in section 6. Is the error associated with using off-line meteorology enough to drive the model errors observed here?

Reply to Comment 4: Thank you for the suggestion. We have now added a discussion of this point to Sect. 6 as follows:

"These findings are consistent with those of Yu et al. (2018), who diagnosed inadequate vertical transport in the current off-line configuration of the GEOS-Chem CTM. Yu et al. (2018) identified as causes i) the off-line convective transport scheme (leading to a +10% bias in modeled ^{222}Rn at the surface, and a -5% bias in the upper troposphere), and ii) off-line archiving of the meteorological fields (+5% model surface bias and -20% upper troposphere bias). Fixing these issues would therefore reduce the errors found here for VOC in the free troposphere (~60% mean low bias) but worsen the aggregated model performance in the PBL (~30% mean low bias). In that case, we would likely see in the model a more consistent low VOC bias throughout the troposphere, which would then indicate errors in overall VOC emissions or other processes."

Specific Remarks:

Remark 1: Page 3, line 118: "The model simulation includes extensive new developments related to atmospheric VOCs. . ." Can you clarify what developments are new in this work? "Latest" may be more appropriate than "new".

Reply to Remark 1: We have modified the wording of that sentence as suggested and now refer the reader to the section where more details may be obtained: "The model simulation includes the latest updates related to atmospheric VOCs (Section 2) and provides a more comprehensive representation of atmospheric organics than has been available for prior model-measurement evaluations."

Remark 2: Page 5 line 180: ". . . implemented into GEOS-Chem as described by Hu et al. (2015) with updated 0.25◦×0.3125◦ distributions of plant functional types and base emission factors". Please clarify the source of the updated plant functional types and base emission factors if different than Hu et. al (2015).

Reply to Remark 2: Thank you for the comment. The plant functional types and emission factor files used here have higher horizontal resolution than originally implemented by Hu et al. (2015), but are derived from the same underlying data version. We have therefore removed the phrase "with updated 0.25˚×0.3125˚ distributions of plant functional types and base emission factors" from the paper.

<u>Remark 3:</u> Figure 2: Please label fluxes to indicate net directionality.

<u>Reply to Remark 3:</u> Thanks for the suggestion. We have clarified in the Figure 2 caption that "Positive fluxes denote sources and negative fluxes denote sinks.".

Reference:

Yu, K., Keller, C. A., Jacob, D. J., Molod, A. M., Eastham, S. D., and Long, M. S.: Errors and improvements in the use of archived meteorological data for chemical transport modeling: an analysis using GEOS-Chem v11-01 driven by GEOS-5 meteorology, Geosci Model Dev, 11, 305-319, https://doi.org/10.5194/gmd-11-305-2018, 2018.

Tables and Figures:

Table R1. EPA National Tier 1 VOC Emission Trends: 2010 - 2014

Source Category	2010	2011	2012	2013	2014
Total without wildfires	14,988	15,263	14,981	14,699	14,416
% change relative to 2013	2.0	3.8	1.9	0.0	-1.9
Transportation	5,061	5,029	4,732	4,435	4,138
% change relative to 2013	14.1	13.4	6.7	0.0	-6.7

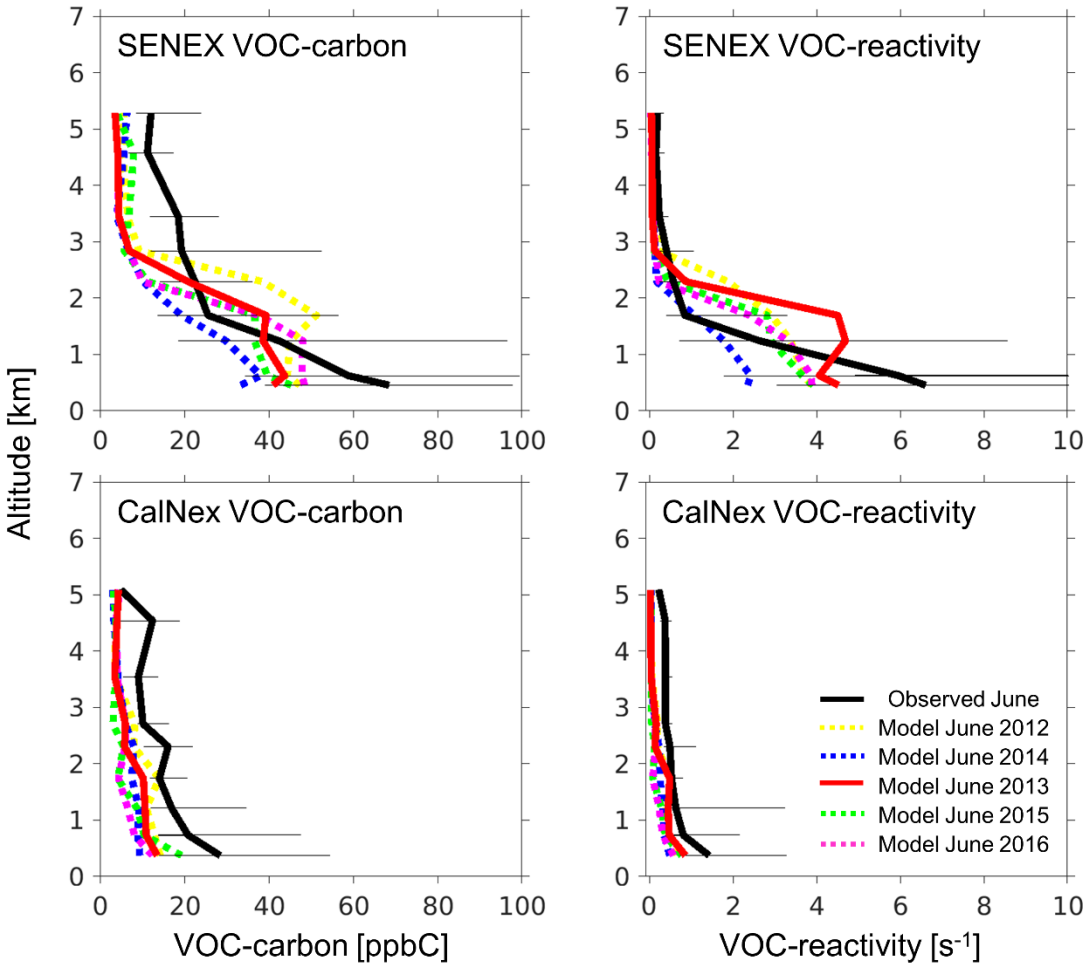

Figure S7. Vertical VOC-carbon and reactivity profiles as measured in 2013 and simulated by GEOS-Chem for June of 2012-2016 along the SENEX and CalNex aircraft flight tracks. Plotted are the observed (solid black lines) and predicted (2013: solid red lines; other years: dashed lines) median profiles, with horizontal bars indicating the 5th-95th percentiles measured for each vertical bin. Bin resolution is 0.5km below 3km and 1km above 3km. VOCs included in the profile correspond to the species shown in Fig. S17 (CalNex) and S18 (SENEX).

Response to **Reviewer #2:**

Thank you for the review.

This is an interesting and well-written paper that investigations VOC concentrations and reactivity in North America using an atmospheric model and a comprehensive analysis of aircraft observations from multiple field studies. The model skill in reproducing observed VOC concentrations and reactivity is good in the PBL and poor in the free troposphere. The subjects addressed in the manuscript are appropriate for ACP.
Photochemical reactions are the main sink for VOC. The authors could consider providing more information and critical evaluation of relevant factors that govern VOC removal rates, such as NOx emissions and O3 boundary conditions. The boundary conditions are from a global model and they have been accepted and used without much discussion or evaluation in the present manuscript.

Thank you for the positive comments. We have prepared a point by point response to the reviewer's comments below.

Comment 1: Are the ozone levels at the model boundaries and their seasonal variations reasonable and consistent with observational analyses by Parrish and Cooper at NOAA?

Reply to Comment 1: To address this question, we evaluate the modeled boundary/background ozone using ozone observation from the recent Atmospheric Tomography Mission (ATom), which sampled a rich set of data over the Pacific and Atlantic Oceans throughout the troposphere across four seasons. To this end, the model was re-run for the ATom period at 2˚×2.5˚ horizontal resolution and sampled along the ATom flight tracks.

Figure S1 shows ATom ozone observations over the Pacific (100˚W-170˚E) superimposed on the modeled monthly mean ozone curtain at ~177.5˚W. We focus discussion here on the northern hemisphere (NH) as most relevant to the boundary conditions for our study domain. We see that the model captures the overall vertical, latitudinal, and seasonal features seen in the observations. Figure S2 shows the observed and modeled probability density functions for ozone in the northern Pacific. The model generally captures the measured ozone variability with R^2 = 0.6-0.9 and normalized mean bias (NMB) of -27% to 5%. The largest discrepancy is seen in spring, likely reflecting insufficient stratosphere-troposphere exchange (also diagnosed by Hu et al. (2017)). Overall, however, the model-measurement comparisons do not point to any persistent, large-scale discrepancies that would alter the conclusions of our paper (particularly given that most campaigns used here, with the exception of DISCOVER-AQ CA, focus on meteorological summer).

We have added Figures S1 and S2 to the Supplement and the following to the Sect. 2: "The Supplement shows an evaluation of these boundary conditions based on Atmospheric Tomography Mission (ATom) (Wofsy et al., 2018) ozone observation in the northern Pacific."

Comment 2: Please provide analogous maps for NOx emissions (anthropogenic, soil, lightning, pyrogenic) to match Figures 2a and 3a for VOC. While NOx is not the focus of the present paper, these emissions are relevant to the analysis as they have strong indirect effects on VOC lifetimes and reactivities.

Reply to Comment 2: Thank you for the comment. As requested we have now added Figures S5 and S6, showing maps of annual NO_x emissions and the fractional contributions by seasons for each emission category.

References:

Hu, L., Jacob, D. J., Liu, X., Zhang, Y., Zhang, L., Kim, P. S., Sulprizio, M. P., and Yantosca, R. M.: Global budget of tropospheric ozone: Evaluating recent model advances with satellite (OMI), aircraft (IAGOS), and ozonesonde observations, Atmos. Environ., https://doi.org/10.1016/j.atmosenv.2017.08.036, 2017.

Wofsy, S. C., Afshar, S., Allen, H. M., Apel, E., Asher, E. C., Barletta, B., Bent, J., Bian, H., Biggs, B. C., Blake, D. R., Blake, N., Bourgeois, I., Brock, C. A., Brune, W. H., Budney, J. W., Bui, T. P., Butler, A., Campuzano-Jost, P., Chang, C. S., Chin, M., Commane, R., Correa, G., Crounse, J. D., Cullis, P. D., Daube, B. C., Day, D. A., Dean-Day, J. M., Dibb, J. E., DiGangi, J. P., Diskin, G. S., Dollner, M., Elkins, J. W., Erdesz, F., Fiore, A. M., Flynn, C. M., Froyd, K., Gesler, D. W., Hall, S. R., Hanisco, T. F., Hannun, R. A., Hills, A. J., Hintsa, E. J., Hoffman, A., Hornbrook, R. S., Huey, L. G., Hughes, S., Jimenez, J. L., Johnson, B. J., Katich, J. M., Keeling, R. F., Kim, M. J., Kupc, A., Lait, L. R., Lamarque, J.-F., Liu, J., McKain, K., Mclaughlin, R. J., Meinardi, S., Miller, D. O., Montzka, S. A., Moore, F. L., Morgan, E. J., Murphy, D. M., Murray, L. T., Nault, B. A., Neuman, J. A., Newman, P. A., Nicely, J. M., Pan, X., Paplawsky, W., Peischl, J., Prather, M. J., Price, D. J., Ray, E., Reeves, J. M., Richardson, M., Rollins, A. W., Rosenlof, K. H., Ryerson, T. B., Scheuer, E., Schill, G. P., Schroder, J. C., Schwarz, J. P., St.Clair, J. M., Steenrod, S. D., Stephens, B. B., Strode, S. A., Sweeney, C., Tanner, D., Teng, A. P., Thames, A. B., Thompson, C. R., Ullmann, K., Veres, P. R., Vieznor, N., Wagner, N. L., Watt, A., Weber, R., Weinzierl, B., Wennberg, P., Williamson, C. J., Wilson, J. C., Wolfe, G. M., Woods, C. T., and Zeng, L. H.: ATom: Merged Atmospheric Chemistry, Trace Gases, and Aerosols. ORNL DAAC, Oak Ridge, Tennessee, USA, https://doi.org/10.3334/ornldaac/1581, 2018.

Figures:

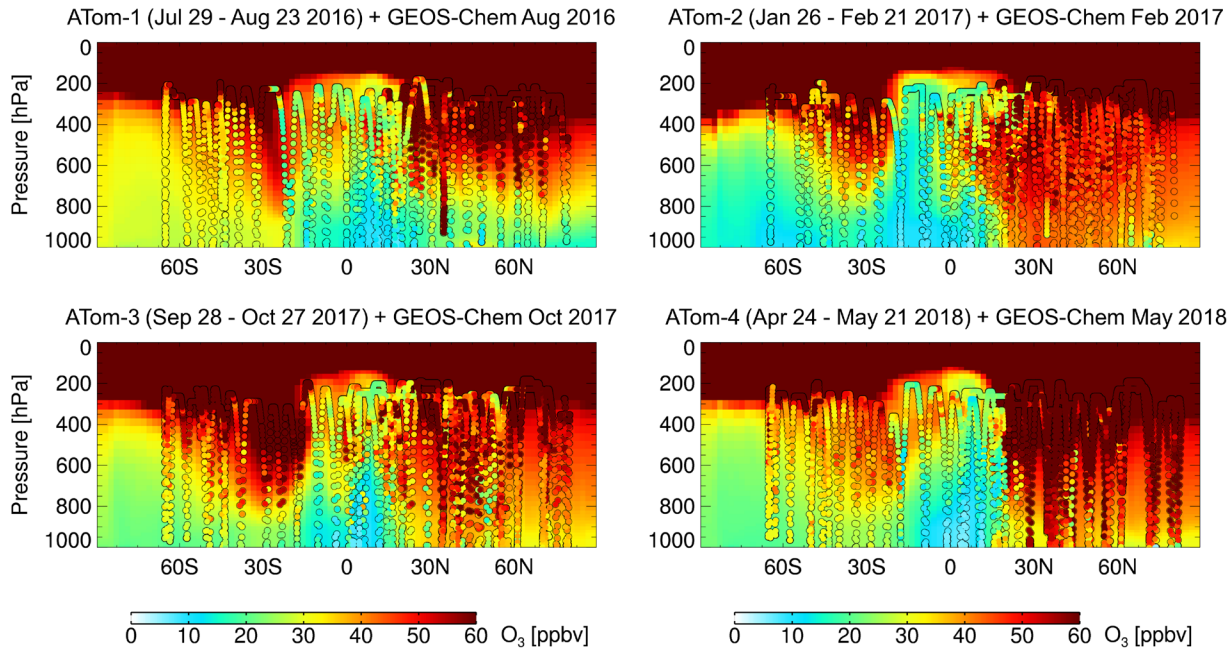

Figure S1. Ozone over the Pacific Ocean. Colored circles show airborne observations from the Atmospheric Tomography Mission (ATom) within 100˚W-170˚E. Plotted in the background is the monthly mean ozone curtain simulated by GEOS-Chem (global simulation at 2˚×2.5˚) at ~177.5˚W for the corresponding month.

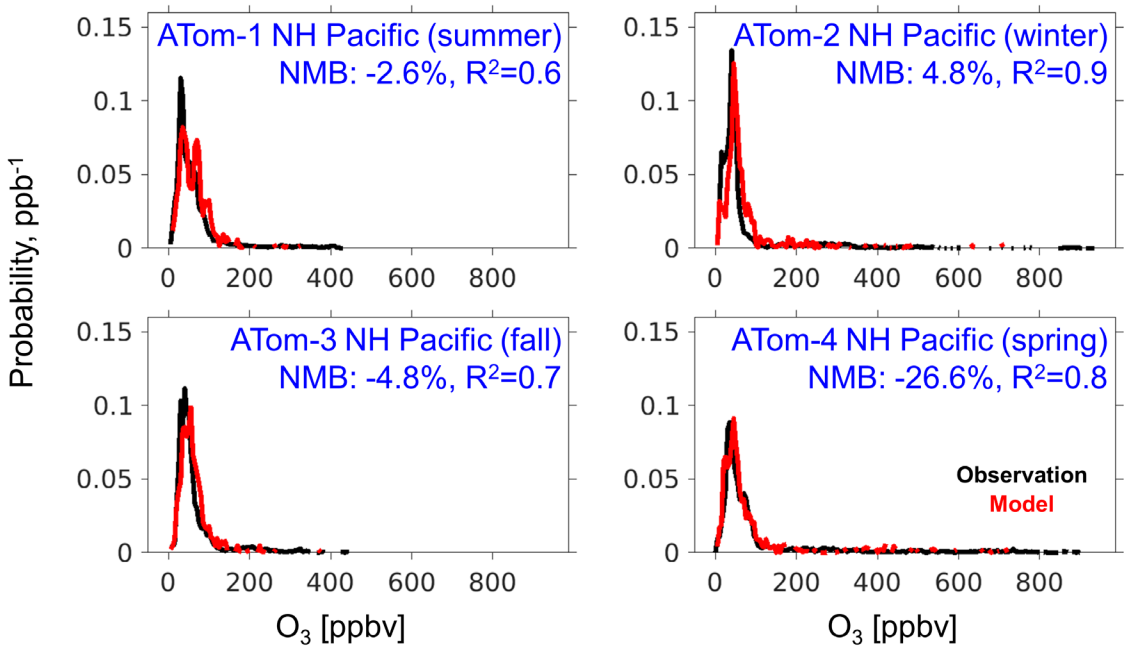

Figure S2. Ozone probability density functions over the northern Pacific (100˚W-170˚E, 0˚-90˚N). Plotted are ATom observations (black) and co-located GEOS-Chem model predictions (red), with correlations and normalized mean biases given inset.

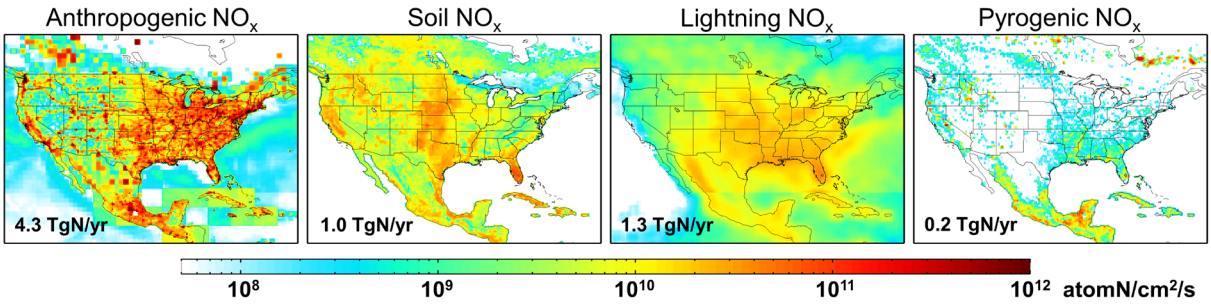

Figure S5. Annual NO_x emission fluxes over North America as simulated by GEOS-Chem for 2013.

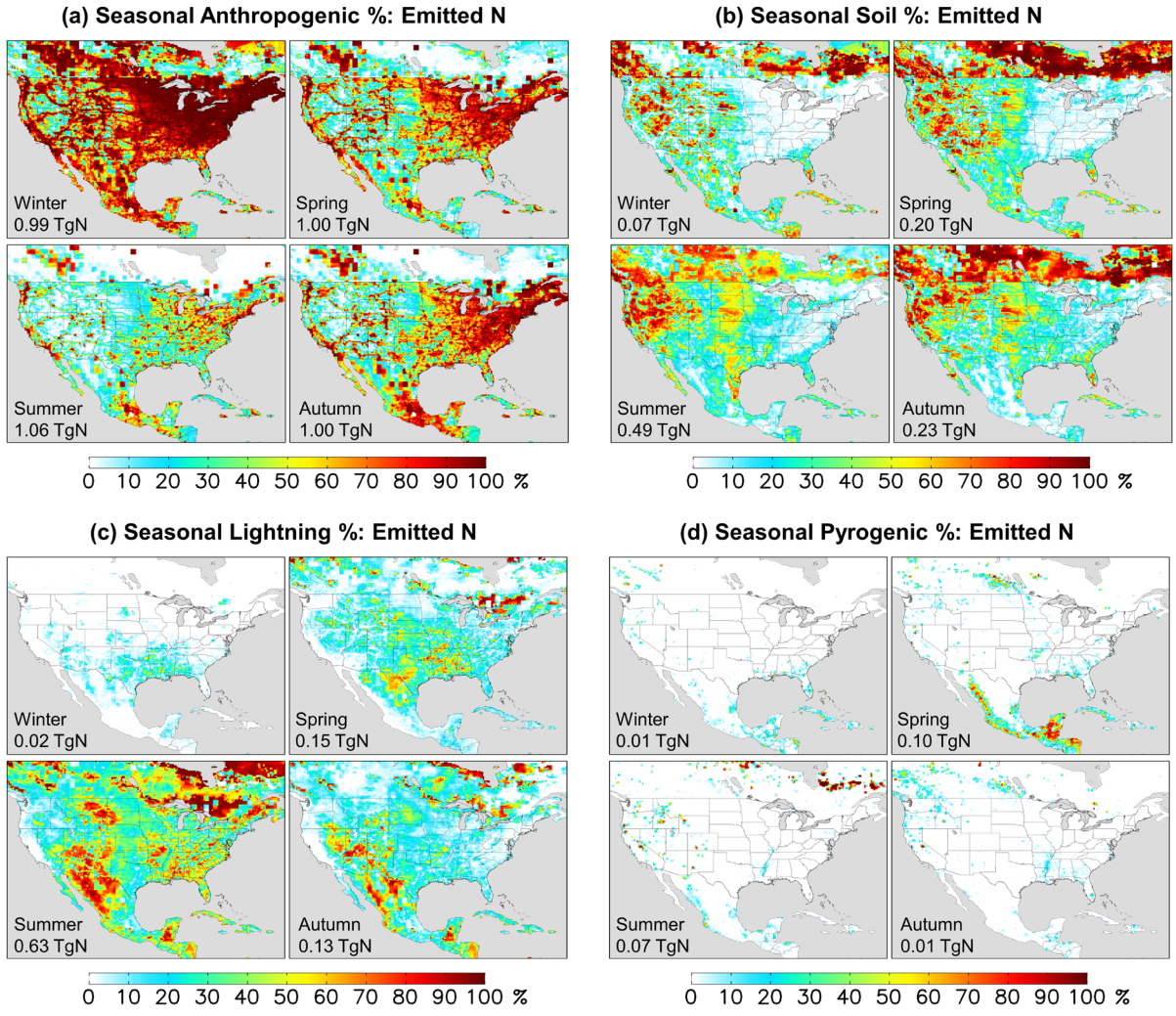

Figure S6. Seasonal contribution of each emission sector to total modeled NO_x emissions.

Revision Checklist:

(minor technical corrections not listed)

Author and acknowledgement updates:

1. Authorship added for Ilann Bourgeois and Chelsea R. Thompson
2. Acknowledgement added for Denise D. Montzka

Revisions relevant to referee comments:

1. From reviewer #1, comment #1: see change at Line 509 and Fig. S7 in supplement
2. From reviewer #1, comment #3: see change at Line 594
3. From reviewer #1, comment #4: see change at Line 575
4. From reviewer #1, remark #1: see change at Line 120
5. From reviewer #1, remark #2: see change at Line 185
6. From reviewer #1, remark #3: see change in Fig. 2 caption
7. From reviewer #2, comment #1: see change at Line 144 and Fig. S1, S2 in supplement
8. From reviewer #2, comment #2: see change at Line 333 and Fig. S5, S6 in supplement

Other revisions:

1. Text change at Line 382
2. Figure 3b, added numbers inset
3. Figure 4d, subtitle changed from "Total modeled OH reactivity" to "Total modeled VOC OH reactivity"
4. Two references added: Wofsy et al. (2018) and Alwe et al. (2019)

On the sources and sinks of atmospheric VOCs: An integrated analysis of recent aircraft campaigns over North America

Xin Chen[1], Dylan B. Millet[1], Hanwant B. Singh[2], Armin Wisthaler[3,4], Eric C. Apel[5], Elliot L. Atlas[6], Donald R. Blake[7], Ilann Bourgeois[8,9], Steven S. Brown[8], John D. Crounse[10~~9~~], Joost A. de Gouw[8,~~9~~10], Frank Flocke[5], Alan Fried[11], Brian G. Heikes[12], Rebecca S. Hornbrook[5], Tomas Mikoviny[4], Kyung-Eun Min[13], Markus Müller[3,*], J. Andrew Neuman[8,~~9~~10], Daniel W. O'Sullivan[14], Jeff Peischl[8,~~9~~10], Gabriele G. Pfister[5], Dirk Richter[12], James M. Roberts[8], Thomas B. Ryerson[8], Stephen Shertz[15], Chelsea R. Thompson[8,9], Victoria Treadaway[12], Patrick R. Veres[8], James Walega[11], Carsten Warneke[8,~~9~~10], Rebecca A. Washenfelder[8], Petter Weibring[11], Bin Yuan[16]

[1]Department of Soil, Water, and Climate, University of Minnesota, Minneapolis-Saint Paul, MN 55108, USA
[2]NASA Ames Research Center, Moffett Field, CA, USA
[3]Institute for Ion Physics and Applied Physics, University of Innsbruck, 6020 Innsbruck, Austria
[4]Department of Chemistry, University of Oslo, Norway
[5]Atmospheric Chemistry Observations & Modeling Laboratory, National Center for Atmospheric Research, Boulder, CO, 80301, USA
[6]Department of Atmospheric Sciences, Rosenstiel School of Marine and Atmospheric Science, University of Miami, Miami, FL, USA
[7]Department of Chemistry, University of California, Irvine, Irvine, CA, USA
[8]Chemical Sciences Division, NOAA Earth System Research Laboratory, Boulder, CO 80305, USA
[9]Cooperative Institute for Research in Environmental Sciences, University of Colorado, Boulder, CO 80309, USA
[~~9~~10]Division of Geological and Planetary Sciences, California Institute of Technology, Pasadena, CA 91125, USA
[~~10~~]~~Cooperative Institute for Research in Environmental Sciences, University of Colorado, Boulder, CO 80309, USA~~
[11]Institute of Arctic & Alpine Research, University of Colorado, Boulder, CO
[12]Graduate School of Oceanography, University of Rhode Island, Narragansett, RI 02882, USA
[13]School of Earth Science and Environmental Engineering, Gwangju Institute of Science and Technology
[14]United States Naval Academy, Chemistry Department, Annapolis, MD, 21401, USA
[15]Atmospheric Chemistry Division, National Center for Atmospheric Research, Boulder, Colorado, USA
[16]Institute for Environmental and Climate Research, Jinan University, Guangzhou, China
*now at: Ionicon Analytik GmbH, Innsbruck, Austria

Correspondence to: Dylan B. Millet (dbm@umn.edu)

Abstract

We apply a high-resolution chemical transport model (GEOS-Chem CTM) with updated treatment of volatile organic compounds (VOCs) and a comprehensive suite of airborne datasets over North America to i) characterize the VOC budget, and ii) test the ability of current models to capture the distribution and reactivity of atmospheric VOCs, over this region. Biogenic emissions dominate the North American VOC budget in the model, accounting for 70% and 95% of annually emitted VOC-carbon and reactivity, respectively. Based on current inventories anthropogenic emissions have declined to the point where biogenic emissions are the dominant summertime source of VOC reactivity even in most major North American cities. Methane oxidation is a 2× larger source of non-methane VOCs (via production of formaldehyde and methyl hydroperoxide) over North America in the model than are anthropogenic emissions. However, anthropogenic VOCs account for over half the ambient VOC loading over the majority of the region owing to their longer aggregate lifetime. Fires can be a significant VOC source

episodically but are small on average. In the planetary boundary layer (PBL), the model exhibits skill in capturing observed variability in total VOC-abundance (R^2 = 0.36) and reactivity (R^2 = 0.54). The same is not true in the free troposphere (FT), where skill is low and there is a persistent low model bias (~60%), with most (27 of 34) model VOCs underestimated by more than a factor of 2. A comparison of PBL:FT concentration ratios over the southeastern US points to a misrepresentation of PBL ventilation as a contributor to these model FT biases. We also find that a relatively small number of VOCs (acetone, methanol, ethane, acetaldehyde, formaldehyde, isoprene + oxidation products, methyl hydroperoxide) drive a large fraction of total ambient VOC reactivity and associated model biases; research to improve understanding of their budgets is thus warranted. A source tracer analysis suggests a current overestimate of biogenic sources for hydroxyacetone, methyl ethyl ketone and glyoxal, an underestimate of biogenic formic acid sources, and an underestimate of peroxyacetic acid production across biogenic and anthropogenic precursors. Future work to improve model representations of vertical transport and to address the VOC biases discussed are needed to advance predictions of ozone and SOA formation.

1. Introduction

Volatile organic compounds (VOCs) play a central role in atmospheric chemistry. Through their influence on the hydroxyl radical (OH), VOCs alter the lifetime of long-lived greenhouse gases (Cubasch et al., 2013), while their oxidation products such as ozone (O_3) and secondary organic aerosols (SOA) degrade human and ecosystem health (EPA, 2018) and alter Earth's radiative balance (Myhre et al., 2013). There are large uncertainties associated with the emissions (Karl et al., 2018; Hatch et al., 2017; Guenther et al., 2012), chemical processing (Caravan et al., 2018; Shaw et al., 2018; Müller et al., 2016a), and sinks of atmospheric VOCs (Iavorivska et al., 2017; Nguyen et al., 2015; Wolfe et al., 2015; Karl et al., 2010). An ensemble of recent airborne campaigns over North America together afford the most expansive picture yet of the atmospheric VOC distribution over this region. Here we apply a high-resolution chemical transport model (nested GEOS-Chem CTM) with a new and highly comprehensive VOC treatment to 1) interpret that observational ensemble in terms of their constraints on the distribution, speciation, and sources of VOC-carbon and reactivity, 2) assess our current scientific ability to capture that distribution across diverse environments, and 3) identify priorities for future research and model improvements.

It is widely recognized that terrestrial ecosystems provide the largest source of VOCs to the global atmosphere, mainly through foliar emissions but also via microbial decomposition of organic material, with an estimated flux of 750-1000 Tg/yr (Safieddine et al., 2017; Guenther et al., 2012). Global anthropogenic VOC emissions are thought to be an order of magnitude lower (e.g., 100-160 Tg/yr (Glasius and Goldstein, 2016; Boucher et al., 2013)), and include contributions from mobile sources such as on-road vehicles and aircraft (Stettler et al., 2011; Parrish, 2006) and from stationary sources such as volatile chemical products, fuel production, distribution, and combustion, and waste treatment (McDonald et al., 2018; Warneke et al., 2014; de Gouw et al., 2012; Millet et al., 2012). Biomass burning, i.e., combustion of any non-fossilized vegetation, leads to an estimated 60-400 Tg/yr of emitted VOCs, though with high uncertainty regarding potential unidentified and/or unmeasured pyrogenic compounds (Giglio et al., 2013; Akagi et al., 2011; Wiedinmyer et al., 2011; Andreae and Merlet, 2001). Ocean-atmosphere VOC fluxes have been investigated with a range of aircraft- and ship-based observations, remote sensing, and modeling approaches for species including isoprene and monoterpenes, other light hydrocarbons, halogenated species, and oxygenated VOCs such as methanol, acetone, formaldehyde, acetaldehyde, glyoxal, and carboxylic acids (Deventer et al., 2018; Kim et al., 2017; Mungall et al., 2017; Coburn et al., 2014; Yang et al., 2014a; Yang et al., 2014b; Beale et al., 2013; Yang et al., 2013; Fischer et al., 2012; Beale et al., 2011; Luo and Yu, 2010; Millet et al., 2010; Shaw et al., 2010; Millet et al., 2008; Read et al., 2008; Palmer and Shaw, 2005; Williams et al., 2004; Singh et al., 2003; Broadgate et

al., 1997; Zhou and Mopper, 1997; Bonsang et al., 1988; Kanakidou et al., 1988) . However, the quantitative role of the ocean as a net global VOC source or sink remains uncertain (Carpenter et al., 2012; Read et al., 2012).

While there have been a large number of studies focusing on one or a small subset of VOCs (a recent Web of Science search for articles with topic terms ("volatile organic compound*") AND ("atmospher*") returned >6,800 results), there have been few integrated studies examining the overall suite of measured species and our ability to capture that ensemble behavior in current CTMs. In one example, de Gouw et al. (2005) examined the photochemical evolution of organic carbon from urban outflow in the northeastern US and found evidence for unidentified aerosol precursors. Later, Goldstein and Galbally (2007) compiled a rough estimate of the total VOC budget and argued that there is a large pool of uncharacterized organic compounds in the atmosphere. Heald et al. (2008) carried out an integrated assessment of total observed organic carbon based on available measurements to that point, and articulated a need for more routine and comprehensive VOC-carbon measurements, while Safieddine et al. (2017) recently performed the first CTM-based budget analysis of total organic carbon on a global scale.

Recent observational work has benefited from new tools (e.g., high-resolution time-of-flight mass spectrometry) that enable a more thorough and time-resolved characterization of VOC-carbon than was previously possible. For instance, new flux measurments have been able for the first time to characterize the two-way surface atmosphere exchange of VOC-carbon simultaneously across the entire mass spectrum (Karl et al., 2018; Millet et al., 2018; Park et al., 2013). In addition, recent studies (Isaacman-VanWertz et al., 2018; Hunter et al., 2017) combining a comprehensive suite of online instrumentation have been able to achieve organic carbon closure (to within error) in a forested environment and in a laboratory oxidation experiment, respectively.

The past decade has thus seen major advances in the scientific community's ability to measure (e.g., Glasius and Goldstein (2016)) as well as model (e.g., Safieddine et al. (2017)) atmospheric organic carbon, and in our laboratory-derived understanding of key VOC oxidation pathways (e.g., (Praske et al., 2018; Ehn et al., 2014; Crounse et al., 2013; Paulot et al., 2009b)). Over the same period, there have been a large number of airborne campaigns over North America that, together, are unprecedented in their chemical and spatial coverage for characterizing VOC distributions over this region. Here, we perform an integrated analysis of these airborne datasets based on a high-resolution chemical transport model (nested GEOS-Chem CTM). The model simulation includes the latest updates~~extensive new developments~~ related to atmospheric VOCs (Sect. 2) and provides a more comprehensive representation of atmospheric organics than has been available for prior model-measurement evaluations. We apply this updated model with the suite of airborne observations to assess present understanding of the processes driving atmospheric VOCs, identify knowledge gaps, and address priorities for future work. We focus in this paper specifically on non-methane VOCs; we exclude intermediate, semi-volatile, low-volatility, and extremely low-volatility organic compounds (IVOC, SVOC, LVOC, ELVOC) because a comparable suite of airborne observations does not exist for these. The Hunter et al. study referenced above found for a ponderosa pine forest that while S/IVOC and E/LVOC species accounted for most of the aerosol-forming material, VOCs dominated the ambient OH reactivity due to non-methane organics, and also provided the majority of the organic carbon mass (Hunter et al., 2017). Likewise, while organic aerosol formation and subsequent deposition is not counted explicitly as a VOC sink in our chemical mechanism, prior work has found this to be only a small fraction (<4%) of the gas-phase VOC budget (Safieddine et al., 2017).

2. Model description

We use the GEOS-Chem CTM (v10-01; www.geos-chem.org) driven by assimilated meteorological fields (Goddard Earth Observation System Forward Processing product, GEOS-FP) from the NASA Goddard Modeling and Assimilation Office (GMAO). Simulations are performed for 2013, the year in which several of the utilized aircraft campaigns took place. The GEOS-FP fields have spatial resolution of 0.25°×0.3125° and temporal resolution of 3-h for 3-D meteorological parameters and 1-h for surface quantities and mixing depths. The North American simulation used here is conducted within a nested framework (130-60°W, 9.75-60°N, 47 vertical layers) at the native GEOS-FP horizontal resolution (Kim et al., 2015), with timesteps of 5-min (transport/convection) and 10-min (emissions/chemistry) (Philip et al., 2016). Dynamic boundary conditions are obtained from a global simulation (4°×5°) with timesteps of 30-min (transport/convection) and 60-min (emissions/chemistry). The Supplement (Fig. S1, S2) shows an evaluation of these boundary conditions based on Atmospheric Tomography Mission (ATom) (Wofsy et al., 2018) ozone observation in the northern Pacific. We use the TPCORE advection algorithm (Lin and Rood, 1996), convective mass fluxes from the GEOS-FP archive (Wu et al., 2007), and the non-local boundary layer mixing scheme described by Lin and McElroy (2010).

A year-long nested model run for 2013 was obtained via 12 parallel month-long simulations. Each of the latter was initialized after a ~1-week nested spin-up of regridded concentration fields from a ~2-year global spin-up. We find that this procedure is sufficient to achieve dynamic steady-state for oxidant and VOC levels in the model, as species that would require longer spin-up (e.g., methane) are prescribed rather than actively simulated in this mechanism.

2.1 Chemistry

The chemical mechanism in this work is based on Millet et al. (2018), with the following modifications. Here we incorporate a more detailed treatment of monoterpene chemistry that is adapted from Fisher et al. (2016), along with updated photo-isomerization yields for acetaldehyde (Millet et al., 2015). Further updates are included for VOC ozonolysis (isoprene, methacrolein, and isoprene hydroxynitrate) (Marais et al., 2016), glyoxal and methyl glyoxal yields from aromatics (Fischer et al., 2014), carboxylic acid production from the hydrolysis of stabilized Criegee intermediates (Millet et al., 2015), and photolysis cross sections for methyl vinyl ketone (MVK) and methacrolein (MACR) nitrates and propanone nitrate (Paulot et al., 2009a). Finally, we apply the carbon mass tracking approach outlined in Safieddine et al. (2017) to ensure carbon closure.

2.2 Deposition

Physical VOC sinks in GEOS-Chem include dry deposition following the Wesely (1989) scheme as implemented by Wang et al. (1998), and wet deposition as described by Amos et al. (2012). Wet deposition assumes liquid-phase-only uptake of VOCs (except formic acid and acetic acid) with a retention efficiency of 1 in warm clouds and 0.02 in mixed clouds (Mari et al., 2000). Ice uptake of formic acid and acetic acid is included based on the Langmuir isotherm model (Paulot et al., 2011).

Henry's law solubility constants (H values; required for calculating dry deposition resistances, gas-phase wet deposition, and air-sea fluxes) are computed following Travis et al. (2016) and Nguyen et al. (2015) for nitric acid, hydrogen peroxide, and a suite of isoprene-derived oxygenated VOCs (isoprene hydroxyl hydroperoxides, isoprene hydroxynitrate, isoprene epoxides, MVK/MACR nitrates, propanone nitrate, glycolaldehyde, hydroxyacetone). Values for lumped ≥C4 alkylnitrates and formaldehyde are based on Marais et al. (2016) and Jacob (2000), respectively, while those for benzene, toluene, and xylene (representing lumped C8 aromatics) are taken from Staudinger and Roberts (2001). The lumped xylene species in the model uses the mean H value from the corresponding individual C8 compounds (o-xylene, m-xylene, p-xylene, ethylbenzene). For other VOCs we use central literature values based on the Sander

(2015) compilation. Carboxylic acids employ an effective H value at pH=7, with lumped ≥C3 acids using the median reported value for propionic acid (Nirmalakhandan and Speece, 1988).

2.3 Emissions

2.3.1 Natural emissions

Biogenic VOC emissions from terrestrial plants are calculated online in GEOS-Chem using the Model of Emissions of Gases and Aerosols from Nature version 2.1 (MEGAN v2.1), implemented into GEOS-Chem as described by Hu et al. (2015) ~~with updated 0.25°×0.3125° distributions of plant functional types and base emission factors~~.

NO_x emissions from microbial processes in soils are estimated as described in Hudman et al. (2012). The annual combined global flux of formic and acetic acids from soils estimated previously by Paulot et al. (2011) corresponds to approximately 10% of this NO_x source, and we therefore determine the formic/acetic acids soil fluxes as 5% (molar ratio) of the Hudman et al. (2012) NO_x flux.

Marine hydrocarbon emissions (for alkanes, alkenes, and isoprene) are estimated following Millet et al. (2015) and Paulot et al. (2011). Air-sea fluxes of oxygenated VOCs are calculated following Johnson (2010), Millet et al. (2010; 2008), and Fischer et al. (2012), with assumed fixed seawater concentrations of 15 nM (acetone), 31 nM (methanol), and 6 nM (acetaldehyde) based on compiled cruise measurements (Beale et al., 2015; Yang et al., 2014a; Yang et al., 2014b; Beale et al., 2013; Yang et al., 2013; Beale et al., 2011; Kameyama et al., 2009; Hudson et al., 2007; Marandino et al., 2005; Williams et al., 2004; Zhou and Mopper, 1997).

2.3.2 Anthropogenic emissions

Global anthropogenic VOC emissions in the model are from the Interpolated ACCMIP-RCP 8.5 inventory for year-2013 (van Vuuren et al., 2011; Lamarque et al., 2010; Riahi et al., 2007) (with a few exceptions; see below). This inventory provides speciated emissions for alkanes/alkenes/alkynes/aromatics, and unspeciated emissions for alcohols/≥C2 aldehydes/ketones/carboxylic acids. For the latter, we apply speciation factors for methanol and ethanol (0.5, 0.375, mass basis), acetaldehyde and ≥C3 aldehydes (0.75, 0.25), and acetone and ≥C4 ketones (0.75, 0.25) based on prior studies (Wells et al., 2012; Millet et al., 2010). Formic acid and acetic acid together are assumed to account for 75% by mass of the total ACCMIP carboxylic acid source (these in turn are partitioned with a 1:2 molar ratio), with ≥C3 carboxylic acids making up the remaining 25% (Paulot et al., 2011).

Global anthropogenic and biofuel emissions of ethane and propane are from Xiao et al. (2008). Global formic and acetic acid emissions from animal agriculture are scaled to the corresponding ammonia source (from EDGAR v4.2 agricultural sectors 4C and 4D) following Paulot et al. (2011). We use global biofuel emissions from Yevich and Logan (2003) for emitted oxygenated VOCs not included in ACCMIP-RCP 8.5 (glycolaldehyde, hydroxyl acetone, glyoxal, and methyl glyoxal). Aircraft emissions are from the AEIC inventory (Stettler et al., 2011), and global anthropogenic NO_x/CO/SO_2/NH_3 emissions are from EDGAR v4.2 (European Commission (EC), 2011).

Over North America, emissions of inorganic species and VOCs (except ethane and propane) from anthropogenic, biofuel, and ship sources are overwritten by the hourly EPA/NEI2011 inventory (Travis et al., 2016; EPA, 2015), with annual scale factors applied to account for recent trends (e.g., the nationally aggregated 2011-2013 emission trend factor for VOCs is 0.971). Molar fluxes of formic and acetic acid over North America from these sources are estimated by scaling those of CO by 2.1×10^{-4} and 4.2×10^{-4}, respectively (Paulot et al., 2011).

222 2.3.3 Biomass burning emissions
223 Open fire emissions are calculated from monthly burned area and fractional fire type contributions from
224 the fourth version of the Global Fire Emissions Database with small fires (GFED4s) (van der Werf et al.,
225 2017) for our simulation year. We use the GFED-recommended species-specific emission factors
226 (http://www.globalfiredata.org/data.html) which are based primarily on Akagi et al. (2011).

227

228 **3. Airborne measurements of VOCs over North America**
229 Figure 1 shows flight tracks for the airborne tropospheric chemistry missions that took place over North
230 America between 2010-2014 and are used here. We have used data from intensive field campaigns using
231 NCAR, NOAA and NASA aircraft that carried a large instrument payload to simultaneously measure
232 many VOCs. Together, they provide a rich dataset for constraining VOC-related processes, as they
233 feature extensive horizontal and vertical sampling throughout the North American troposphere and
234 include a range of observing strategies such as survey transects, racetrack gradients/walls, and spirals.
235 Table 1 summarizes the campaigns in terms of sampling time period, region, as well as aircraft platform
236 and flight ceiling, with instrumental measurement details and references provided in Table S1. Below, we
237 briefly introduce the overall goals and instrument payload for each campaign.

238 The Studies of Emissions and Atmospheric Composition, Clouds, and Climate Coupling by Regional
239 Surveys (SEAC^{4}RS 2013; Aug-Sep 2013) (Toon et al., 2016; SEAC^{4}RS Science Team, 2013) was
240 conducted over the southeastern US and targeted a broad range of goals including quantifying the
241 regional distribution of anthropogenic, biomass burning, and biogenic chemicals, characterizing their re-
242 distribution through convection, and identifying their impacts on boundary layer and upper tropospheric
243 chemistry. The deployed NASA DC-8 aircraft has a flight ceiling of 12.5 km above sea level (ASL),
244 enabling deep vertical profiling. The SEAC^{4}RS VOC payload included a chemical ionization mass
245 spectrometer using CF_3O^- reagent ions (CIT-CIMS (CF_3O^-)), a separate CIMS measuring peroxy acetyl
246 nitrate (PAN-CIMS), a proton-transfer-reaction mass spectrometer (PTR-MS), in situ airborne
247 formaldehyde measurements by laser induced fluorescence (ISAF-LIF), thermal dissociation LIF (TD-
248 LIF), and a whole air sampler (WAS). Specific VOCs measured by each instrument are listed in Table S1.

249 The Southeast Nexus (SENEX; Jun 2013) campaign (Warneke et al., 2016) was part of the Southeast
250 Atmosphere Study (SAS). The NOAA WP-3D aircraft sampled the boundary layer through mid-
251 troposphere (up to 6.4 km ASL), targeting both natural and anthropogenic emissions. Onboard VOC
252 instruments included WAS, ISAF-LIF, PAN-CIMS, and PTR-MS. SENEX also featured in-situ
253 measurements of carboxylic acids by two separate CIMS using iodide reagent ions (I^--CIMS) and of
254 glyoxal via airborne cavity enhanced spectrometer (ACES) (Table S1).

255 The Deep Convective Clouds and Chemistry (DC3; May-Jun 2012) field experiments took place over the
256 central US and were specifically designed to investigate changes in upper tropospheric composition and
257 chemistry during and after deep convective events (Barth et al., 2015; DC3 Science Team, 2013). During
258 DC3 the NASA DC-8 and GV aircraft sampled storm outflow up to 13 km ASL through spirals and wall
259 sampling. The VOC payload included PTR-MS, a Trace Organic Gas Analyzer (TOGA), CIT-CIMS
260 (CF_3O^-), PAN-CIMS, ISAF-LIF, TD-LIF, and WAS.

261 The California Research at the Nexus of Air Quality and Climate Change (CalNex; May-June 2010)
262 campaign studied air quality and climate over California and offshore (Ryerson et al., 2013). The NOAA
263 WP-3D aircraft sampled the troposphere up to 5 km ASL, and carried out survey tracks over the northern,
264 central, and southern San Joaquin Valley and Los Angeles basin, with spirals over targeted urban and
265 agricultural sources. VOCs were measured onboard by PTR-MS, PAN-CIMS, and WAS.

DISCOVER-AQ (Deriving Information on Surface Conditions from Column and Vertically Resolved Observations Relevant to Air Quality) (Crawford and Pickering, 2014; DISCOVER-AQ Science Team, 2014) included four separate airborne campaigns: DISCOVER-AQ DC (Jun-Jul 2011) over Baltimore-Washington DC, DISCOVER-AQ CA (Jan-Feb 2013) over the San Joaquin Valley, DISCOVER-AQ TX (Sep 2013) over Houston, and DISCOVER-AQ CO (Jul-Aug 2014) over the Denver Colorado urban region. The NASA P3-B aircraft (8.5 km ASL ceiling) was employed in each case, with frequent and repeated spirals to characterize the vertical structure of the troposphere. The VOC payload included a difference frequency generation absorption spectrometer (DFGAS) and time-of-flight PTR-MS (PTR-ToF-MS; quadrupole PTR-MS was used for DISCOVER-AQ DC).

FRAPPÉ (Front Range Air Pollution and Photochemistry Experiment; Jul-Aug 2014) took place jointly with DISCOVER-AQ CO, with the employed NCAR C-130 aircraft (8 km ASL ceiling) sampling the broader mountain-plain areas over northern Colorado. The VOC payload included PTR-MS, a compact atmospheric multi-species spectrometer (CAMS), TOGA, peroxide CIMS (PCIMS), PAN-CIMS, and WAS.

We use 1-minute merged data from each campaign to match the frequency at which the GEOS-Chem output is sampled along the aircraft flight tracks. For species co-measured by multiple instruments during the same campaign, we select one measurement primarily based on time response (≤ 1-min sampling rate preferred), while also considering data availability and nominal accuracy. For example, VOCs measured by PTR-MS, TOGA or CAMS (for ethane) take precedence over contemporaneous WAS observations due to the higher time resolution. The ISAF-LIF, DFGAS and CAMS instruments are specifically designed for formaldehyde, and we use these observations (rather than WAS, TOGA, or PTR-MS) in all cases with the exception of CalNex (where PTR-MS was the only available HCHO measurement). PTR-MS and TOGA measurements during FRAPPÉ are highly correlated but with 5-30% discrepancies across compounds (Fig. S3~~18~~). We therefore repeated our main analyses using data from each instrument (see Fig. 5~~-8, 6~~ and Table S2~~-5, S3~~), and find that the conclusions are not significantly changed. Similar sensitivity tests are done for formaldehyde, which had concurrent observations during DC3-DC-8 (DFGAS, ISAF-LIF) and during SEAC^{4}RS (CAMS, ISAF-LIF), as well as for formic acid, which had concurrent observations during SENEX (NOAA CIMS, UW CIMS) (Fig. S4~~19~~).

One concern when combining multiple measurements is the differing time resolution between instruments. For example, the WAS systems collect discrete samples separated by up to 10 min, while TOGA collects a 35 second integrated sample on alternate minutes. Many other instruments used here have significantly higher time resolution. To address this issue, when mapping aggregated quantities (i.e., total VOC-carbon; Fig. 5), we consider only those datapoints with complete species coverage (no missing data within a given campaign's payload). Overall, this yields ~7000 (4500) 1-min averaged observational datapoints in the PBL (FT), distributed over ~900 (1700) ~25km model grid cells. Finally, to avoid comparing a single modeled value with multiple observations falling into the same model gridbox and timestep, all measurements and model output are averaged and gridded to unique model gridbox-timestep combinations.

4. Simulated VOC budget over North America

4.1 Biogenic emissions dominate the VOC budget on a carbon basis

Figure 2a depicts the annual VOC budget (in C units) over North America in 2013 as simulated by GEOS-Chem. A buffer of ten model grid boxes along each lateral boundary has been omitted to exclude unrealistic conditions near the edge of the nested domain. Total fluxes are indicated for each source and

sink term, representing the sum over all grid boxes within the plotted region. The net transport flux in/out of the domain is estimated from the accumulated product of the daily average eastward/northward wind components and VOC number density at the boundaries. In this way, we achieve regional VOC-carbon closure to within 3%.

We see in Fig. 2a that biogenic emissions are the dominant annual VOC-carbon source over North America, accounting for 71% (40 TgC) of the model total. Anthropogenic emissions account for 23% (13 TgC), while VOC emissions from fires can be important in particular locations and seasons but are minor when integrated over the domain as a whole (3 TgC, 5%). Prior studies have estimated that biogenic VOC emissions are 10-12× larger than anthropogenic emissions on a global basis (Safieddine et al., 2017; Glasius and Goldstein, 2016; Boucher et al., 2013; Guenther et al., 2012; Goldstein and Galbally, 2007); our results for North America, while indicating a greater relative importance for anthropogenic emissions than in the global mean, still show that biogenic VOC-carbon emissions are ~3× anthropogenic sources even in this industrialized region. Finally, while methane is not considered as a VOC for the purpose of our analysis, its oxidation generates formaldehyde and methyl hydroperoxide, corresponding to a VOC source of 30 TgC/y over our North American domain. Methane oxidation is thus >2× larger as a non-methane VOC source over this region than anthropogenic emissions, though this source is diffuse and not-collocated with land-based fluxes.

During winter (Fig. 3a), we find in the model that anthropogenic sources account for the majority (54%) of emitted VOC-carbon over the domain as a whole; this fraction would be significantly higher if we were to exclude the US Gulf States, Mexico, and Central America where substantial biogenic emissions persist throughout the year. However, during summer the modeled domain-wide anthropogenic contribution is only 12%; then, it is only in the most polluted regions, where biogenic emissions are low, that anthropogenic emissions provide the main source of atmospheric reactive carbon.

Analogous sets of figures for NO_x are provided in the supplement (Fig. S5, S6).

4.2 Biogenic VOC emissions even more dominant on a reactivity basis

The predominance of biogenic over anthropogenic VOCs in North America is even more pronounced when we account for the chemical reactivity of the various species. A common metric for assessing this is the OH reactivity ($\sum k_i n_i$, where k_i and n_i are the OH reaction rate coefficient and atmospheric number density for chemical i), which quantifies the OH loss rate associated with the ambient loadings of various species. In this paper, we use the term 'VOC reactivity' to refer specifically to that portion of the OH reactivity driven by VOCs. A related, emissions-focused measure is the OH reactivity flux: i.e., $\sum k_i F_i$, where F_i is the surface flux for VOC i (in molecular units). Since the reactivity flux is equivalent to a (mixing-height scaled) time-derivative of OH reactivity (Millet et al., 2018), it provides a direct measure of how a given surface flux affects ambient OH reactivity.

Figure 2b maps the modeled OH reactivity flux associated with biogenic, anthropogenic and pyrogenic VOC emissions. We see that biogenic sources in the model account for 95% of the annual reactivity-weighted VOC source over North America as a whole, with anthropogenic sources contributing just 3%. This biogenic predominance continues throughout the year, with biogenic VOCs making up 88% of the modeled domain-aggregated reactivity flux even during winter (though with strong spatial gradients; Fig. 3b). During summer, that fraction increases to 96%.

There has been a substantial decrease in transportation-related VOC emissions over the past several decades in the US (McDonald et al., 2013; Parrish, 2006) (e.g., a factor of ~50-100 decrease was inferred over Los Angeles from 1960-2010 (Warneke et al., 2012)). According to current inventories (Fig. 3), anthropogenic emissions have declined to the point where biogenic emissions are the dominant

summertime source of VOC reactivity even in many major North American cities. Only in a small number of pollution hotspots (Fig. 3) are anthropogenic emissions the main source of VOC-related OH reactivity driving summertime production of ozone and other secondary products.

4.3 Anthropogenic species comprise over half of the ambient VOC-carbon burden over most of North America

Figure 4 (panels b, c, e, and f) shows the fractional contribution to the ambient near-surface VOC burden from anthropogenic and biogenic emissions. We quantify these contributions via model sensitivity tests with modified (-10%) biogenic and anthropogenic VOC emissions; the contribution from each emission category is then obtained by dividing the relative change in ambient VOC-carbon or reactivity by the relative emission perturbation. Partitioning the ambient VOC loading in this way provides an alternate framing of the VOC budget compared to the discussion above, which examined the VOC source flux magnitudes themselves.

While anthropogenic species make up only a small fraction of the total emitted VOC mass (~23%; Fig. 2a~~1~~), they account for more than half of the ambient near-surface VOC-carbon abundance over most of the North American domain (the median fraction in Fig. 4c is 57%). This is due to the longer aggregate model lifetime for anthropogenic versus biogenic VOCs: because of this, away from major biogenic source regions the ambient VOC-carbon loading predominantly reflects anthropogenic species. However, many of these areas have relatively low total VOC-carbon loading (Fig. 4a). The corollary of the above finding is that the ambient VOC-driven OH reactivity is controlled by biogenic species, and this is also apparent in Fig. 4 (panels e and f).

4.4 Fate of reactive carbon over North America

The predominance of biogenic VOCs (in terms of total emitted VOC-carbon) combined with their relatively short ensemble lifetime leads to a spatial correlation between biogenic VOC emissions and total VOC sinks (e.g., over the southeastern US; Fig. 2a). Fig. 2a shows that of the 86 TgC of non-methane VOC added annually to the North American atmosphere through emissions, transport, and CH_4 oxidation, 62 TgC (72%) is oxidized to $CO+CO_2$ in the model. If we exclude the oxidation of methane (nearly 100% of which goes on to form CO and CO_2), then of the 56 TgC/y of primary VOCs emitted over North America, 32 TgC/y (57%) is ultimately oxidized to $CO+CO_2$ within the domain of Fig. 2. Oxidation of non-methane VOCs therefore provides an atmospheric CO+CO2 source over this region ~~slightly larger~~greater than that from methane oxidation (30 TgC/y), and greater than that from direct anthropogenic CO emissions (also 30 TgC/y).

Other removal processes include deposition (dry, 10 TgC/y; wet, 7 TgC/y) and net transport out of the domain (10 TgC/y). While global studies have found that wet deposition is a ~50% larger sink of organic carbon than is dry deposition (Safieddine et al., 2017; Kanakidou et al., 2012), the increased role for dry deposition found here is consistent with the higher continental coverage of our regional domain.

In the case of the VOC reactivity budget (Fig. 2b), we find in GEOS-Chem that chemical degradation is by far the largest sink (83%) of emitted reactivity, with physical removal via deposition (14%) and transport out of the domain (3%) making up the remainder.

5. Observed versus predicted distribution of VOC-carbon and reactivity over North America

In this section we use the aircraft campaigns described earlier to characterize the distribution of VOCs over North America, and assess the ability of the GEOS-Chem model to capture that distribution in terms of total carbon loading and associated reactivity.

For each campaign we use the 1-minute merge products provided by the NASA Langley Research Center (LaRC) and the NOAA Earth System Research Laboratory Chemical Science Division (ESRL CSD) (Table 1), and sample the model along the flight tracks at the time of measurement. Measurements have been filtered to remove fresh biomass burning (CH_3CN > 0.2 ppbv) and pollution plumes (NO_2 > 4 ppbv or NO_x/NO_y > 0.4), and restricted to daytime measurements over continental North America. Model-measurement comparisons are performed for the planetary boundary layer (PBL, defined here as <2 km AGL) and free troposphere (FT, >3 km AGL) based on unique gridbox-timestep combinations.

For the purposes of model-measurement comparison we restrict the observed VOCs to those that are explicitly simulated by GEOS-Chem (Millet et al., 2018). This restricted set of VOCs nonetheless encompasses those species believed to be most important in terms of abundance and reactivity (Heald et al., 2008), and allows an apples-to-apples comparison between observations and model. For cases where multiple VOCs are measured together as a single quantity, the corresponding modeled VOCs are likewise summed. Similarly, measured VOCs are summed to match those that are lumped in the model.

VOC OH reactivities are calculated from the measured and simulated species concentrations and corresponding pressure- and temperature-dependent rate coefficients for reaction with OH. For species that are detected together but simulated separately, we use the modeled ratio to partition the measured sum in calculating the combined OH reactivity. For species that are lumped in the model but measured separately, we apply the bulk OH reaction rate coefficient from the model to the summed measurements.

In the case of C3 and C4 ketones and aldehydes, the model includes a dedicated tracer for acetone (ACET) and lumped tracers for ≥C4 ketones (MEK) and ≥C3 aldehydes (RCHO). On the other hand, these species are measured by PTR-MS as Σ(acetone+propanal) and Σ(MEK+butanal) and by TOGA as individual species. When analyzing the PTR-MS data we therefore partition the PTR-MS observations based on the median aldehyde:ketone ratio measured by TOGA during FRAPPÉ and DC3 (0.009 for propanal:acetone and 0.09 for butanal:MEK).

5.1 Total observed VOC-carbon and reactivity over North America

Figure 5 (left panels) shows the resulting total VOC-carbon as observed over North America, which averages 27 ppbC in the PBL when considering all the aircraft campaigns as a single statistical ensemble. However, the campaigns span a range of instrumental payloads, seasons, and locations: campaigns with the most comprehensive VOC instrument payloads and that occur during summer reveal total PBL VOC loadings generally >60 ppbC, and up to 133 ppbC over the central and southeastern US. Campaigns over the northeastern and western US, with more limited VOC payloads, show PBL VOC loadings that average 20 ppbC and at times exceed 50 ppbC. Total VOC loadings in the FT (Fig. 5~~a~~) drop by a factor of ~3 or more from those in the PBL across all environments, with an ensemble spatial mean of 9 ppbC.

The observed VOC-carbon loadings summarized above and plotted in Fig. 5 are broadly similar to those reported over the US by Heald et al. (2008) (averaging 8-84 ppbC with 83-97% in the gas-phase at 273K and 1013hPa), who synthesized the gas- and aerosol- phase organic carbon observations up to that time. However, observations over the US used in that study were primarily from ground-based campaigns. The 10 airborne studies carried out since then and used here allow a more comprehensive spatial description of VOCs across the North American airshed. The combined dataset employed here also includes a number of additional multifunctional VOCs that can now be quantified thanks to measurement advances in the intervening decade (Glasius and Goldstein, 2016).

Figure 6 (left panels) shows the total OH reactivity arising from the set of observed VOC. The aggregated spatial mean VOC reactivity is 2 s^{-1} in the PBL, declining to 0.13 s^{-1} in the FT. Compared to the VOC-carbon loading, the reactivity has a much larger vertical falloff (10-20× decrease from the PBL to the FT),

and greater spatial variability within the PBL. The observed VOC reactivity within the PBL is generally >6 s^{-1} over the southeastern US, 2-6 s^{-1} over the northeastern US, and <2 s^{-1} over the central and western US. The highest observed VOC reactivity (24 s^{-1}) over the southeastern US is comparable to ground-based measurements in that region (10-25 s^{-1}) during the SOAS study (Feiner et al., 2016; Kaiser et al., 2016).

The importance of biogenic VOCs for reactive carbon loading and, especially, reactivity in the PBL is evident in the maps shown in Fig. 5-6. For example, Fig. 6 shows sharply defined areas of elevated VOC reactivity in the PBL over the forests of the southeastern US, with strong horizontal gradients and much lower observed reactivity elsewhere. Similar patterns, though less starkly defined, are evident in the measured VOC-carbon distribution (Fig. 5). The highly reactive nature of many biogenic VOCs (especially isoprene and some of its oxidation products) explain their disproportionate impact on reactivity given their relative abundance, as well as the much larger spatial gradients for VOC reactivity than for total VOC-carbon.

5.2 Speciated drivers of ambient VOC-carbon and reactivity

Figures 7 and 8 show the species driving ambient VOC-carbon and reactivity as a function of their carbon oxidation state (OS_c) and size (carbon number, n_c) (Kroll et al., 2011). Within the PBL (Fig. 7b), we find that the total mean VOC-carbon is largely driven by small and relatively reduced VOCs (e.g., acetone, methanol and alkanes), though some more oxidized species (e.g., formic acid, methyl hydroperoxide, formaldehyde, other isoprene oxidation products) also make significant contributions. These smaller VOCs would represent an even larger portion of the total molar VOC-loading.

In the FT (Fig. 7a), mean abundances decline by ~2-fold or more for all measured VOCs relative to the PBL. Here, a few small, reduced (low-OS_c), and relatively long-lived species dominate the overall VOC-carbon loading, with acetone, methanol, and ethane (τ ~ 12-50 days at OH = 10^6 molecules/cm^3) together averaging 6.4 ppbC, compared to only 3.6 ppbC for the mean sum of all other observed species.

However, ambient OH reactivity is driven by a different set of VOCs. Figure 8 shows that within the PBL, formaldehyde (0.34 s^{-1}), acetaldehyde (0.19 s^{-1}), isoprene hydroxyhydroperoxides + epoxides (0.21 s^{-1}), methylhydroperoxide (0.17 s^{-1}), and isoprene (0.11 s^{-1}) make the largest contributions to the mean observed VOC reactivity. Compared to the case for VOC-carbon loading (Fig. 7b), we see in the reactivity distribution a more prominent role for a number of higher-n_c (and more reactive) compounds.

On average, the observed VOC reactivity is more than a factor of 10 lower in the FT than in the PBL, with formaldehyde (0.03 s^{-1}) and acetaldehyde (0.02 s^{-1}) still making the largest contributions to the total. Whereas the FT VOC-carbon loading is dominated by a few small VOCs (Fig. 7a), Figure 8a shows that the FT VOC reactivity is provided by a wider suite of species due to the offsetting effects of abundance and lifetime. In other words, we see important FT reactivity contributions (in the mean) from both highly-reactive (but low-abundance) VOCs such as isoprene, and from less-reactive (but highly-abundant) VOCs such as methanol.

5.3 Accuracy of CTM-predicted VOC-carbon and reactivity

Figures 5 and 6 also portray the ability of the GEOS-Chem CTM to represent the measured distribution of VOCs over North America. In the PBL, the model exhibits significant skill at capturing atmospheric variability in VOC-carbon and reactivity: spatial model-measurement R^2 values are 0.36 and 0.54, respectively. The same is not true in the FT, where the model-measurement correlations are R^2 <0.1 for both VOC-carbon and VOC OH reactivity. This lack of explanatory power suggests that the primary drivers of VOC abundance and reactivity in the FT are not well-understood or represented in current models.

We also see in Fig. 5 and 6 that the model tends to underestimate the observed VOC-carbon and reactivity in the PBL across most of the sampled environments, with a normalized mean bias (NMB) of -37% and -34%, respectively. This corresponds to a mean reactive carbon underestimate in the PBL of 10 ppbC and a reactivity underestimate of 0.6 s^{-1}. A bias of this magnitude is equivalent to ~2× the reactivity of methane (at 2ppm) or 0.5× that of CO (at 200 ppb), and is therefore important for accurately representing atmospheric OH chemistry and ozone production.

While on average the CTM underpredicts the abundance and reactivity of VOCs in the PBL, this is not the case everywhere. There are areas shown in Fig. 5 and 6 where the model either agrees with the observations or is too high - in particular over the northern Sacramento Valley and the southeastern US. Regarding the former, large methanol and acetaldehyde emissions from rice fields, with strong enhancements after flooding, were previously inferred based on the same CalNex observations over the Central Valley (Peischl et al., 2012; Warneke et al., 2011). Indeed, we find here a model overestimate of total VOC-carbon for this region before flooding and a low bias after flooding, suggesting that agricultural VOC emissions are not currently well-represented in the model. On the other hand, over the southeastern US, where biogenic emissions predominate and VOC loading is highest across all sampled areas, both the PBL VOC-carbon (observed mean of 48 ppbC) and VOC reactivity (4.5 s^{-1}) are captured by the model with low mean bias (<14% for both).

In contrast to the PBL where both positive and negative model discrepancies occur, aloft in the FT the model exhibits a large negative bias for both VOC-carbon (-64%) and reactivity (-63%) that manifests essentially everywhere. Such a severe discrepancy has implications for our understanding of FT HO_x cycling (Brune et al., 2018; Mao et al., 2009), ozone production at higher altitudes where its climatic effects are strongest (Apel et al., 2015; Bertram et al., 2007), and possibly, secondary organic aerosol loading (Bianchi et al., 2016; Cappa, 2016; Kirkby et al., 2016; Trostl et al., 2016; Heald et al., 2005). We explore potential causes for these observed discrepancies in Sect. 6.1.

Given the range in measurement years spanned by the aircraft measurements, we performed a set of one-month simulations spanning multiple years to assess the potential impact of interannual variability on these findings. Results (see Fig. S7 and text following) suggest that the key features of the model-measurement comparisons discussed here are robust across years.

5.4 Key VOCs driving model biases in atmospheric VOC-carbon and reactivity

Figure 7b shows that the overall low model bias for VOC-carbon in the PBL manifests for 23 out of 34 individual VOCs, with these exhibiting normalized biases ranging from -1% to -90% (Fig. S8~~1~~b and S9~~2~~b). In general, the largest absolute carbon biases are seen for the more abundant VOCs (Fig. 7b), and largest reactivity biases for the more reactive VOCs (Fig. 8b). Just two compounds (acetone and methanol) account for almost half of the mean negative VOC-carbon bias seen in the PBL (4.3 of 9 ppbC). For VOC -reactivity, four compounds (methyl hydroperoxide, acetaldehyde, formaldehyde, and isoprene) together account for 70% of the mean model bias in the PBL (-0.34 of -0.47 s^{-1}).

Aloft in the FT (Fig. 7a and 8a), we see appreciable relative biases manifest across nearly all model compounds (ranging from -7% to -100%; Fig. S8~~1~~a and S9~~2~~a), with 29 ~~of~~ out of 34 VOCs biased low in the model by more than a factor of 2. Acetone, methanol, and ethane are predominant in driving the overall model VOC-carbon underestimate: these three species have a combined model bias of -3.3 ppbC, versus a total of only -2.1 ppbC for all other underestimated VOCs combined. Significant discrepancies in model simulated FT VOC -reactivity are driven by both abundant but less reactive VOCs, and by reactive (but less abundant) VOCs, with acetaldehyde having by far the largest absolute bias overall (-0.015 s^{-1}).

The above comparisons point to research priorities for improving current model representations of atmospheric VOCs. Along with highly abundant VOCs (such as acetone, methanol, and ethane), acetaldehyde, formaldehyde, isoprene (plus its oxidation products), and methyl hydroperoxide drive a large fraction of total VOC ~~-~~reactivity and associated model biases. Advancing our current ability to model the sources, chemistry, and physical removal of this relatively small number of species could substantially improve predictions of VOC-carbon and reactivity distributions.

6. Role of vertical transport in driving a persistent model VOC underestimate in the free troposphere over North America

In Sect. 5 we demonstrated that VOC abundance and reactivity are consistently underestimated by the model in the free troposphere across environments and compounds. Potential explanations for these missing FT VOCs include chemical effects (e.g., model biases in FT VOC production and loss rates) as well as dynamical effects (e.g., model biases in PBL-FT mixing). To help distinguish between these two, we plot in Fig. 9a the modeled versus observed mean PBL:FT ratio (mixing ratio units) for each VOC across the entire SEAC^{4}RS campaign. We see that all data fall above the 1:1 ratio line, showing that the model is overestimating the PBL:FT ratio to a similar degree across all VOCs regardless of source, lifetime, and chemical properties. This consistency across compounds points to a misdiagnosis of PBL ventilation as a likely explanation for the persistent VOC underestimate in the FT (at least over the SEAC^{4}RS domain), since other tenable mechanisms would not be expected to affect all VOCs in such a consistent way. In particular: i) a missing FT photochemical VOC source would not explain the PBL:FT discrepancy seen for primary VOCs; ii) a model bias in dry deposition or wet scavenging would differentially affect polar and soluble versus nonpolar and less soluble species; and iii) a model OH bias would impact reactive and longer-lived species to differing degrees. ~~-~~Findings similar to those shown in Fig. 9a are obtained for other campaigns over the southern and eastern US (SENEX, DISCOVER-AQ DC, DISCOVER-AQ TX) but not consistently elsewhere (DC3, DISCOVER-AQ CO, FRAPPÉ, DISCOVER-AQ CA, CalNex). Since the southeastern US is the major source of North American VOC-carbon and reactivity (Fig. 2), such a mixing bias would yield a significant model underestimate of the total amount of reactive organic carbon that is transported to the North American FT.

We can explore this issue further by considering a two-box model to conceptualize VOC partitioning between the PBL and FT. In that case, for an example VOC that is directly emitted and then subject to chemical loss by OH, PBL-FT mixing, and deposition (PBL only), the steady-state PBL:FT ratio would be linearly related to the OH rate coefficient k_{OH} with a slope determined by OH and by the PBL ventilation rate, and with an intercept determined by the PBL-FT mixing rates. Figure S10~~3~~ shows that the same holds for secondary VOCs. While dilution with PBL and FT background air will also affect the PBL:FT ratio, its effect in this simplified framework will diminish as the extent of the domain considered increases, and for shorter-lived species.

Of the aircraft campaigns considered, SEAC^{4}RS comes closest to the above approximation due to the larger spatial domain sampled by the DC8 aircraft. The modeled and observed PBL:FT ratios for this campaign are plotted in Fig. 9b as a function of k_{OH}. For both model and measurements, there is an approximately linear relationship, with the model generally capturing the observed PBL:FT vs. k_{OH} slope. However, with only a couple of exceptions (e.g., HCHO, C_2H_2), there is a clear offset between the two populations that manifests in a consistent way for both primary and secondary VOCs and across lifetimes. The offset persists even after correcting for a potential 40% PBL depth overestimate (Zhu et al., 2016) in the GEOS fields (Fig. S11~~4~~). The same conclusions are obtained if we instead examine the PBL:(PBL+FT) or (PBL+FT):PBL ratios to minimize any potential influence from spurious ratios caused

by near-detection-limit VOC measurements (not shown). Overall, the above comparisons implicates PBL:FT mixing as a likely player in the pervasive model VOC biases found in the FT.

These findings are consistent with those of Yu et al. (2018), who diagnosed inadequate vertical transport in the current off-line configuration of the GEOS-Chem CTM. Yu et al. (2018) identified as causes i) the off-line convective transport scheme (leading to a +10% bias in modeled ^{222}Rn at the surface, and a -5% bias in the upper troposphere), and ii) off-line archiving of the meteorological fields (+5% model surface bias and -20% upper troposphere bias). Fixing these issues would therefore reduce the errors found here for VOC in the free troposphere (~60% mean low bias) but worsen the aggregated model performance in the PBL (~30% mean low bias). In that case, we would likely see in the model a more consistent low VOC bias throughout the troposphere, which would then indicate errors in overall VOC emissions or other processes.

7. Role of biogenic versus anthropogenic sources in driving model biases for key oxygenated VOCs in the North American boundary layer

Section 5 demonstrated the critical role that certain light OVOCs (e.g., formaldehyde, acetaldehyde, methanol, acetone, methyl hydroperoxide) play in defining atmospheric VOC-carbon loading and associated reactivity, and in driving model biases in those quantities. We see in Fig. 7~~6~~ that while the GEOS-Chem model underestimates the abundance of most OVOCs in the PBL, some species are overestimated (analogous discrepancies are seen in the average vertical profiles; Fig. S12~~5~~-21~~4~~). We therefore investigate in this section the likely role of biogenic versus anthropogenic sources in driving the observed model biases for key OVOCs.

To this end, a unique pair of biogenic ($\mathcal{B}_{OVOC}$) and anthropogenic ($\mathcal{A}_{OVOC}$) source tracers was developed for each OVOC based on the mixing ratio difference along the flight track for that species between the model base-case and simulations with either i) all biogenic VOC emissions perturbed by 10%, or ii) all anthropogenic VOC emissions perturbed by 10% (see Sect. 4.3). $\mathcal{B}_{OVOC}$ thus represents the integrated influence of direct biogenic emissions plus oxidation of biogenic precursors for a given OVOC along the aircraft flight track, based on the model simulation. $\mathcal{A}_{OVOC}$ is likewise a marker for the combined influence of primary plus secondary anthropogenic sources. We find that the above tracers are best able to capture the observed in-PBL OVOC variance for the SEAC^{4}RS, SENEX, and DISCOVER-AQ TX campaigns (Table S6~~4~~), arguing that the allocation of model VOC sources has the highest spatial reliability over the southeastern US region. We therefore focus our source-tracer interpretation on these specific campaigns.

Figure 10 plots the model bias for select OVOCs as a function of $\mathcal{B}_{OVOC}$ and $\mathcal{A}_{OVOC}$, and shows that in several cases the model OVOC errors exhibit a clear relationship with one (or both) of these source tracers. For example, the positive model bias seen previously (Fig. 7~~6~~) for hydroxyacetone (HAC), methyl ethyl ketone (MEK), and glyoxal (CHOCHO) is strongly correlated with the biogenic source tracer $\mathcal{B}_{OVOC}$ for each species, with the largest model overestimates occurring when $\mathcal{B}_{OVOC}$ is high. This points to a current model overestimate of the biogenic sources of HAC, MEK, and CHOCHO, either due to biases in their precursor emissions (e.g., (Kaiser et al., 2018; Zhu et al., 2016; Wolfe et al., 2015)) or in their chemical formation mechanisms (e.g., (Miller et al., 2017; Li et al., 2016)). Model sink errors may also play a role (e.g., (Curry et al., 2018)); however, to explain the results in Fig. 10, such biases would need to be spatially correlated with emissions.

Conversely, in the case of formic acid (HCOOH) the model bias becomes more negative with increasing biogenic influence (consistent results are obtained with either the UW or NOAA measurements, Fig.

S2216), which is consistent with earlier findings (Alwe et al., 2019; Millet et al., 2015; Stavrakou et al., 2012) pointing to an underestimated biogenic source of HCOOH or its precursors over the southeastern US. The negative model bias seen for PAA (Fig. 7) increases with both $\mathcal{B}_{OVOC}$ and $\mathcal{A}_{OVOC}$ (Fig. 10), which may indicate a generic underestimate of PAA production across biogenic and anthropogenic VOCs or an overestimation of its chemical loss.

Findings for other OVOCs tend to be less clear and/or less consistent across these campaigns. Acetaldehyde (CH_3CHO) is biased low in the model, on average, across the aircraft campaigns (Fig. 7), and there is some indication that this is partly due to underrepresented anthropogenic sources (Fig. 10, S2215-S2417). Acetone and methanol are strongly underestimated by the model (Fig. 7), which drives a significant part of the overall model VOC-carbon bias over North America. However, Fig. 10 shows that while the model bias is negative under low values of $\mathcal{B}_{OVOC}$, it is positive under high values of $\mathcal{B}_{OVOC}$ (this is specifically the case for SEAC^{4}RS and DISCOVER-AQ TX; Fig. S2215-S2417): this may indicate a model overestimate of direct biogenic emissions combined with an underestimate of regional background concentrations or of other sources.

8. Summary

We performed an integrated analysis of the atmospheric VOC budget over North America based on an ensemble of recent airborne observations interpreted with an updated version of the GEOS-Chem CTM. 86 TgC of non-methane VOC is added annually to the North American atmosphere in the model through emissions (biogenic: 40 TgC; anthropogenic 13 TgC; fires: 3 TgC), and CH_4 oxidation (30 TgC/y). Of that, 62 TgC is oxidized to CO/CO_2, with the rest removed by deposition (dry: 7 TgC/y; wet: 10 TgC/y) and net transport out of the domain (10 TgC/y).

The simulated North American VOC budget shows the dominance of biogenic VOC emissions on a carbon basis (71%) and even more markedly on a reactivity basis (95%). Anthropogenic emissions provide the dominant summertime source of VOC-carbon and reactivity only in a fairly small number of pollution hotspots, and annually is >2× smaller as a source of non-methane VOC over North America than is methane oxidation. Nevertheless, anthropogenic VOCs provide more than half of the ambient VOC-carbon burden over the majority of the region due to their longer average lifetime relative to biogenic species.

While on-road VOC emissions in North America have undergone a substantial decrease in the past few decades (McDonald et al., 2013; Warneke et al., 2012), recent studies have pointed to the importance of i) emerging VOC sources from oil and gas facilities (Li et al., 2017; Pfister et al., 2017), ii) volatile chemical products (McDonald et al., 2018), and iii) unexpectedly large urban OVOC fluxes (Karl et al., 2018). It is possible that such sources are not well captured in current inventories such as those used here, which in turn could alter the budget understanding above. These areas require further research to better understand the importance of such emissions for atmospheric chemistry, and to test and improve their representation in models.

Based on the collective aircraft observations, we find that total ambient VOC-carbon over North America is dominated by small and relatively reduced VOCs (e.g., acetone, methanol, alkanes), along with some oxidized species (e.g., formic acid, methyl hydroperoxide, formaldehyde, other isoprene oxidation products) that are also substantial VOC-carbon reservoirs in the planetary boundary layer (PBL). In the free troposphere (FT), acetone, methanol, and ethane together average 6 ppbC over the ensemble of airborne data, compared to only 4 ppbC for the sum of all other measured VOCs. Formaldehyde and acetaldehyde provide the largest source of VOC reactivity, on average, in both the PBL and FT, with a

range of other reactive (but less abundant) and abundant (but less reactive) species also making significant contributions.

The GEOS-Chem CTM with state-of-science VOC treatment captures a significant portion of the observed ambient variability for VOC-carbon (R^2 = 0.36) and reactivity (0.54) in the PBL, but not in the FT (0.07 and 0.04) – suggesting that the main factors influencing VOC abundances in the FT are inadequately represented in current models. The GEOS-Chem model exhibits both underestimates and overestimates of the observed VOC-carbon and reactivity in the PBL, depending on location, with an overall normalized mean bias of -37% (carbon) and -34% (reactivity). This mean bias is equivalent to ~2× the reactivity of methane at 2 ppm or 0.5× that of CO at 200 ppb, and is therefore important from the point of view of accurately predicting OH chemistry and ozone production.

In the FT, the model exhibits a persistent low bias (~60%) for VOC-carbon and reactivity that manifests essentially everywhere. A comparison of modeled versus observed PBL:FT VOC concentration ratios over the southeastern US suggests that inadequate PBL ventilation in the model may play a role in driving the observed FT biases. Recent work has sought to improve CTM transport performance through improved spatial resolution (e.g., (Zhuang et al., 2018; Yu et al., 2016)), through use of a cubed-sphere rather than regular Cartesian grid (e.g., (Eastham et al., 2018; Yu et al., 2018)), and by integration into earth system models with online coupled meteorology (e.g., (Hu et al., 2018; Long et al., 2015)). Further work is needed to specifically assess model treatment of PBL-FT coupling (e.g., using PAN:NO_x or other diagnostic quantities) and PBL depths to improve tracer simulations in the FT.

We used a source tracer analysis to investigate the likely role of biogenic versus anthropogenic sources in driving model biases for key oxygenated VOCs. Results point to a current overestimate of the (primary + secondary) biogenic sources of hydroxyacetone, methyl ethyl ketone, and glyoxal and an underestimate of the biogenic sources of formic acid. Results also suggest a possible underestimate of the anthropogenic sources of acetaldehyde, along with an underestimate of peroxyacetic acid production across both biogenic and anthropogenic precursors. Finally, we find that a relatively modest number of individual VOCs (acetone, methanol, ethane, acetaldehyde, formaldehyde, isoprene + oxidation products, methyl hydroperoxide) drive a significant fraction of the total ambient VOC-carbon and reactivity (and associated model biases) across many environments. These species therefore merit further research to better understand their budgets and to improve model representation of VOC chemistry and the resulting effects on SOA, O_3, and other oxidants.

Data availability

Aircraft data used here are available at NASA LaRC (https://www-air.larc.nasa.gov/missions.htm) and NOAA ESRL ESD (https://esrl.noaa.gov/csd/field.html). GEOS-Chem model code is available at www.geos-chem.org.

Author contributions

X. Chen, D. B. Millet, H. B. Singh, and A. Wisthaler designed the study. X. Chen and D. B. Millet led the model development, simulations, all analyses, and manuscript preparation. The following authors provided measurements used in the analysis and contributed to manuscript preparation and data interpretation: A. Wisthaler, T. Mikoviny, and M. Müller (DC3, SEAC^{4}RS, and DISCOVER-AQ PTR-MS), E. C. Apel and H. S. Hornbrook (TOGA), E. L. Atlas (CalNex WAS), D. R. Blake (CalNex, SEAC^{4}RS, and FRAPPÉ WAS), S. S. Brown, K.-E. Min, and R. A. Washenfelder (SENEX glyoxal), J.

D. Crounse (CIT-CIMS), J. A. de Gouw and C. Warneke (CalNex and SENEX PTR-MS), F. Flocke, G. G. Pfister, and S. Shertz (FRAPPÉ PTR-MS and PAN-CIMS), A. Fried, D. Richter, J. Walega, and P. Weibring (DFGAS and CAMS formaldehyde), B. G. Heikes, D. W. O'Sullivan, and V. Treadaway (PCIMS), J. A. Neuman (SENEX NOAA CIMS HCOOH), T. B. Ryerson, I. Bourgeois, ~~and~~ J. Peischl, and C. R. Thompson (NOAA NO_yO_3), J. M. Roberts (CalNex and SENEX PAN), P. R. Veres (SENEX PAN), and B. Yuan (other PTR-MS data).

Acknowledgements

This research was supported by NASA Atmospheric Composition Campaign Data Analysis and Modelling (ACCDAM) program (Grant NNX14AP89G). Computing resources were provided by the Minnesota Supercomputing Institute (https://www.msi.umn.edu) at the University of Minnesota. We acknowledge the ECCAD database (http://eccad.sedoo.fr) for hosting emission inventories used in this work. We thank Kelley Wells, Katie Travis, Seb Eastham, Joel Thornton, Paul Wennberg, and Gao Chen for their assistance and useful discussions.

We thank the CalNex, DC3, SENEX, SEAC^{4}RS, DISCOVER-AQ, and FRAPPÉ teams for making this work possible. In particular, we acknowledge the contributions of Martin Graus (SENEX PTR-MS), Jessica Gilman (SENEX WAS), Lisa Kaser (FRAPPÉ PTR-MS), Joel Thornton, Ben Lee and Felipe Lopez-Hilfiker (UW CIMS), Thomas Hanisco and Glenn Wolfe (ISAF-LIF), Ronald Cohen (TD-LIF), Greg Huey (GIT CIMS), Andrew Weinheimer and Denise Montzka (NCAR NO_x/NO_y), and Tara Yacovitch and Scott Herndon (DISCOVER-AQ Colorado ethane).

A. Wisthaler~~,~~ acknowledges the Austrian Federal Ministry for Transport, Innovation and Technology (bmvit) through the Austrian Space Applications Programme (ASAP) of the Austrian Research Promotion Agency (FFG) for supporting the PTR-MS measurements during DC3, SEAC^{4}RS and DISCOVER-AQ. T.M. was supported by an appointment to the NASA Postdoctoral Program at the Langley Research Center administered by Oak Ridge Associated Universities through a contract with NASA.

F. Flocke~~,~~ and G. G. Pfister~~,~~ thank the State of Colorado/Colorado Department of Public Health and Environment and the National Science Foundation (NSF) for funding of FRAPPÉ. The National Center for Atmospheric Research is sponsored by NSF.

References

Akagi, S. K., Yokelson, R. J., Wiedinmyer, C., Alvarado, M. J., Reid, J. S., Karl, T., Crounse, J. D., and Wennberg, P. O.: Emission factors for open and domestic biomass burning for use in atmospheric models, Atmos. Chem. Phys., 11, 4039-4072, https://doi.org/10.5194/acp-11-4039-2011, 2011.

Alwe, H. D., Millet, D. B., Chen, X., Raff, J. D., Payne, Z. C., and Fledderman, K.: Oxidation of Volatile Organic Compounds as the Major Source of Formic Acid in a Mixed Forest Canopy, Geophys Res Lett, 46, 2940-2948, https://doi.org/10.1029/2018GL081526, 2019.

Amos, H. M., Jacob, D. J., Holmes, C. D., Fisher, J. A., Wang, Q., Yantosca, R. M., Corbitt, E. S., Galarneau, E., Rutter, A. P., Gustin, M. S., Steffen, A., Schauer, J. J., Graydon, J. A., St Louis, V. L., Talbot, R. W., Edgerton, E. S., Zhang, Y., and Sunderland, E. M.: Gas-particle partitioning of atmospheric Hg(II) and its effect on global mercury deposition, Atmos. Chem. Phys., 12, 591-603, https://doi.org/10.5194/acp-12-591-2012, 2012.

Andreae, M. O., and Merlet, P.: Emission of trace gases and aerosols from biomass burning, Global Biogeochem Cy, 15, 955-966, https://doi.org/10.1029/2000gb001382, 2001.

Apel, E. C., Emmons, L. K., Karl, T., Flocke, F., Hills, A. J., Madronich, S., Lee-Taylor, J., Fried, A., Weibring, P., Walega, J., Richter, D., Tie, X., Mauldin, L., Campos, T., Weinheimer, A., Knapp, D., Sive, B., Kleinman, L., Springston, S., Zaveri, R., Ortega, J., Voss, P., Blake, D., Baker, A., Warneke, C., Welsh-Bon, D., de Gouw, J., Zheng, J., Zhang, R., Rudolph, J., Junkermann, W., and Riemer, D. D.: Chemical evolution of volatile organic compounds in the outflow of the Mexico City Metropolitan area, Atmos. Chem. Phys., 10, 2353-2375, https://doi.org/10.5194/acp-10-2353-2010, 2010.

Apel, E. C., Hornbrook, R. S., Hills, A. J., Blake, N. J., Barth, M. C., Weinheimer, A., Cantrell, C., Rutledge, S. A., Basarab, B., Crawford, J., Diskin, G., Homeyer, C. R., Campos, T., Flocke, F., Fried, A., Blake, D. R., Brune, W., Pollack, I., Peischl, J., Ryerson, T., Wennberg, P. O., Crounse, J. D., Wisthaler, A., Mikoviny, T., Huey, G., Heikes, B., O'Sullivan, D., and Riemer, D. D.: Upper tropospheric ozone production from lightning NOx-impacted convection: Smoke ingestion case study from the DC3 campaign, J. Geophys. Res. Atmos., 120, 2505-2523, https://doi.org/10.1002/2014JD022121, 2015.

Barth, M. C., Cantrell, C. A., Brune, W. H., Rutledge, S. A., Crawford, J. H., Huntrieser, H., Carey, L. D., MacGorman, D., Weisman, M., Pickering, K. E., Bruning, E., Anderson, B., Apel, E., Biggerstaff, M., Campos, T., Campuzano-Jost, P., Cohen, R., Crounse, J., Day, D. A., Diskin, G., Flocke, F., Fried, A., Garland, C., Heikes, B., Honomichl, S., Hornbrook, R., Huey, L. G., Jimenez, J. L., Lang, T., Lichtenstern, M., Mikoviny, T., Nault, B., O'Sullivan, D., Pan, L. L., Peischl, J., Pollack, I., Richter, D., Riemer, D., Ryerson, T., Schlager, H., St Clair, J., Walega, J., Weibring, P., Weinheimer, A., Wennberg, P., Wisthaler, A., Wooldridge, P. J., and Ziegler, C.: The Deep Convective Clouds and Chemistry (DC3) Field Campaign, B Am Meteorol Soc, 96, 1281-1309, https://doi.org/10.1175/Bams-D-13-00290.1, 2015.

Beale, R., Liss, P. S., Dixon, J. L., and Nightingale, P. D.: Quantification of oxygenated volatile organic compounds in seawater by membrane inlet-proton transfer reaction/mass spectrometry, Anal. Chim. Acta, 706, 128-134, https://doi.org/10.1016/j.aca.2011.08.023, 2011.

Beale, R., Dixon, J. L., Arnold, S. R., Liss, P. S., and Nightingale, P. D.: Methanol, acetaldehyde, and acetone in the surface waters of the Atlantic Ocean, J. Geophys. Res. Oceans, 118, 5412-5425, https://doi.org/10.1002/jgrc.20322, 2013.

Beale, R., Dixon, J. L., Smyth, T. J., and Nightingale, P. D.: Annual study of oxygenated volatile organic compounds in UK shelf waters, Mar. Chem., 171, 96-106, https://doi.org/10.1016/j.marchem.2015.02.013, 2015.

Bertram, T. H., Perring, A. E., Wooldridge, P. J., Crounse, J. D., Kwan, A. J., Wennberg, P. O., Scheuer, E., Dibb, J., Avery, M., Sachse, G., Vay, S. A., Crawford, J. H., McNaughton, C. S., Clarke, A., Pickering, K. E., Fuelberg, H., Huey, G., Blake, D. R., Singh, H. B., Hall, S. R., Shetter, R. E., Fried, A., Heikes, B. G., and Cohen, R. C.: Direct measurements of the convective recycling of the upper troposphere, Science, 315, 816-820, https://doi.org/10.1126/science.1134548, 2007.

Bianchi, F., Trostl, J., Junninen, H., Frege, C., Henne, S., Hoyle, C. R., Molteni, U., Herrmann, E., Adamov, A., Bukowiecki, N., Chen, X., Duplissy, J., Gysel, M., Hutterli, M., Kangasluoma, J., Kontkanen, J., Kurten, A., Manninen, H. E., Munch, S., Perakyla, O., Petaja, T., Rondo, L., Williamson, C., Weingartner, E., Curtius, J., Worsnop, D. R., Kulmala, M., Dommen, J., and Baltensperger, U.: New particle formation in the free troposphere: A question of chemistry and timing, Science, 352, 1109-1112, https://doi.org/10.1126/science.aad5456, 2016.

Blake, N. J., Blake, D. R., Swanson, A. L., Atlas, E., Flocke, F., and Rowland, F. S.: Latitudinal, vertical, and seasonal variations of C1-C4 alkyl nitrates in the troposphere over the Pacific Ocean during PEM-Tropics A and B: Oceanic and continental sources, J. Geophys. Res. Atmos., 108, https://doi.org/10.1029/2001jd001444, 2003.

Bonsang, B., Kanakidou, M., Lambert, G., and Monfray, P.: The marine source of C2-C6 aliphatic-hydrocarbons, J. Atmos. Chem., 6, 3-20, https://doi.org/10.1007/Bf00048328, 1988.

Boucher, O., Randall, D., Artaxo, P., Bretherton, C., Feingold, G., Forster, C., Kerminen, V. M., Kondo, Y., Liao, H., Lohmann, U., Rasch, P., Satheesh, S. K., Sherwood, S., and Stevens, B.: Clouds and aerosols, in: Climate Change 2013: The Physical Science Basis. Contribution of Working Group I to the Fifth Assessment Report of the Intergovernmental Panel on Climate Change, edited by: Stocker, T. F., Qin, D., Plattner, G.-K., Tignor, M., Allen, S. K., Boschung, J., Nauels, A., Xia, Y., Bex, V., and Midgley, P. M., Cambridge University Press, Cambridge, United Kingdom and New York, NY, USA, 571–658, 2013.

Broadgate, W. J., Liss, P. S., and Penkett, S. A.: Seasonal emissions of isoprene and other reactive hydrocarbon gases from the ocean, Geophys Res Lett, 24, 2675-2678, https://doi.org/10.1029/97gl02736, 1997.

Brune, W. H., Ren, X. R., Zhang, L., Mao, J. Q., Miller, D. O., Anderson, B. E., Blake, D. R., Cohen, R. C., Diskin, G. S., Hall, S. R., Hanisco, T. F., Huey, L. G., Nault, B. A., Peisch, J., Pollack, I., Ryerson, T. B., Shingler, T., Sorooshian, A., Ullmann, K., Wisthaler, A., and Wooldridge, P. J.: Atmospheric oxidation in the presence of clouds during the Deep Convective Clouds and Chemistry (DC3) study, Atmos. Chem. Phys., 18, 14493-14510, https://doi.org/10.5194/acp-18-14493-2018, 2018.

Cappa, C.: Atmospheric science: Unexpected player in particle formation, Nature, 533, 478-479, https://doi.org/10.1038/533478a, 2016.

Caravan, R. L., Khan, M. A. H., Zador, J., Sheps, L., Antonov, I. O., Rotavera, B., Ramasesha, K., Au, K., Chen, M. W., Rosch, D., Osborn, D. L., Fittschen, C., Schoemaecker, C., Duncianu, M., Grira, A., Dusanter, S., Tomas, A., Percival, C. J., Shallcross, D. E., and Taatjes, C. A.: The reaction of hydroxyl and methylperoxy radicals is not a major source of atmospheric methanol, Nat. Commun., 9, 4343, https://doi.org/10.1038/s41467-018-06716-x, 2018.

Carpenter, L. J., Archer, S. D., and Beale, R.: Ocean-atmosphere trace gas exchange, Chem. Soc. Rev., 41, 6473-6506, https://doi.org/10.1039/c2cs35121h, 2012.

Cazorla, M., Wolfe, G. M., Bailey, S. A., Swanson, A. K., Arkinson, H. L., and Hanisco, T. F.: A new airborne laser-induced fluorescence instrument for in situ detection of formaldehyde throughout the troposphere and lower stratosphere, Atmos. Meas. Tech., 8, 541-552, https://doi.org/10.5194/amt-8-541-2015, 2015.

Coburn, S., Ortega, I., Thalman, R., Blomquist, B., Fairall, C. W., and Volkamer, R.: Measurements of diurnal variations and eddy covariance (EC) fluxes of glyoxal in the tropical marine boundary layer: description of the Fast LED-CE-DOAS instrument, Atmos. Meas. Tech., 7, 3579-3595, https://doi.org/10.5194/amt-7-3579-2014, 2014.

Colman, J. J., Swanson, A. L., Meinardi, S., Sive, B. C., Blake, D. R., and Rowland, F. S.: Description of the analysis of a wide range of volatile organic compounds in whole air samples collected during PEM-tropics A and B, Anal. Chem., 73, 3723-3731, https://doi.org/10.1021/ac010027g, 2001.

Crawford, J. H., and Pickering, K. E.: Advancing Strategies for Air Quality Observations in the Next Decade, Environ. Manage, 4-7, 2014.

Crounse, J. D., McKinney, K. A., Kwan, A. J., and Wennberg, P. O.: Measurement of gas-phase hydroperoxides by chemical ionization mass spectrometry, Anal. Chem., 78, 6726-6732, https://doi.org/10.1021/ac0604235, 2006.

Crounse, J. D., Nielsen, L. B., Jørgensen, S., Kjaergaard, H. G., and Wennberg, P. O.: Autoxidation of Organic Compounds in the Atmosphere, J. Phys. Chem. Lett., 4, 3513-3520, https://doi.org/10.1021/jz4019207, 2013.

Cubasch, U., Wuebbles, D., Chen, D., Facchini, M. C., Frame, C. L., Mahowald, N., and Winther, J.-G.: Introduction, in: Climate Change 2013: The Physical Science Basis. Contribution of Working Group I to the Fifth Assessment Report of the Intergovernmental Panel on Climate Change, edited by: Stocker, T. F., Qin, D., Plattner, G.-K., Tignor, M., Allen, S. K., Boschung, J., Nauels, A., Xia, Y., Bex, V., and Midgley, P. M., Cambridge University Press, Cambridge, United Kingdom and New York, NY, USA, 119–158, 2013.

824 Curry, L. A., Tsui, W. G., and McNeill, V. F.: Technical note: Updated parameterization of the reactive uptake of glyoxal and
825 methylglyoxal by atmospheric aerosols and cloud droplets, Atmos. Chem. Phys., 18, 9823-9830, https://doi.org/10.5194/acp-18-
826 9823-2018, 2018.

827 DC3 Science Team: DC3 Field Campaign Data from DC-8 aircraft. NASA Langley Atmospheric Science Data Center DAAC,
828 https://doi.org/10.5067/aircraft/dc3/dc8/aerosol-tracegas, 2013.

829 de Gouw, J., and Warneke, C.: Measurements of volatile organic compounds in the earth's atmosphere using proton-transfer-
830 reaction mass spectrometry, Mass Spectrom. Rev., 26, 223-257, https://doi.org/10.1002/mas.20119, 2007.

831 de Gouw, J. A., Middlebrook, A. M., Warneke, C., Goldan, P. D., Kuster, W. C., Roberts, J. M., Fehsenfeld, F. C., Worsnop, D.
832 R., Canagaratna, M. R., Pszenny, A. A. P., Keene, W. C., Marchewka, M., Bertman, S. B., and Bates, T. S.: Budget of organic
833 carbon in a polluted atmosphere: Results from the New England Air Quality Study in 2002, J. Geophys. Res. Atmos., 110,
834 https://doi.org/10.1029/2004jd005623, 2005.

835 de Gouw, J. A., Gilman, J. B., Borbon, A., Warneke, C., Kuster, W. C., Goldan, P. D., Holloway, J. S., Peischl, J., Ryerson, T.
836 B., Parrish, D. D., Gentner, D. R., Goldstein, A. H., and Harley, R. A.: Increasing atmospheric burden of ethanol in the United
837 States, Geophys Res Lett, 39, https://doi.org/10.1029/2012gl052109, 2012.

838 Deventer, M. J., Jiao, Y., Knox, H., Anderson, F., Ferner, M. C., Lewis, J. A., and Rhew, R. C.: Ecosystem-scale measurements
839 of methyl halide fluxes from a brackish tidal marsh invaded with perennial pepperweed (lepidium latifolium), J. Geophys. Res.
840 Biogeosci., 123, 2104-2120, https://doi.org/10.1029/2018JG004536, 2018.

841 DiGangi, J. P., Boyle, E. S., Karl, T., Harley, P., Turnipseed, A., Kim, S., Cantrell, C., Maudlin, R. L., Zheng, W., Flocke, F.,
842 Hall, S. R., Ullmann, K., Nakashima, Y., Paul, J. B., Wolfe, G. M., Desai, A. R., Kajii, Y., Guenther, A., and Keutsch, F. N.:
843 First direct measurements of formaldehyde flux via eddy covariance: implications for missing in-canopy formaldehyde sources,
844 Atmos. Chem. Phys., 11, 10565-10578, https://doi.org/10.5194/acp-11-10565-2011, 2011.

845 DISCOVER-AQ Science Team: DISCOVER-AQ P-3B Aircraft In-situ Trace Gas Measurements. NASA Langley Atmospheric
846 Science Data Center DAAC, https://doi.org/10.5067/aircraft/discover-aq/aerosol-tracegas, 2014.

847 Eastham, S. D., Long, M. S., Keller, C. A., Lundgren, E., Yantosca, R. M., Zhuang, J. W., Li, C., Lee, C. J., Yannetti, M., Auer,
848 B. M., Clune, T. L., Kouatchou, J., Putman, W. M., Thompson, M. A., Trayanov, A. L., Molod, A. M., Martin, R. V., and Jacob,
849 D. J.: GEOS-Chem High Performance (GCHP v11-02c): a next-generation implementation of the GEOS-Chem chemical
850 transport model for massively parallel applications, Geosci Model Dev, 11, 2941-2953, https://doi.org/10.5194/gmd-11-2941-
851 2018, 2018.

852 Ehn, M., Thornton, J. A., Kleist, E., Sipila, M., Junninen, H., Pullinen, I., Springer, M., Rubach, F., Tillmann, R., Lee, B., Lopez-
853 Hilfiker, F., Andres, S., Acir, I. H., Rissanen, M., Jokinen, T., Schobesberger, S., Kangasluoma, J., Kontkanen, J., Nieminen, T.,
854 Kurten, T., Nielsen, L. B., Jorgensen, S., Kjaergaard, H. G., Canagaratna, M., Maso, M. D., Berndt, T., Petaja, T., Wahner, A.,
855 Kerminen, V. M., Kulmala, M., Worsnop, D. R., Wildt, J., and Mentel, T. F.: A large source of low-volatility secondary organic
856 aerosol, Nature, 506, 476-479, https://doi.org/10.1038/nature13032, 2014.

857 EPA: 2011 National Emissions Inventory Data & Documentation, available at: https://www.epa.gov/air-emissions-
858 inventories/2011-national-emission-inventory-nei-report, last access: 8 Feb 2018, 2015.

859 EPA: Technical Support Document EPA's 2014 National Air Toxics Assessment, available at:
860 https://www.epa.gov/sites/production/files/2018-09/documents/2014_nata_technical_support_document.pdf last access: 25 Sep
861 2018, 2018.

862 European Commission (EC): Joint Research Centre (JRC)/Netherlands Environmental Assessment Agency (PBL), Emission
863 Database for Global Atmospheric Research (EDGAR), release version 4.2. http://edgar.jrc.ec.europa.eu, 2011.

864 Feiner, P. A., Brune, W. H., Miller, D. O., Zhang, L., Cohen, R. C., Romer, P. S., Goldstein, A. H., Keutsch, F. N., Skog, K. M.,
865 Wennberg, P. O., Nguyen, T. B., Teng, A. P., DeGouw, J., Koss, A., Wild, R. J., Brown, S. S., Guenther, A., Edgerton, E.,
866 Baumann, K., and Fry, J. L.: Testing atmospheric oxidation in an alabama forest, J Atmos Sci, 73, 4699-4710,
867 https://doi.org/10.1175/Jas-D-16-0044.1, 2016.

868 Fischer, E. V., Jacob, D. J., Millet, D. B., Yantosca, R. M., and Mao, J.: The role of the ocean in the global atmospheric budget of
869 acetone, Geophys Res Lett, 39, n/a-n/a, https://doi.org/10.1029/2011gl050086, 2012.

Fischer, E. V., Jacob, D. J., Yantosca, R. M., Sulprizio, M. P., Millet, D. B., Mao, J., Paulot, F., Singh, H. B., Roiger, A., Ries, L., Talbot, R. W., Dzepina, K., and Deolal, S. P.: Atmospheric peroxyacetyl nitrate (PAN): a global budget and source attribution, Atmos. Chem. Phys., 14, 2679-2698, https://doi.org/10.5194/acp-14-2679-2014, 2014.

Fisher, J. A., Jacob, D. J., Travis, K. R., Kim, P. S., Marais, E. A., Miller, C. C., Yu, K., Zhu, L., Yantosca, R. M., Sulprizio, M. P., Mao, J., Wennberg, P. O., Crounse, J. D., Teng, A. P., Nguyen, T. B., St Clair, J. M., Cohen, R. C., Romer, P., Nault, B. A., Wooldridge, P. J., Jimenez, J. L., Campuzano-Jost, P., Day, D. A., Hu, W., Shepson, P. B., Xiong, F., Blake, D. R., Goldstein, A. H., Misztal, P. K., Hanisco, T. F., Wolfe, G. M., Ryerson, T. B., Wisthaler, A., and Mikoviny, T.: Organic nitrate chemistry and its implications for nitrogen budgets in an isoprene- and monoterpene-rich atmosphere: constraints from aircraft (SEAC(4)RS) and ground-based (SOAS) observations in the Southeast US, Atmos. Chem. Phys., 16, 5969-5991, https://doi.org/10.5194/acp-16-5969-2016, 2016.

Fried, A., Cantrell, C., Olson, J., Crawford, J. H., Weibring, P., Walega, J., Richter, D., Junkermann, W., Volkamer, R., Sinreich, R., Heikes, B. G., O'Sullivan, D., Blake, D. R., Blake, N., Meinardi, S., Apel, E., Weinheimer, A., Knapp, D., Perring, A., Cohen, R. C., Fuelberg, H., Shetter, R. E., Hall, S. R., Ullmann, K., Brune, W. H., Mao, J., Ren, X., Huey, L. G., Singh, H. B., Hair, J. W., Riemer, D., Diskin, G., and Sachse, G.: Detailed comparisons of airborne formaldehyde measurements with box models during the 2006 INTEX-B and MILAGRO campaigns: potential evidence for significant impacts of unmeasured and multi-generation volatile organic carbon compounds, Atmos. Chem. Phys., 11, 11867-11894, https://doi.org/10.5194/acp-11-11867-2011, 2011.

Giglio, L., Randerson, J. T., and van der Werf, G. R.: Analysis of daily, monthly, and annual burned area using the fourth-generation global fire emissions database (GFED4), J. Geophys. Res. Biogeosci., 118, 317-328, https://doi.org/10.1002/jgrg.20042, 2013.

Gilman, J. B., Kuster, W. C., Goldan, P. D., Herndon, S. C., Zahniser, M. S., Tucker, S. C., Brewer, W. A., Lerner, B. M., Williams, E. J., Harley, R. A., Fehsenfeld, F. C., Warneke, C., and de Gouw, J. A.: Measurements of volatile organic compounds during the 2006 TexAQS/GoMACCS campaign: Industrial influences, regional characteristics, and diurnal dependencies of the OH reactivity, J. Geophys. Res. Atmos., 114, https://doi.org/10.1029/2008jd011525, 2009.

Glasius, M., and Goldstein, A. H.: Recent discoveries and future challenges in atmospheric organic chemistry, Environ. Sci. Technol., 50, 2754-2764, https://doi.org/10.1021/acs.est.5b05105, 2016.

Goldstein, A. H., and Galbally, I. E.: Known and unexplored organic constituents in the earth's atmosphere, Environ. Sci. Technol., 41, 1514-1521, https://doi.org/10.1021/Es072476p, 2007.

Guenther, A. B., Jiang, X., Heald, C. L., Sakulyanontvittaya, T., Duhl, T., Emmons, L. K., and Wang, X.: The Model of Emissions of Gases and Aerosols from Nature version 2.1 (MEGAN2.1): an extended and updated framework for modeling biogenic emissions, Geosci Model Dev, 5, 1471-1492, https://doi.org/10.5194/gmd-5-1471-2012, 2012.

Hatch, L. E., Yokelson, R. J., Stockwell, C. E., Veres, P. R., Simpson, I. J., Blake, D. R., Orlando, J. J., and Barsanti, K. C.: Multi-instrument comparison and compilation of non-methane organic gas emissions from biomass burning and implications for smoke-derived secondary organic aerosol precursors, Atmos. Chem. Phys., 17, 1471-1489, https://doi.org/10.5194/acp-17-1471-2017, 2017.

Heald, C. L., Jacob, D. J., Park, R. J., Russell, L. M., Huebert, B. J., Seinfeld, J. H., Liao, H., and Weber, R. J.: A large organic aerosol source in the free troposphere missing from current models, Geophys Res Lett, 32, n/a-n/a, https://doi.org/10.1029/2005gl023831, 2005.

Heald, C. L., Goldstein, A. H., Allan, J. D., Aiken, A. C., Apel, E., Atlas, E. L., Baker, A. K., Bates, T. S., Beyersdorf, A. J., Blake, D. R., Campos, T., Coe, H., Crounse, J. D., DeCarlo, P. F., de Gouw, J. A., Dunlea, E. J., Flocke, F. M., Fried, A., Goldan, P., Griffin, R. J., Herndon, S. C., Holloway, J. S., Holzinger, R., Jimenez, J. L., Junkermann, W., Kuster, W. C., Lewis, A. C., Meinardi, S., Millet, D. B., Onasch, T., Polidori, A., Quinn, P. K., Riemer, D. D., Roberts, J. M., Salcedo, D., Sive, B., Swanson, A. L., Talbot, R., Warneke, C., Weber, R. J., Weibring, P., Wennberg, P. O., Worsnop, D. R., Wittig, A. E., Zhang, R., Zheng, J., and Zheng, W.: Total observed organic carbon (TOOC) in the atmosphere: a synthesis of North American observations, Atmos. Chem. Phys., 8, 2007-2025, https://doi.org/10.5194/acp-8-2007-2008, 2008.

Hottle, J. R., Huisman, A. J., DiGangi, J. P., Kammrath, A., Galloway, M. M., Coens, K. L., and Keutsch, F. N.: A laser induced fluorescence-based instrument for in-situ measurements of atmospheric formaldehyde, Environ. Sci. Technol., 43, 790-795, https://doi.org/10.1021/es801621f, 2009.

Hu, L., Millet, D. B., Baasandorj, M., Griffis, T. J., Turner, P., Helmig, D., Curtis, A. J., and Hueber, J.: Isoprene emissions and impacts over an ecological transition region in the US Upper Midwest inferred from tall tower measurements, J. Geophys. Res. Atmos., 120, 3553-3571, https://doi.org/10.1002/2014JD022732, 2015.

Hu, L., Keller, C. A., Long, M. S., Sherwen, T., Auer, B., Da Silva, A., Nielsen, J. E., Pawson, S., Thompson, M. A., Trayanov, A. L., Travis, K. R., Grange, S. K., Evans, M. J., and Jacob, D. J.: Global simulation of tropospheric chemistry at 12.5 km resolution: performance and evaluation of the GEOS-Chem chemical module (v10-1) within the NASA GEOS Earth system model (GEOS-5 ESM), Geosci Model Dev, 11, 4603-4620, https://doi.org/10.5194/gmd-11-4603-2018, 2018.

Hudman, R. C., Moore, N. E., Mebust, A. K., Martin, R. V., Russell, A. R., Valin, L. C., and Cohen, R. C.: Steps towards a mechanistic model of global soil nitric oxide emissions: implementation and space based-constraints, Atmos. Chem. Phys., 12, 7779-7795, https://doi.org/10.5194/acp-12-7779-2012, 2012.

Hudson, E. D., Okuda, K., and Ariya, P. A.: Determination of acetone in seawater using derivatization solid-phase microextraction, Anal. Bioanal. Chem., 388, 1275-1282, https://doi.org/10.1007/s00216-007-1324-x, 2007.

Huey, L. G.: Measurement of trace atmospheric species by chemical ionization mass spectrometry: speciation of reactive nitrogen and future directions, Mass Spectrom. Rev., 26, 166-184, https://doi.org/10.1002/mas.20118, 2007.

Hunter, J. F., Day, D. A., Palm, B. B., Yatavelli, R. L. N., Chan, A. H., Kaser, L., Cappellin, L., Hayes, P. L., Cross, E. S., Carrasquillo, A. J., Campuzano-Jost, P., Stark, H., Zhao, Y. L., Hohaus, T., Smith, J. N., Hansel, A., Karl, T., Goldstein, A. H., Guenther, A., Worsnop, D. R., Thornton, J. A., Heald, C. L., Jimenez, J. L., and Kroll, J. H.: Comprehensive characterization of atmospheric organic carbon at a forested site, Nat Geosci, 10, 748-+, https://doi.org/10.1038/NGEO3018, 2017.

Iavorivska, L., Boyer, E. W., and Grimm, J. W.: Wet atmospheric deposition of organic carbon: An underreported source of carbon to watersheds in the northeastern United States, J. Geophys. Res. Atmos., 122, 3104-3115, https://doi.org/10.1002/2016JD026027, 2017.

Isaacman-VanWertz, G., Massoli, P., O'Brien, R., Lim, C., Franklin, J. P., Moss, J. A., Hunter, J. F., Nowak, J. B., Canagaratna, M. R., Misztal, P. K., Arata, C., Roscioli, J. R., Herndon, S. T., Onasch, T. B., Lambe, A. T., Jayne, J. T., Su, L., Knopf, D. A., Goldstein, A. H., Worsnop, D. R., and Kroll, J. H.: Chemical evolution of atmospheric organic carbon over multiple generations of oxidation, Nat. Chem., 10, 462-468, https://doi.org/10.1038/s41557-018-0002-2, 2018.

Jacob, D. J.: Heterogeneous chemistry and tropospheric ozone, Atmos. Environ., 34, 2131-2159, https://doi.org/10.1016/S1352-2310(99)00462-8, 2000.

Johnson, M. T.: A numerical scheme to calculate temperature and salinity dependent air-water transfer velocities for any gas, Ocean Sci., 6, 913-932, https://doi.org/10.5194/os-6-913-2010, 2010.

Kaiser, J., Skog, K. M., Baumann, K., Bertman, S. B., Brown, S. B., Brune, W. H., Crounse, J. D., de Gouw, J. A., Edgerton, E. S., Feiner, P. A., Goldstein, A. H., Koss, A., Misztal, P. K., Nguyen, T. B., Olson, K. F., St Clair, J. M., Teng, A. P., Toma, S., Wennberg, P. O., Wild, R. J., Zhang, L., and Keutsch, F. N.: Speciation of OH reactivity above the canopy of an isoprene-dominated forest, Atmos. Chem. Phys., 16, 9349-9359, https://doi.org/10.5194/acp-16-9349-2016, 2016.

Kaiser, J., Jacob, D. J., Zhu, L., Travis, K. R., Fisher, J. A., Abad, G. G., Zhang, L., Zhang, X. S., Fried, A., Crounse, J. D., St Clair, J. M., and Wisthaler, A.: High-resolution inversion of OMI formaldehyde columns to quantify isoprene emission on ecosystem-relevant scales: application to the southeast US, Atmos. Chem. Phys., 18, 5483-5497, https://doi.org/10.5194/acp-18-5483-2018, 2018.

Kameyama, S., Tanimoto, H., Inomata, S., Tsunogai, U., Ooki, A., Yokouchi, Y., Takeda, S., Obata, H., and Uematsu, M.: Equilibrator inlet-proton transfer reaction-mass spectrometry (EI-PTR-MS) for sensitive, high-resolution measurement of dimethyl sulfide dissolved in seawater, Anal. Chem., 81, 9021-9026, https://doi.org/10.1021/ac901630h, 2009.

Kanakidou, M., Bonsang, B., Leroulley, J. C., Lambert, G., Martin, D., and Sennequier, G.: Marine source of atmospheric acetylene, Nature, 333, 51-52, https://doi.org/10.1038/333051a0, 1988.

Kanakidou, M., Duce, R. A., Prospero, J. M., Baker, A. R., Benitez-Nelson, C., Dentener, F. J., Hunter, K. A., Liss, P. S., Mahowald, N., Okin, G. S., Sarin, M., Tsigaridis, K., Uematsu, M., Zamora, L. M., and Zhu, T.: Atmospheric fluxes of organic N and P to the global ocean, Global Biogeochem Cy, 26, https://doi.org/10.1029/2011gb004277, 2012.

963 Karl, T., Harley, P., Emmons, L., Thornton, B., Guenther, A., Basu, C., Turnipseed, A., and Jardine, K.: Efficient atmospheric
964 cleansing of oxidized organic trace gases by vegetation, Science, 330, 816-819, https://doi.org/10.1126/science.1192534, 2010.

965 Karl, T., Striednig, M., Graus, M., Hammerle, A., and Wohlfahrt, G.: Urban flux measurements reveal a large pool of oxygenated
966 volatile organic compound emissions, Proc. Natl. Acad. Sci. U.S.A., 115, 1186-1191, https://doi.org/10.1073/pnas.1714715115,
967 2018.

968 Kaser, L., Karl, T., Schnitzhofer, R., Graus, M., Herdlinger-Blatt, I. S., DiGangi, J. P., Sive, B., Turnipseed, A., Hornbrook, R.
969 S., Zheng, W., Flocke, F. M., Guenther, A., Keutsch, F. N., Apel, E., and Hansel, A.: Comparison of different real time VOC
970 measurement techniques in a ponderosa pine forest, Atmos. Chem. Phys., 13, 2893-2906, https://doi.org/10.5194/acp-13-2893-
971 2013, 2013.

972 Kim, M. J., Novak, G. A., Zoerb, M. C., Yang, M. X., Blomquist, B. W., Huebert, B. J., Cappa, C. D., and Bertram, T. H.: Air-
973 Sea exchange of biogenic volatile organic compounds and the impact on aerosol particle size distributions, Geophys Res Lett, 44,
974 3887-3896, https://doi.org/10.1002/2017GL072975, 2017.

975 Kim, P. S., Jacob, D. J., Fisher, J. A., Travis, K., Yu, K., Zhu, L., Yantosca, R. M., Sulprizio, M. P., Jimenez, J. L., Campuzano-
976 Jost, P., Froyd, K. D., Liao, J., Hair, J. W., Fenn, M. A., Butler, C. F., Wagner, N. L., Gordon, T. D., Welti, A., Wennberg, P. O.,
977 Crounse, J. D., St Clair, J. M., Teng, A. P., Millet, D. B., Schwarz, J. P., Markovic, M. Z., and Perring, A. E.: Sources,
978 seasonality, and trends of southeast US aerosol: an integrated analysis of surface, aircraft, and satellite observations with the
979 GEOS-Chem chemical transport model, Atmos. Chem. Phys., 15, 10411-10433, https://doi.org/10.5194/acp-15-10411-2015,
980 2015.

981 Kim, S., Huey, L. G., Stickel, R. E., Tanner, D. J., Crawford, J. H., Olson, J. R., Chen, G., Brune, W. H., Ren, X., Lesher, R.,
982 Wooldridge, P. J., Bertram, T. H., Perring, A., Cohen, R. C., Lefer, B. L., Shetter, R. E., Avery, M., Diskin, G., and Sokolik, I.:
983 Measurement of HO2NO2 in the free troposphere during the intercontinental chemical transport experiment - North America
984 2004, J. Geophys. Res. Atmos., 112, https://doi.org/10.1029/2006jd007676, 2007.

985 Kirkby, J., Duplissy, J., Sengupta, K., Frege, C., Gordon, H., Williamson, C., Heinritzi, M., Simon, M., Yan, C., Almeida, J.,
986 Trostl, J., Nieminen, T., Ortega, I. K., Wagner, R., Adamov, A., Amorim, A., Bernhammer, A. K., Bianchi, F., Breitenlechner,
987 M., Brilke, S., Chen, X., Craven, J., Dias, A., Ehrhart, S., Flagan, R. C., Franchin, A., Fuchs, C., Guida, R., Hakala, J., Hoyle, C.
988 R., Jokinen, T., Junninen, H., Kangasluoma, J., Kim, J., Krapf, M., Kurten, A., Laaksonen, A., Lehtipalo, K., Makhmutov, V.,
989 Mathot, S., Molteni, U., Onnela, A., Perakyla, O., Piel, F., Petaja, T., Praplan, A. P., Pringle, K., Rap, A., Richards, N. A.,
990 Riipinen, I., Rissanen, M. P., Rondo, L., Sarnela, N., Schobesberger, S., Scott, C. E., Seinfeld, J. H., Sipila, M., Steiner, G.,
991 Stozhkov, Y., Stratmann, F., Tome, A., Virtanen, A., Vogel, A. L., Wagner, A. C., Wagner, P. E., Weingartner, E., Wimmer, D.,
992 Winkler, P. M., Ye, P., Zhang, X., Hansel, A., Dommen, J., Donahue, N. M., Worsnop, D. R., Baltensperger, U., Kulmala, M.,
993 Carslaw, K. S., and Curtius, J.: Ion-induced nucleation of pure biogenic particles, Nature, 533, 521-526,
994 https://doi.org/10.1038/nature17953, 2016.

995 Kroll, J. H., Donahue, N. M., Jimenez, J. L., Kessler, S. H., Canagaratna, M. R., Wilson, K. R., Altieri, K. E., Mazzoleni, L. R.,
996 Wozniak, A. S., Bluhm, H., Mysak, E. R., Smith, J. D., Kolb, C. E., and Worsnop, D. R.: Carbon oxidation state as a metric for
997 describing the chemistry of atmospheric organic aerosol, Nat. Chem., 3, 133-139, https://doi.org/10.1038/nchem.948, 2011.

998 Lamarque, J. F., Bond, T. C., Eyring, V., Granier, C., Heil, A., Klimont, Z., Lee, D., Liousse, C., Mieville, A., Owen, B., Schultz,
999 M. G., Shindell, D., Smith, S. J., Stehfest, E., Van Aardenne, J., Cooper, O. R., Kainuma, M., Mahowald, N., McConnell, J. R.,
1000 Naik, V., Riahi, K., and van Vuuren, D. P.: Historical (1850-2000) gridded anthropogenic and biomass burning emissions of
1001 reactive gases and aerosols: methodology and application, Atmos. Chem. Phys., 10, 7017-7039, https://doi.org/10.5194/acp-10-
1002 7017-2010, 2010.

1003 Lee, B. H., Lopez-Hilfiker, F. D., Mohr, C., Kurten, T., Worsnop, D. R., and Thornton, J. A.: An iodide-adduct high-resolution
1004 time-of-flight chemical-ionization mass spectrometer: application to atmospheric inorganic and organic compounds, Environ.
1005 Sci. Technol., 48, 6309-6317, https://doi.org/10.1021/es500362a, 2014.

1006 Lerner, B. M., Gilman, J. B., Aikin, K. C., Atlas, E. L., Goldan, P. D., Graus, M., Hendershot, R., Isaacman-VanWertz, G. A.,
1007 Koss, A., Kuster, W. C., Lueb, R. A., McLaughlin, R. J., Peischl, J., Sueper, D., Ryerson, T. B., Tokarek, T. W., Warneke, C.,
1008 Yuan, B., and de Gouw, J. A.: An improved, automated whole air sampler and gas chromatography mass spectrometry analysis
1009 system for volatile organic compounds in the atmosphere, Atmos. Meas. Tech., 10, 291-313, https://doi.org/10.5194/amt-10-291-
1010 2017, 2017.

Li, J., Mao, J., Min, K. E., Washenfelder, R. A., Brown, S. S., Kaiser, J., Keutsch, F. N., Volkamer, R., Wolfe, G. M., Hanisco, T. F., Pollack, I. B., Ryerson, T. B., Graus, M., Gilman, J. B., Lerner, B. M., Warneke, C., de Gouw, J. A., Middlebrook, A. M., Liao, J., Welti, A., Henderson, B. H., McNeill, V. F., Hall, S. R., Ullmann, K., Donner, L. J., Paulot, F., and Horowitz, L. W.: Observational constraints on glyoxal production from isoprene oxidation and its contribution to organic aerosol over the Southeast United States, J. Geophys. Res. Atmos., 121, 9849-9861, https://doi.org/10.1002/2016JD025331, 2016.

Li, S. M., Leithead, A., Moussa, S. G., Liggio, J., Moran, M. D., Wang, D., Hayden, K., Darlington, A., Gordon, M., Staebler, R., Makar, P. A., Stroud, C. A., McLaren, R., Liu, P. S. K., O'Brien, J., Mittermeier, R. L., Zhang, J., Marson, G., Cober, S. G., Wolde, M., and Wentzell, J. J. B.: Differences between measured and reported volatile organic compound emissions from oil sands facilities in Alberta, Canada, Proc. Natl. Acad. Sci. U.S.A., 114, E3756-E3765, https://doi.org/10.1073/pnas.1617862114, 2017.

Lin, J. T., and McElroy, M. B.: Impacts of boundary layer mixing on pollutant vertical profiles in the lower troposphere: Implications to satellite remote sensing, Atmos. Environ., 44, 1726-1739, https://doi.org/10.1016/j.atmosenv.2010.02.009, 2010.

Lin, S. J., and Rood, R. B.: Multidimensional flux-form semi-Lagrangian transport schemes, Mon Weather Rev, 124, 2046-2070, https://doi.org/10.1175/1520-0493(1996)124<2046:Mffslt>2.0.Co;2, 1996.

Long, M. S., Yantosca, R., Nielsen, J. E., Keller, C. A., da Silva, A., Sulprizio, M. P., Pawson, S., and Jacob, D. J.: Development of a grid-independent GEOS-Chem chemical transport model (v9-02) as an atmospheric chemistry module for Earth system models, Geosci Model Dev, 8, 595-602, https://doi.org/10.5194/gmd-8-595-2015, 2015.

Luo, G., and Yu, F.: A numerical evaluation of global oceanic emissions of alpha-pinene and isoprene, Atmos. Chem. Phys., 10, 2007-2015, https://doi.org/10.5194/acp-10-2007-2010, 2010.

Mao, J., Ren, X., Brune, W. H., Olson, J. R., Crawford, J. H., Fried, A., Huey, L. G., Cohen, R. C., Heikes, B., Singh, H. B., Blake, D. R., Sachse, G. W., Diskin, G. S., Hall, S. R., and Shetter, R. E.: Airborne measurement of OH reactivity during INTEX-B, Atmos. Chem. Phys., 9, 163-173, https://doi.org/10.5194/acp-9-163-2009, 2009.

Marais, E. A., Jacob, D. J., Jimenez, J. L., Campuzano-Jost, P., Day, D. A., Hu, W., Krechmer, J., Zhu, L., Kim, P. S., Miller, C. C., Fisher, J. A., Travis, K., Yu, K., Hanisco, T. F., Wolfe, G. M., Arkinson, H. L., Pye, H. O. T., Froyd, K. D., Liao, J., and McNeill, V. F.: Aqueous-phase mechanism for secondary organic aerosol formation from isoprene: application to the southeast United States and co-benefit of SO2 emission controls, Atmos. Chem. Phys., 16, 1603-1618, https://doi.org/10.5194/acp-16-1603-2016, 2016.

Marandino, C. A., De Bruyn, W. J., Miller, S. D., Prather, M. J., and Saltzman, E. S.: Oceanic uptake and the global atmospheric acetone budget, Geophys Res Lett, 32, https://doi.org/10.1029/2005gl023285, 2005.

Mari, C., Jacob, D. J., and Bechtold, P.: Transport and scavenging of soluble gases in a deep convective cloud, J. Geophys. Res. Atmos., 105, 22255-22267, https://doi.org/10.1029/2000jd900211, 2000.

McDonald, B. C., Gentner, D. R., Goldstein, A. H., and Harley, R. A.: Long-term trends in motor vehicle emissions in u.s. urban areas, Environ. Sci. Technol., 47, 10022-10031, https://doi.org/10.1021/es401034z, 2013.

McDonald, B. C., de Gouw, J. A., Gilman, J. B., Jathar, S. H., Akherati, A., Cappa, C. D., Jimenez, J. L., Lee-Taylor, J., Hayes, P. L., McKeen, S. A., Cui, Y. Y., Kim, S. W., Gentner, D. R., Isaacman-VanWertz, G., Goldstein, A. H., Harley, R. A., Frost, G. J., Roberts, J. M., Ryerson, T. B., and Trainer, M.: Volatile chemical products emerging as largest petrochemical source of urban organic emissions, Science, 359, 760-764, https://doi.org/10.1126/science.aaq0524, 2018.

Miller, C. C., Jacob, D. J., Marais, E. A., Yu, K. R., Travis, K. R., Kim, P. S., Fisher, J. A., Zhu, L., Wolfe, G. M., Hanisco, T. F., Keutsch, F. N., Kaiser, J., Min, K. E., Brown, S. S., Washenfelder, R. A., Abad, G. G., and Chance, K.: Glyoxal yield from isoprene oxidation and relation to formaldehyde: chemical mechanism, constraints from SENEX aircraft observations, and interpretation of OMI satellite data, Atmos. Chem. Phys., 17, 8725-8738, https://doi.org/10.5194/acp-17-8725-2017, 2017.

Millet, D. B., Jacob, D. J., Custer, T. G., de Gouw, J. A., Goldstein, A. H., Karl, T., Singh, H. B., Sive, B. C., Talbot, R. W., Warneke, C., and Williams, J.: New constraints on terrestrial and oceanic sources of atmospheric methanol, Atmos. Chem. Phys., 8, 6887-6905, https://doi.org/10.5194/acp-8-6887-2008, 2008.

Millet, D. B., Guenther, A., Siegel, D. A., Nelson, N. B., Singh, H. B., de Gouw, J. A., Warneke, C., Williams, J., Eerdekens, G., Sinha, V., Karl, T., Flocke, F., Apel, E., Riemer, D. D., Palmer, P. I., and Barkley, M.: Global atmospheric budget of

acetaldehyde: 3-D model analysis and constraints from in-situ and satellite observations, Atmos. Chem. Phys., 10, 3405-3425, https://doi.org/10.5194/acp-10-3405-2010, 2010.

Millet, D. B., Apel, E., Henze, D. K., Hill, J., Marshall, J. D., Singh, H. B., and Tessum, C. W.: Natural and anthropogenic ethanol sources in North America and potential atmospheric impacts of ethanol fuel use, Environ. Sci. Technol., 46, 8484-8492, https://doi.org/10.1021/es300162u, 2012.

Millet, D. B., Baasandorj, M., Farmer, D. K., Thornton, J. A., Baumann, K., Brophy, P., Chaliyakunnel, S., de Gouw, J. A., Graus, M., Hu, L., Koss, A., Lee, B. H., Lopez-Hilfiker, F. D., Neuman, J. A., Paulot, F., Peischl, J., Pollack, I. B., Ryerson, T. B., Warneke, C., Williams, B. J., and Xu, J.: A large and ubiquitous source of atmospheric formic acid, Atmos. Chem. Phys., 15, 6283-6304, https://doi.org/10.5194/acp-15-6283-2015, 2015.

Millet, D. B., Alwe, H. D., Chen, X., Deventer, M. J., Griffis, T. J., Holzinger, R., Bertman, S. B., Rickly, P. S., Stevens, P. S., Leonardis, T., Locoge, N., Dusanter, S., Tyndall, G. S., Alvarez, S. L., Erickson, M. H., and Flynn, J. H.: Bidirectional ecosystem-atmosphere fluxes of volatile organic compounds across the mass spectrum: How many matter?, Acs Earth Space Chem, 2, 764-777, https://doi.org/10.1021/acsearthspacechem.8b00061, 2018.

Min, K. E., Washenfelder, R. A., Dube, W. P., Langford, A. O., Edwards, P. M., Zarzana, K. J., Stutz, J., Lu, K., Rohrer, F., Zhang, Y., and Brown, S. S.: A broadband cavity enhanced absorption spectrometer for aircraft measurements of glyoxal, methylglyoxal, nitrous acid, nitrogen dioxide, and water vapor, Atmos. Meas. Tech., 9, 423-440, https://doi.org/10.5194/amt-9-423-2016, 2016.

Müller, J. F., Liu, Z., Nguyen, V. S., Stavrakou, T., Harvey, J. N., and Peeters, J.: The reaction of methyl peroxy and hydroxyl radicals as a major source of atmospheric methanol, Nat. Commun., 7, 13213, https://doi.org/10.1038/ncomms13213, 2016a.

Müller, M., Mikoviny, T., Feil, S., Haidacher, S., Hanel, G., Hartungen, E., Jordan, A., Mark, L., Mutschlechner, P., Schottkowsky, R., Sulzer, P., Crawford, J. H., and Wisthaler, A.: A compact PTR-ToF-MS instrument for airborne measurements of volatile organic compounds at high spatiotemporal resolution, Atmos. Meas. Tech., 7, 3763-3772, https://doi.org/10.5194/amt-7-3763-2014, 2014.

Müller, M., Anderson, B. E., Beyersdorf, A. J., Crawford, J. H., Diskin, G. S., Eichler, P., Fried, A., Keutsch, F. N., Mikoviny, T., Thornhill, K. L., Walega, J. G., Weinheimer, A. J., Yang, M., Yokelson, R. J., and Wisthaler, A.: In situ measurements and modeling of reactive trace gases in a small biomass burning plume, Atmos. Chem. Phys., 16, 3813-3824, https://doi.org/10.5194/acp-16-3813-2016, 2016b.

Mungall, E. L., Abbatt, J. P. D., Wentzell, J. J. B., Lee, A. K. Y., Thomas, J. L., Blais, M., Gosselin, M., Miller, L. A., Papakyriakou, T., Willis, M. D., and Liggio, J.: Microlayer source of oxygenated volatile organic compounds in the summertime marine Arctic boundary layer, Proc. Natl. Acad. Sci. U.S.A., 114, 6203-6208, https://doi.org/10.1073/pnas.1620571114, 2017.

Myhre, G., Shindell, D., Bréon, F.-M., Collins, W., Fuglestvedt, J., Huang, J., Koch, D., Lamarque, J.-F., Lee, D., Mendoza, B., Nakajima, T., Robock, A., Stephens, G., Takemura, T., and Zhang, H.: Anthropogenic and natural radiative forcing, in: Climate Change 2013: The Physical Science Basis. Contribution of Working Group I to the Fifth Assessment Report of the Intergovernmental Panel on Climate Change, edited by: Stocker, T. F., Qin, D., Plattner, G.-K., Tignor, M., Allen, S. K., Boschung, J., Nauels, A., Xia, Y., Bex, V., and Midgley, P. M., Cambridge University Press, Cambridge, United Kingdom and New York, NY, USA, 659–740, 2013.

Nguyen, T. B., Crounse, J. D., Teng, A. P., St Clair, J. M., Paulot, F., Wolfe, G. M., and Wennberg, P. O.: Rapid deposition of oxidized biogenic compounds to a temperate forest, Proc. Natl. Acad. Sci. U.S.A., 112, E392-401, https://doi.org/10.1073/pnas.1418702112, 2015.

Nirmalakhandan, N. N., and Speece, R. E.: QSAR model for predicting Henry's constant, Environ. Sci. Technol., 22, 1349-1357, https://doi.org/10.1021/es00176a016, 1988.

O'Sullivan, D. W., Silwal, I. K. C., McNeill, A. S., Treadaway, V., and Heikes, B. G.: Quantification of gas phase hydrogen peroxide and methyl peroxide in ambient air: Using atmospheric pressure chemical ionization mass spectrometry with O2−, and O2−(CO2) reagent ions, Int. J. Mass Spectrom., 424, 16-26, https://doi.org/10.1016/j.ijms.2017.11.015, 2018.

Osthoff, H. D., Roberts, J. M., Ravishankara, A. R., Williams, E. J., Lerner, B. M., Sommariva, R., Bates, T. S., Coffman, D., Quinn, P. K., Dibb, J. E., Stark, H., Burkholder, J. B., Talukdar, R. K., Meagher, J., Fehsenfeld, F. C., and Brown, S. S.: High

levels of nitryl chloride in the polluted subtropical marine boundary layer, Nat Geosci, 1, 324-328, https://doi.org/10.1038/ngeo177, 2008.

Palmer, P. I., and Shaw, S. L.: Quantifying global marine isoprene fluxes using MODIS chlorophyll observations, Geophys Res Lett, 32, https://doi.org/10.1029/2005gl022592, 2005.

Park, J. H., Goldstein, A. H., Timkovsky, J., Fares, S., Weber, R., Karlik, J., and Holzinger, R.: Active atmosphere-ecosystem exchange of the vast majority of detected volatile organic compounds, Science, 341, 643-647, https://doi.org/10.1126/science.1235053, 2013.

Parrish, D. D.: Critical evaluation of US on-road vehicle emission inventories, Atmos. Environ., 40, 2288-2300, https://doi.org/10.1016/j.atmosenv.2005.11.033, 2006.

Paulot, F., Crounse, J. D., Kjaergaard, H. G., Kroll, J. H., Seinfeld, J. H., and Wennberg, P. O.: Isoprene photooxidation: new insights into the production of acids and organic nitrates, Atmos. Chem. Phys., 9, 1479-1501, https://doi.org/10.5194/acp-9-1479-2009, 2009a.

Paulot, F., Crounse, J. D., Kjaergaard, H. G., Kurten, A., St Clair, J. M., Seinfeld, J. H., and Wennberg, P. O.: Unexpected epoxide formation in the gas-phase photooxidation of isoprene, Science, 325, 730-733, 10.1126/science.1172910, 2009b.

Paulot, F., Wunch, D., Crounse, J. D., Toon, G. C., Millet, D. B., DeCarlo, P. F., Vigouroux, C., Deutscher, N. M., Abad, G. G., Notholt, J., Warneke, T., Hannigan, J. W., Warneke, C., de Gouw, J. A., Dunlea, E. J., De Maziere, M., Griffith, D. W. T., Bernath, P., Jimenez, J. L., and Wennberg, P. O.: Importance of secondary sources in the atmospheric budgets of formic and acetic acids, Atmos. Chem. Phys., 11, 1989-2013, https://doi.org/10.5194/acp-11-1989-2011, 2011.

Peischl, J., Ryerson, T. B., Holloway, J. S., Trainer, M., Andrews, A. E., Atlas, E. L., Blake, D. R., Daube, B. C., Dlugokencky, E. J., Fischer, M. L., Goldstein, A. H., Guha, A., Karl, T., Kofler, J., Kosciuch, E., Misztal, P. K., Perring, A. E., Pollack, I. B., Santoni, G. W., Schwarz, J. P., Spackman, J. R., Wofsy, S. C., and Parrish, D. D.: Airborne observations of methane emissions from rice cultivation in the Sacramento Valley of California, J. Geophys. Res. Atmos., 117, n/a-n/a, https://doi.org/10.1029/2012jd017994, 2012.

Pfister, G., Flocke, F., Hornbrook, R., Orlando, J., Lee, S., and Schroeder, J.: FRAPPÉ Final Report: Process-Based and Regional Source Impact Analysis for FRAPPÉ and DISCOVER-AQ 2014, available at: https://www.colorado.gov/airquality/tech_doc_repository.aspx?action=open&file=FRAPPE-NCAR_Final_Report_July2017.pdf, last access: 13 Jan 2019, 2017.

Philip, S., Martin, R. V., and Keller, C. A.: Sensitivity of chemistry-transport model simulations to the duration of chemical and transport operators: a case study with GEOS-Chem v10-01, Geosci Model Dev, 9, 1683-1695, https://doi.org/10.5194/gmd-9-1683-2016, 2016.

Pollack, I. B., Lerner, B. M., and Ryerson, T. B.: Evaluation of ultraviolet light-emitting diodes for detection of atmospheric NO2 by photolysis - chemiluminescence, J. Atmos. Chem., 65, 111-125, https://doi.org/10.1007/s10874-011-9184-3, 2010.

Praske, E., Otkjaer, R. V., Crounse, J. D., Hethcox, J. C., Stoltz, B. M., Kjaergaard, H. G., and Wennberg, P. O.: Atmospheric autoxidation is increasingly important in urban and suburban North America, Proc. Natl. Acad. Sci. U.S.A., 115, 64-69, https://doi.org/10.1073/pnas.1715540115, 2018.

Read, K. A., Mahajan, A. S., Carpenter, L. J., Evans, M. J., Faria, B. V., Heard, D. E., Hopkins, J. R., Lee, J. D., Moller, S. J., Lewis, A. C., Mendes, L., McQuaid, J. B., Oetjen, H., Saiz-Lopez, A., Pilling, M. J., and Plane, J. M.: Extensive halogen-mediated ozone destruction over the tropical Atlantic Ocean, Nature, 453, 1232-1235, https://doi.org/10.1038/nature07035, 2008.

Read, K. A., Carpenter, L. J., Arnold, S. R., Beale, R., Nightingale, P. D., Hopkins, J. R., Lewis, A. C., Lee, J. D., Mendes, L., and Pickering, S. J.: Multiannual observations of acetone, methanol, and acetaldehyde in remote tropical atlantic air: implications for atmospheric OVOC budgets and oxidative capacity, Environ. Sci. Technol., 46, 11028-11039, https://doi.org/10.1021/es302082p, 2012.

Riahi, K., Grubler, A., and Nakicenovic, N.: Scenarios of long-term socio-economic and environmental development under climate stabilization, Technol. Forecasting Social Change, 74, 887-935, https://doi.org/10.1016/j.techfore.2006.05.026, 2007.

Richter, D., Weibring, P., Walega, J. G., Fried, A., Spuler, S. M., and Taubman, M. S.: Compact highly sensitive multi-species airborne mid-IR spectrometer, Appl. Phys. B: Lasers Opt., 119, 119-131, https://doi.org/10.1007/s00340-015-6038-8, 2015.

Ryerson, T. B., Buhr, M. P., Frost, G. J., Goldan, P. D., Holloway, J. S., Hubler, G., Jobson, B. T., Kuster, W. C., McKeen, S. A., Parrish, D. D., Roberts, J. M., Sueper, D. T., Trainer, M., Williams, J., and Fehsenfeld, F. C.: Emissions lifetimes and ozone formation in power plant plumes, J. Geophys. Res. Atmos., 103, 22569-22583, https://doi.org/10.1029/98jd01620, 1998.

Ryerson, T. B., Huey, L. G., Knapp, K., Neuman, J. A., Parrish, D. D., Sueper, D. T., and Fehsenfeld, F. C.: Design and initial characterization of an inlet for gas-phase NOy measurements from aircraft, J. Geophys. Res. Atmos., 104, 5483-5492, https://doi.org/10.1029/1998jd100087, 1999.

Ryerson, T. B., Andrews, A. E., Angevine, W. M., Bates, T. S., Brock, C. A., Cairns, B., Cohen, R. C., Cooper, O. R., de Gouw, J. A., Fehsenfeld, F. C., Ferrare, R. A., Fischer, M. L., Flagan, R. C., Goldstein, A. H., Hair, J. W., Hardesty, R. M., Hostetler, C. A., Jimenez, J. L., Langford, A. O., McCauley, E., McKeen, S. A., Molina, L. T., Nenes, A., Oltmans, S. J., Parrish, D. D., Pederson, J. R., Pierce, R. B., Prather, K., Quinn, P. K., Seinfeld, J. H., Senff, C. J., Sorooshian, A., Stutz, J., Surratt, J. D., Trainer, M., Volkamer, R., Williams, E. J., and Wofsy, S. C.: The 2010 California Research at the Nexus of Air Quality and Climate Change (CalNex) field study, J. Geophys. Res. Atmos., 118, 5830-5866, https://doi.org/10.1002/jgrd.50331, 2013.

Safieddine, S. A., Heald, C. L., and Henderson, B. H.: The global nonmethane reactive organic carbon budget: A modeling perspective, Geophys Res Lett, 44, 3897-3906, https://doi.org/10.1002/2017GL072602, 2017.

Sander, R.: Compilation of Henry's law constants (version 4.0) for water as solvent, Atmos. Chem. Phys., 15, 4399-4981, https://doi.org/10.5194/acp-15-4399-2015, 2015.

Schauffler, S. M., Atlas, E. L., Donnelly, S. G., Andrews, A., Montzka, S. A., Elkins, J. W., Hurst, D. F., Romashkin, P. A., Dutton, G. S., and Stroud, V.: Chlorine budget and partitioning during the Stratospheric Aerosol and Gas Experiment (SAGE) III Ozone Loss and Validation Experiment (SOLVE), J. Geophys. Res. Atmos., 108, https://doi.org/10.1029/2001jd002040, 2003.

SEAC^{4}RS Science Team: SEAC^{4}RS Field Campaign Data. NASA Langley Atmospheric Science Data Center DAAC, https://doi.org/10.5067/aircraft/seac4rs/aerosol-tracegas-cloud, 2013.

Shaw, M. F., Sztáray, B., Whalley, L. K., Heard, D. E., Millet, D. B., Jordan, M. J., Osborn, D. L., and Kable, S. H.: Photo-tautomerization of acetaldehyde as a photochemical source of formic acid in the troposphere, Nat. Commun., 9, 2584, 2018.

Shaw, S. L., Gantt, B., and Meskhidze, N.: Production and emissions of marine isoprene and monoterpenes: A review, Adv Meteorol, 2010, 1-24, https://doi.org/10.1155/2010/408696, 2010.

Singh, H. B., Tabazadeh, A., Evans, M. J., Field, B. D., Jacob, D. J., Sachse, G., Crawford, J. H., Shetter, R., and Brune, W. H.: Oxygenated volatile organic chemicals in the oceans: Inferences and implications based on atmospheric observations and air-sea exchange models, Geophys Res Lett, 30, https://doi.org/10.1029/2003gl017933, 2003.

Slusher, D. L., Huey, L. G., Tanner, D. J., Flocke, F. M., and Roberts, J. M.: A thermal dissociation-chemical ionization mass spectrometry (TD-CIMS) technique for the simultaneous measurement of peroxyacyl nitrates and dinitrogen pentoxide, J. Geophys. Res. Atmos., 109, https://doi.org/10.1029/2004jd004670, 2004.

St Clair, J. M., McCabe, D. C., Crounse, J. D., Steiner, U., and Wennberg, P. O.: Chemical ionization tandem mass spectrometer for the in situ measurement of methyl hydrogen peroxide, Rev. Sci. Instrum., 81, 094102, https://doi.org/10.1063/1.3480552, 2010.

Staudinger, J., and Roberts, P. V.: A critical compilation of Henry's law constant temperature dependence relations for organic compounds in dilute aqueous solutions, Chemosphere, 44, 561-576, https://doi.org/10.1016/S0045-6535(00)00505-1, 2001.

Stavrakou, T., Muller, J. F., Peeters, J., Razavi, A., Clarisse, L., Clerbaux, C., Coheur, P. F., Hurtmans, D., De Maziere, M., Vigouroux, C., Deutscher, N. M., Griffith, D. W. T., Jones, N., and Paton-Walsh, C.: Satellite evidence for a large source of formic acid from boreal and tropical forests, Nat Geosci, 5, 26-30, https://doi.org/10.1038/NGEO1354, 2012.

Stettler, M. E. J., Eastham, S., and Barrett, S. R. H.: Air quality and public health impacts of UK airports. Part I: Emissions, Atmos. Environ., 45, 5415-5424, https://doi.org/10.1016/j.atmosenv.2011.07.012, 2011.

Toon, O. B., Maring, H., Dibb, J., Ferrare, R., Jacob, D. J., Jensen, E. J., Luo, Z. J., Mace, G. G., Pan, L. L., Pfister, L., Rosenlof, K. H., Redemann, J., Reid, J. S., Singh, H. B., Thompson, A. M., Yokelson, R., Minnis, P., Chen, G., Jucks, K. W., and Pszenny, A.: Planning, implementation, and scientific goals of the Studies of Emissions and Atmospheric Composition, Clouds and Climate Coupling by Regional Surveys (SEAC(4)RS) field mission, J. Geophys. Res. Atmos., 121, 4967-5009, https://doi.org/10.1002/2015JD024297, 2016.

Travis, K. R., Jacob, D. J., Fisher, J. A., Kim, P. S., Marais, E. A., Zhu, L., Yu, K., Miller, C. C., Yantosca, R. M., Sulprizio, M. P., Thompson, A. M., Wennberg, P. O., Crounse, J. D., St Clair, J. M., Cohen, R. C., Laughner, J. L., Dibb, J. E., Hall, S. R., Ullmann, K., Wolfe, G. M., Pollack, I. B., Peischl, J., Neuman, J. A., and Zhou, X.: Why do Models Overestimate Surface Ozone in the Southeastern United States?, Atmos. Chem. Phys., 16, 13561-13577, https://doi.org/10.5194/acp-16-13561-2016, 2016.

Treadaway, V., Heikes, B. G., McNeill, A. S., Silwal, I. K. C., and O'Sullivan, D. W.: Measurement of formic acid, acetic acid and hydroxyacetaldehyde, hydrogen peroxide, and methyl peroxide in air by chemical ionization mass spectrometry: airborne method development, Atmos. Meas. Tech., 11, 1901-1920, https://doi.org/10.5194/amt-11-1901-2018, 2018.

Trostl, J., Chuang, W. K., Gordon, H., Heinritzi, M., Yan, C., Molteni, U., Ahlm, L., Frege, C., Bianchi, F., Wagner, R., Simon, M., Lehtipalo, K., Williamson, C., Craven, J. S., Duplissy, J., Adamov, A., Almeida, J., Bernhammer, A. K., Breitenlechner, M., Brilke, S., Dias, A., Ehrhart, S., Flagan, R. C., Franchin, A., Fuchs, C., Guida, R., Gysel, M., Hansel, A., Hoyle, C. R., Jokinen, T., Junninen, H., Kangasluoma, J., Keskinen, H., Kim, J., Krapf, M., Kurten, A., Laaksonen, A., Lawler, M., Leiminger, M., Mathot, S., Mohler, O., Nieminen, T., Onnela, A., Petaja, T., Piel, F. M., Miettinen, P., Rissanen, M. P., Rondo, L., Sarnela, N., Schobesberger, S., Sengupta, K., Sipila, M., Smith, J. N., Steiner, G., Tome, A., Virtanen, A., Wagner, A. C., Weingartner, E., Wimmer, D., Winkler, P. M., Ye, P. L., Carslaw, K. S., Curtius, J., Dommen, J., Kirkby, J., Kulmala, M., Riipinen, I., Worsnop, D. R., Donahue, N. M., and Baltensperger, U.: The role of low-volatility organic compounds in initial particle growth in the atmosphere, Nature, 533, 527-+, https://doi.org/10.1038/nature18271, 2016.

van der Werf, G. R., Randerson, J. T., Giglio, L., van Leeuwen, T. T., Chen, Y., Rogers, B. M., Mu, M. Q., van Marle, M. J. E., Morton, D. C., Collatz, G. J., Yokelson, R. J., and Kasibhatla, P. S.: Global fire emissions estimates during 1997-2016, Earth Syst. Sci. Data, 9, 697-720, https://doi.org/10.5194/essd-9-697-2017, 2017.

van Vuuren, D. P., Edmonds, J., Kainuma, M., Riahi, K., Thomson, A., Hibbard, K., Hurtt, G. C., Kram, T., Krey, V., Lamarque, J. F., Masui, T., Meinshausen, M., Nakicenovic, N., Smith, S. J., and Rose, S. K.: The representative concentration pathways: an overview, Clim. Change, 109, 5-31, https://doi.org/10.1007/s10584-011-0148-z, 2011.

Wang, Y. H., Jacob, D. J., and Logan, J. A.: Global simulation of tropospheric O3-NOx-hydrocarbon chemistry 1. Model formulation, J. Geophys. Res. Atmos., 103, 10713-10725, https://doi.org/10.1029/98jd00158, 1998.

Warneke, C., de Gouw, J. A., Nowak, J. B., and Peischl, J.: Volatile organic compound emissions from agriculture in Central Valley, California, Abstr. Pap. Am. Chem. Soc., 242, 1, 2011.

Warneke, C., de Gouw, J. A., Holloway, J. S., Peischl, J., Ryerson, T. B., Atlas, E., Blake, D., Trainer, M., and Parrish, D. D.: Multiyear trends in volatile organic compounds in Los Angeles, California: Five decades of decreasing emissions, J. Geophys. Res. Atmos., 117, n/a-n/a, https://doi.org/10.1029/2012jd017899, 2012.

Warneke, C., Geiger, F., Edwards, P. M., Dube, W., Petron, G., Kofler, J., Zahn, A., Brown, S. S., Graus, M., Gilman, J. B., Lerner, B. M., Peischl, J., Ryerson, T. B., de Gouw, J. A., and Roberts, J. M.: Volatile organic compound emissions from the oil and natural gas industry in the Uintah Basin, Utah: oil and gas well pad emissions compared to ambient air composition, Atmos. Chem. Phys., 14, 10977-10988, https://doi.org/10.5194/acp-14-10977-2014, 2014.

Warneke, C., Trainer, M., de Gouw, J. A., Parrish, D. D., Fahey, D. W., Ravishankara, A. R., Middlebrook, A. M., Brock, C. A., Roberts, J. M., Brown, S. S., Neuman, J. A., Lerner, B. M., Lack, D., Law, D., Hubler, G., Pollack, I., Sjostedt, S., Ryerson, T. B., Gilman, J. B., Liao, J., Holloway, J., Peischl, J., Nowak, J. B., Aikin, K., Min, K. E., Washenfelder, R. A., Graus, M. G., Richardson, M., Markovic, M. Z., Wagner, N. L., Welti, A., Veres, P. R., Edwards, P., Schwarz, J. P., Gordon, T., Dube, W. P., McKeen, S., Brioude, J., Ahmadov, R., Bougiatioti, A., Lin, J. J., Nenes, A., Wolfe, G. M., Hanisco, T. F., Lee, B. H., Lopez-Hilfiker, F. D., Thornton, J. A., Keutsch, F. N., Kaiser, J., Mao, J., and Hatch, C.: Instrumentation and measurement strategy for the NOAA SENEX aircraft campaign as part of the Southeast Atmosphere Study 2013, Atmos. Meas. Tech., 9, 3063-3093, https://doi.org/10.5194/amt-9-3063-2016, 2016.

Weibring, P., Richter, D., Walega, J. G., Rippe, L., and Fried, A.: Difference frequency generation spectrometer for simultaneous multispecies detection, Opt. Express, 18, 27670-27681, https://doi.org/10.1364/OE.18.027670, 2010.

Weinheimer, A. J., Walega, J. G., Ridley, B. A., Gary, B. L., Blake, D. R., Blake, N. J., Rowland, F. S., Sachse, G. W., Anderson, B. E., and Collins, J. E.: Meridional distributions of NOx, NOy and other species in the lower stratosphere and upper troposphere during AASE II, Geophys Res Lett, 21, 2583-2586, https://doi.org/10.1029/94gl01897, 1994.

Wells, K. C., Millet, D. B., Hu, L., Cady-Pereira, K. E., Xiao, Y., Shephard, M. W., Clerbaux, C. L., Clarisse, L., Coheur, P. F., Apel, E. C., de Gouw, J., Warneke, C., Singh, H. B., Goldstein, A. H., and Sive, B. C.: Tropospheric methanol observations from space: retrieval evaluation and constraints on the seasonality of biogenic emissions, Atmos. Chem. Phys., 12, 5897-5912, https://doi.org/10.5194/acp-12-5897-2012, 2012.

Wesely, M. L.: Parameterization of surface resistances to gaseous dry deposition in regional-scale numerical models, Atmos. Environ., 23, 1293-1304, https://doi.org/10.1016/0004-6981(89)90153-4, 1989.

Wiedinmyer, C., Akagi, S. K., Yokelson, R. J., Emmons, L. K., Al-Saadi, J. A., Orlando, J. J., and Soja, A. J.: The Fire INventory from NCAR (FINN): a high resolution global model to estimate the emissions from open burning, Geosci Model Dev, 4, 625-641, https://doi.org/10.5194/gmd-4-625-2011, 2011.

Williams, J., Holzinger, R., Gros, V., Xu, X., Atlas, E., and Wallace, D. W. R.: Measurements of organic species in air and seawater from the tropical Atlantic, Geophys Res Lett, 31, https://doi.org/10.1029/2004gl020012, 2004.

Wisthaler, A., Hansel, A., Dickerson, R. R., and Crutzen, P. J.: Organic trace gas measurements by PTR-MS during INDOEX 1999, J. Geophys. Res. Atmos., 107, https://doi.org/10.1029/2001jd000576, 2002.

Wofsy, S. C., Afshar, S., Allen, H. M., Apel, E., Asher, E. C., Barletta, B., Bent, J., Bian, H., Biggs, B. C., Blake, D. R., Blake, N., Bourgeois, I., Brock, C. A., Brune, W. H., Budney, J. W., Bui, T. P., Butler, A., Campuzano-Jost, P., Chang, C. S., Chin, M., Commane, R., Correa, G., Crounse, J. D., Cullis, P. D., Daube, B. C., Day, D. A., Dean-Day, J. M., Dibb, J. E., DiGangi, J. P., Diskin, G. S., Dollner, M., Elkins, J. W., Erdesz, F., Fiore, A. M., Flynn, C. M., Froyd, K., Gesler, D. W., Hall, S. R., Hanisco, T. F., Hannun, R. A., Hills, A. J., Hintsa, E. J., Hoffman, A., Hornbrook, R. S., Huey, L. G., Hughes, S., Jimenez, J. L., Johnson, B. J., Katich, J. M., Keeling, R. F., Kim, M. J., Kupc, A., Lait, L. R., Lamarque, J.-F., Liu, J., McKain, K., Mclaughlin, R. J., Meinardi, S., Miller, D. O., Montzka, S. A., Moore, F. L., Morgan, E. J., Murphy, D. M., Murray, L. T., Nault, B. A., Neuman, J. A., Newman, P. A., Nicely, J. M., Pan, X., Paplawsky, W., Peischl, J., Prather, M. J., Price, D. J., Ray, E., Reeves, J. M., Richardson, M., Rollins, A. W., Rosenlof, K. H., Ryerson, T. B., Scheuer, E., Schill, G. P., Schroder, J. C., Schwarz, J. P., St.Clair, J. M., Steenrod, S. D., Stephens, B. B., Strode, S. A., Sweeney, C., Tanner, D., Teng, A. P., Thames, A. B., Thompson, C. R., Ullmann, K., Veres, P. R., Vieznor, N., Wagner, N. L., Watt, A., Weber, R., Weinzierl, B., Wennberg, P., Williamson, C. J., Wilson, J. C., Wolfe, G. M., Woods, C. T., and Zeng, L. H.: ATom: Merged Atmospheric Chemistry, Trace Gases, and Aerosols. ORNL DAAC, Oak Ridge, Tennessee, USA, https://doi.org/10.3334/ornldaac/1581, 2018.

Wolfe, G. M., Hanisco, T. F., Arkinson, H. L., Bui, T. P., Crounse, J. D., Dean-Day, J., Goldstein, A., Guenther, A., Hall, S. R., Huey, G., Jacob, D. J., Karl, T., Kim, P. S., Liu, X., Marvin, M. R., Mikoviny, T., Misztal, P. K., Nguyen, T. B., Peischl, J., Pollack, I., Ryerson, T., St Clair, J. M., Teng, A., Travis, K. R., Ullmann, K., Wennberg, P. O., and Wisthaler, A.: Quantifying sources and sinks of reactive gases in the lower atmosphere using airborne flux observations, Geophys Res Lett, 42, 8231-8240, https://doi.org/10.1002/2015GL065839, 2015.

Wooldridge, P. J., Perring, A. E., Bertram, T. H., Flocke, F. M., Roberts, J. M., Singh, H. B., Huey, L. G., Thornton, J. A., Wolfe, G. M., Murphy, J. G., Fry, J. L., Rollins, A. W., LaFranchi, B. W., and Cohen, R. C.: Total Peroxy Nitrates (ΣPNs) in the atmosphere: the Thermal Dissociation-Laser Induced Fluorescence (TD-LIF) technique and comparisons to speciated PAN measurements, Atmos. Meas. Tech., 3, 593-607, https://doi.org/10.5194/amt-3-593-2010, 2010.

Wu, S. L., Mickley, L. J., Jacob, D. J., Logan, J. A., Yantosca, R. M., and Rind, D.: Why are there large differences between models in global budgets of tropospheric ozone?, J. Geophys. Res. Atmos., 112, https://doi.org/10.1029/2006jd007801, 2007.

Xiao, Y. P., Logan, J. A., Jacob, D. J., Hudman, R. C., Yantosca, R., and Blake, D. R.: Global budget of ethane and regional constraints on US sources, J. Geophys. Res. Atmos., 113, https://doi.org/10.1029/2007jd009415, 2008.

Yacovitch, T. I., Herndon, S. C., Roscioli, J. R., Floerchinger, C., McGovern, R. M., Agnese, M., Petron, G., Kofler, J., Sweeney, C., Karion, A., Conley, S. A., Kort, E. A., Nahle, L., Fischer, M., Hildebrandt, L., Koeth, J., McManus, J. B., Nelson, D. D., Zahniser, M. S., and Kolb, C. E.: Demonstration of an ethane spectrometer for methane source identification, Environ. Sci. Technol., 48, 8028-8034, http://doi.org/10.1021/es501475q, 2014.

Yang, M., Nightingale, P. D., Beale, R., Liss, P. S., Blomquist, B., and Fairall, C.: Atmospheric deposition of methanol over the Atlantic Ocean, Proc. Natl. Acad. Sci. U.S.A., 110, 20034-20039, https://doi.org/10.1073/pnas.1317840110, 2013.

Yang, M., Beale, R., Liss, P., Johnson, M., Blomquist, B., and Nightingale, P.: Air-sea fluxes of oxygenated volatile organic compounds across the Atlantic Ocean, Atmos. Chem. Phys., 14, 7499-7517, https://doi.org/10.5194/acp-14-7499-2014, 2014a.

Yang, M. X., Blomquist, B. W., and Nightingale, P. D.: Air-sea exchange of methanol and acetone during HiWinGS: Estimation of air phase, water phase gas transfer velocities, J. Geophys. Res. Oceans, 119, 7308-7323, https://doi.org/10.1002/2014JC010227, 2014b.

Yevich, R., and Logan, J. A.: An assessment of biofuel use and burning of agricultural waste in the developing world, Global Biogeochem Cy, 17, https://doi.org/10.1029/2002gb001952, 2003.

Yu, K., Keller, C. A., Jacob, D. J., Molod, A. M., Eastham, S. D., and Long, M. S.: Errors and improvements in the use of archived meteorological data for chemical transport modeling: an analysis using GEOS-Chem v11-01 driven by GEOS-5 meteorology, Geosci Model Dev, 11, 305-319, https://doi.org/10.5194/gmd-11-305-2018, 2018.

Yu, K. R., Jacob, D. J., Fisher, J. A., Kim, P. S., Marais, E. A., Miller, C. C., Travis, K. R., Zhu, L., Yantosca, R. M., Sulprizio, M. P., Cohen, R. C., Dibb, J. E., Fried, A., Mikoviny, T., Ryerson, T. B., Wennberg, P. O., and Wisthaler, A.: Sensitivity to grid resolution in the ability of a chemical transport model to simulate observed oxidant chemistry under high-isoprene conditions, Atmos. Chem. Phys., 16, 4369-4378, https://doi.org/10.5194/acp-16-4369-2016, 2016.

Zheng, W., Flocke, F. M., Tyndall, G. S., Swanson, A., Orlando, J. J., Roberts, J. M., Huey, L. G., and Tanner, D. J.: Characterization of a thermal decomposition chemical ionization mass spectrometer for the measurement of peroxy acyl nitrates (PANs) in the atmosphere, Atmos. Chem. Phys., 11, 6529-6547, https://doi.org/10.5194/acp-11-6529-2011, 2011.

Zhou, X. L., and Mopper, K.: Photochemical production of low-molecular-weight carbonyl compounds in seawater and surface microlayer and their air-sea exchange, Mar. Chem., 56, 201-213, https://doi.org/10.1016/S0304-4203(96)00076-X, 1997.

Zhu, L., Jacob, D. J., Kim, P. S., Fisher, J. A., Yu, K., Travis, K. R., Mickley, L. J., Yantosca, R. M., Sulprizio, M. P., De Smedt, I., Abad, G. G., Chance, K., Li, C., Ferrare, R., Fried, A., Hair, J. W., Hanisco, T. F., Richter, D., Scarino, A. J., Walega, J., Weibring, P., and Wolfe, G. M.: Observing atmospheric formaldehyde (HCHO) from space: validation and intercomparison of six retrievals from four satellites (OMI, GOME2A, GOME2B, OMPS) with SEAC(4)RS aircraft observations over the Southeast US, Atmos. Chem. Phys., 16, 13477-13490, https://doi.org/10.5194/acp-16-13477-2016, 2016.

Zhuang, J. W., Jacob, D. J., and Eastham, S. D.: The importance of vertical resolution in the free troposphere for modeling intercontinental plumes, Atmos. Chem. Phys., 18, 6039-6055, https://doi.org/10.5194/acp-18-6039-2018, 2018.

Table 1. Overview of aircraft campaigns used here[a].

	Aircraft platform	Aircraft ceiling	Timeframe	Sampling region	Campaign overview and data DOI if applicable
CalNex	NOAA WP-3D	7600m	May – Jul 2010	California and offshore	Ryerson et al. (2013)
DC3	NASA DC-8	12500m	May – Jun 2012	Northeastern Colorado, west Texas to central Oklahoma, and northern Alabama	Barth et al. (2015) DC3 Science Team (2013)
	NSF/NCAR GV	15500m			
SENEX	NOAA WP-3D	7600m	Jun – Jul 2013	Southeastern US	Warneke et al. (2016)
SEAC^{4}RS	NASA DC-8	12500m	Aug – Sep 2013	Southeastern US and Gulf of Mexico	Toon et al. (2016) SEAC^{4}RS Science Team (2013)
DISCOVER-AQ	NASA P-3B	8500m	Jun – Jul 2011	Baltimore-Washington, D.C.	Crawford and Pickering (2014) DISCOVER-AQ Science Team (2014)
			Jan – Feb 2013	San Joaquin Valley, California	
			Sep 2013	Houston, Texas	
			Jul – Aug 2014	Denver, Colorado	
FRAPPÉ	NCAR C-130	7900m	Jul – Aug 2014	Northern Colorado	Pfister et al. (2017)

[a]See measurement details in Table S1 (O'Sullivan et al., 2018; Treadaway et al., 2018; Lerner et al., 2017; Min et al., 2016; Müller et al., 2016b; Cazorla et al., 2015; Richter et al., 2015; Lee et al., 2014; Müller et al., 2014; Yacovitch et al., 2014; Kaser et al., 2013; DiGangi et al., 2011; Fried et al., 2011; Zheng et al., 2011; Apel et al., 2010; Pollack et al., 2010; St Clair et al., 2010; Weibring et al., 2010; Wooldridge et al., 2010; Gilman et al., 2009; Hottle et al., 2009; Osthoff et al., 2008; de Gouw and Warneke, 2007; Huey, 2007; Kim et al., 2007; Crounse et al., 2006; Slusher et al., 2004; Blake et al., 2003; Schauffler et al., 2003; Wisthaler et al., 2002; Colman et al., 2001; Ryerson et al., 1999; Ryerson et al., 1998; Weinheimer et al., 1994).

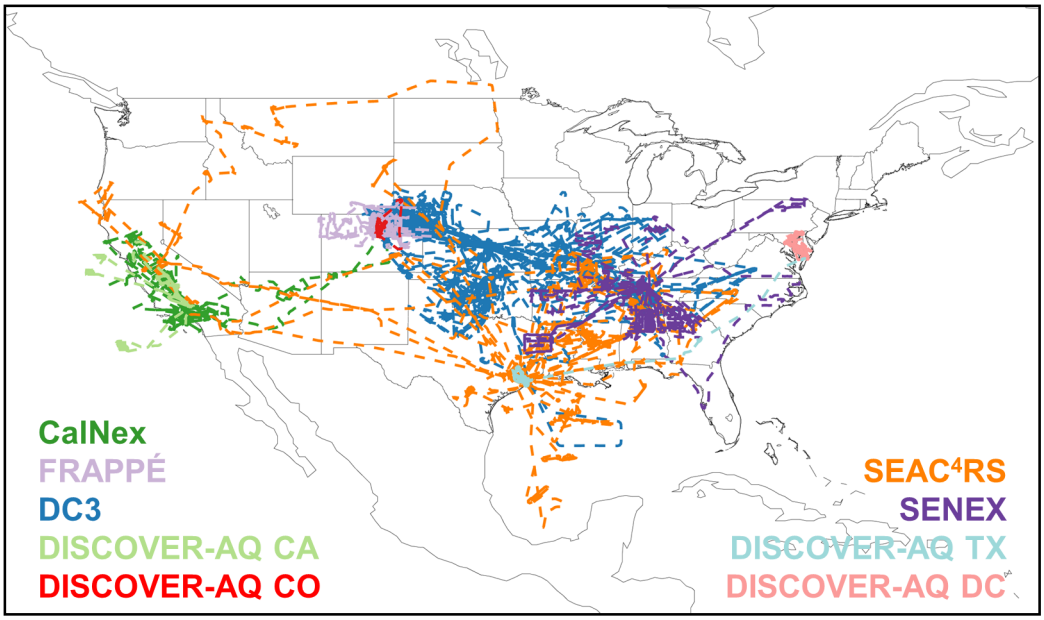

Figure 1. Flight tracks for the aircraft campaigns used in this study: CalNex (May-Jun 2010), FRAPPÉ (Jul-Aug 2014), DC3 (May-Jun 2012), DISCOVER-AQ CA (Jan-Feb 2013), DISCOVER-AQ CO (Jul-Aug 2014), SEAC^{4}RS (Aug-Sep 2013), SENEX (Jun 2013), DISCOVER-AQ TX (Sep 2013), and DISCOVER-AQ DC (Jun-Jul 2011).

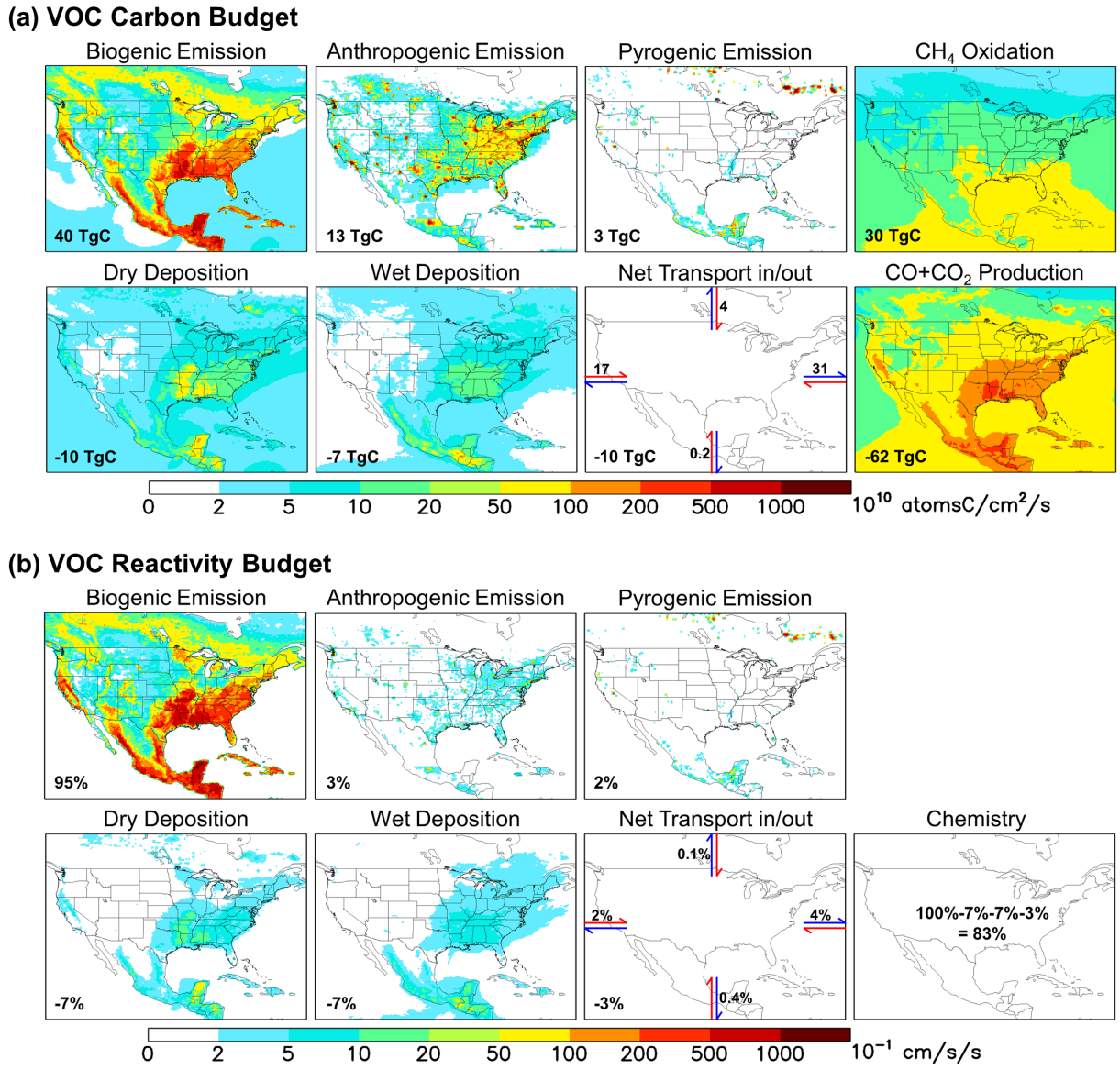

Figure 2. Annual VOC-carbon (a) and reactivity (b) budgets over North America as simulated by GEOS-Chem for 2013. For panel (a) the annually integrated flux for each source/sink is given inset. For panel (b) all VOC fluxes are weighted by the corresponding OH reaction rate coefficient at 298 K to derive a VOC reactivity budget. Values inset indicat~~ing~~ the fraction of total emitted reactivity produced or removed by that source/sink/transport process. Positive fluxes denote sources and negative fluxes denote sinks.

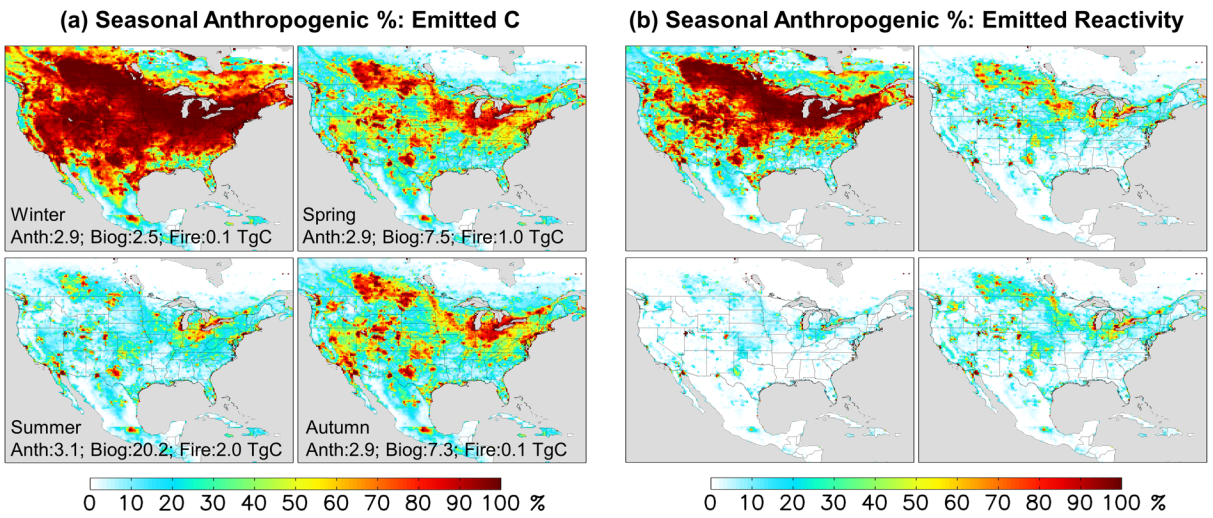

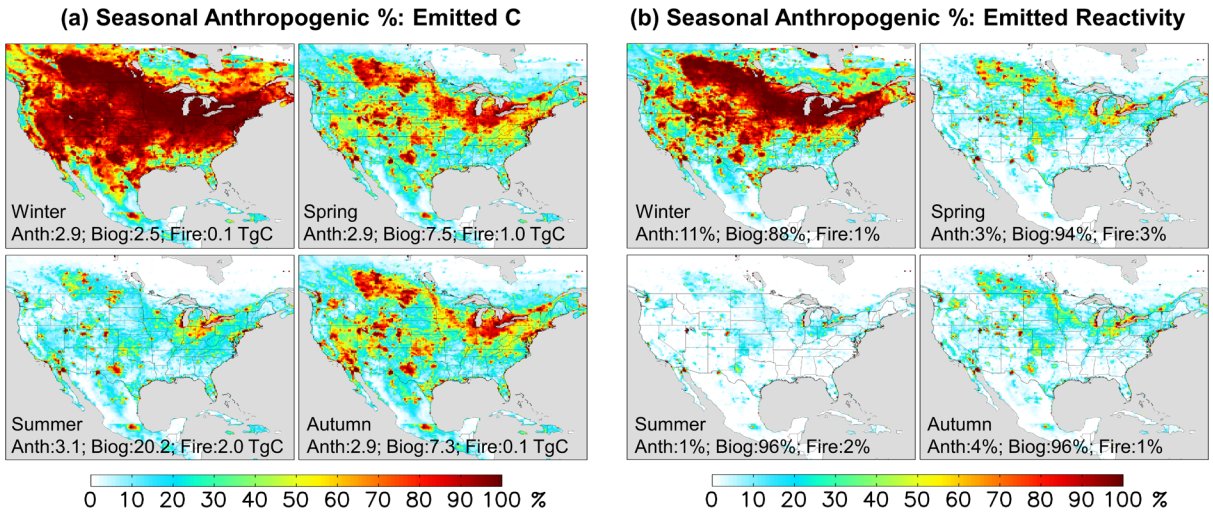

Figure 3. Seasonal anthropogenic contribution to total VOC-carbon emissions (panel a) and to total reactivity-weighted VOC emissions (panel b). Numbers inset indicate the domain-aggregated emissions (panel a) or domain-wide contribution to reactivity-weighted emissions (panel b) from anthropogenic, biogenic, and biomass burning sources.

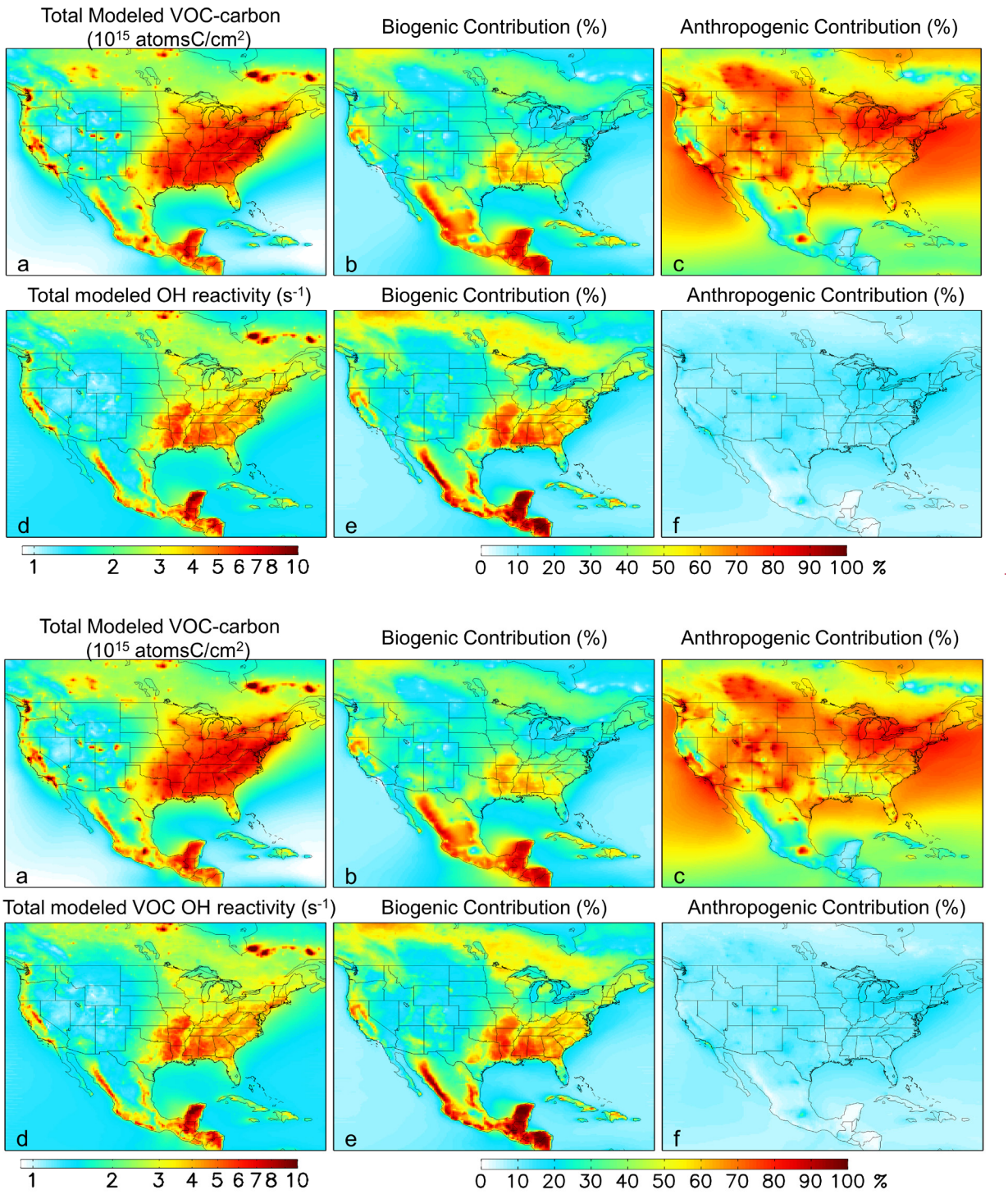

Figure 4. Distribution and source attribution of ambient VOC-carbon and associated OH reactivity over North America. Panels (a) and (d): total VOC-carbon and VOC-driven OH reactivity as simulated in the lowest model layer (below ~130m). Panel (b) and (e): ambient VOC-carbon and reactivity attributed to biogenic VOC emissions. Panel (c) and (f): ambient VOC-carbon and reactivity attributed to anthropogenic VOC emissions. Source attributions are derived based on model sensitivity tests with 10% modified anthropogenic or biogenic emissions, as described in-text.

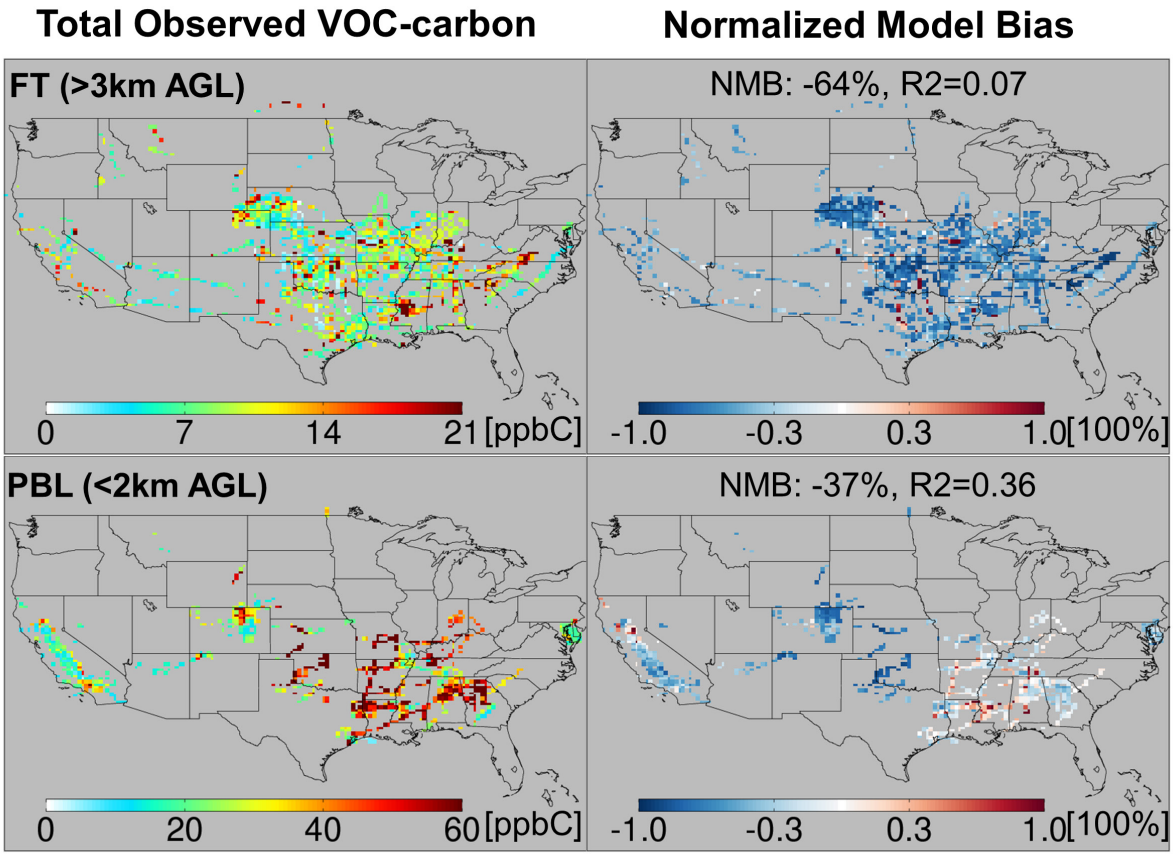

Figure 5. Total observed VOC-carbon loading (left) over North America in the planetary boundary layer (<2 km AGL) and free troposphere (>3 km AGL). In the right-hand panels the GEOS-Chem model simulation is compared to co-located aircraft observation with the normalized mean bias given inset. Note that the sampling season and instrument payload vary among campaigns.

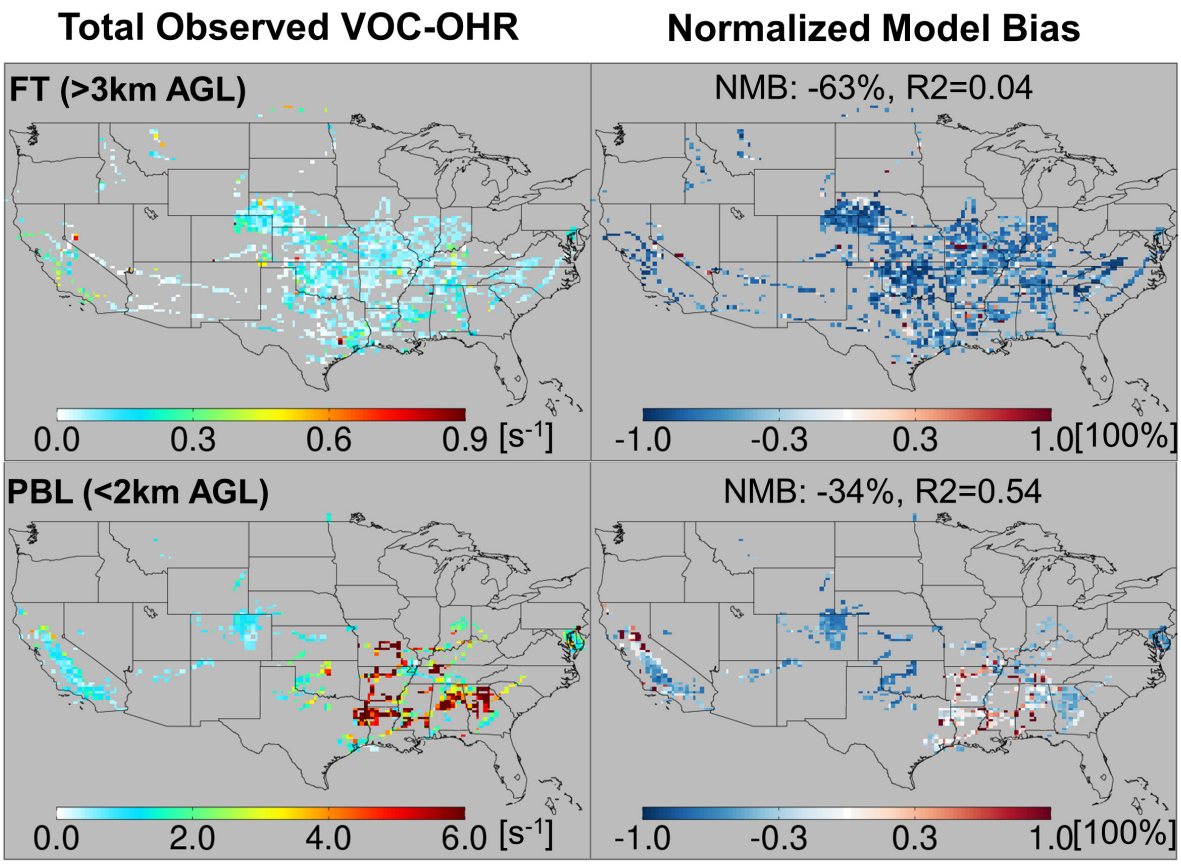

Figure 6. Total observed VOC reactivity (left) over North America in the planetary boundary layer (<2 km AGL) and free troposphere (>3 km AGL). In the right-hand panels, the GEOS-Chem model simulation is compared to co-located aircraft observation with the normalized mean bias given inset. Note that the sampling season and instrument payload vary among campaigns.

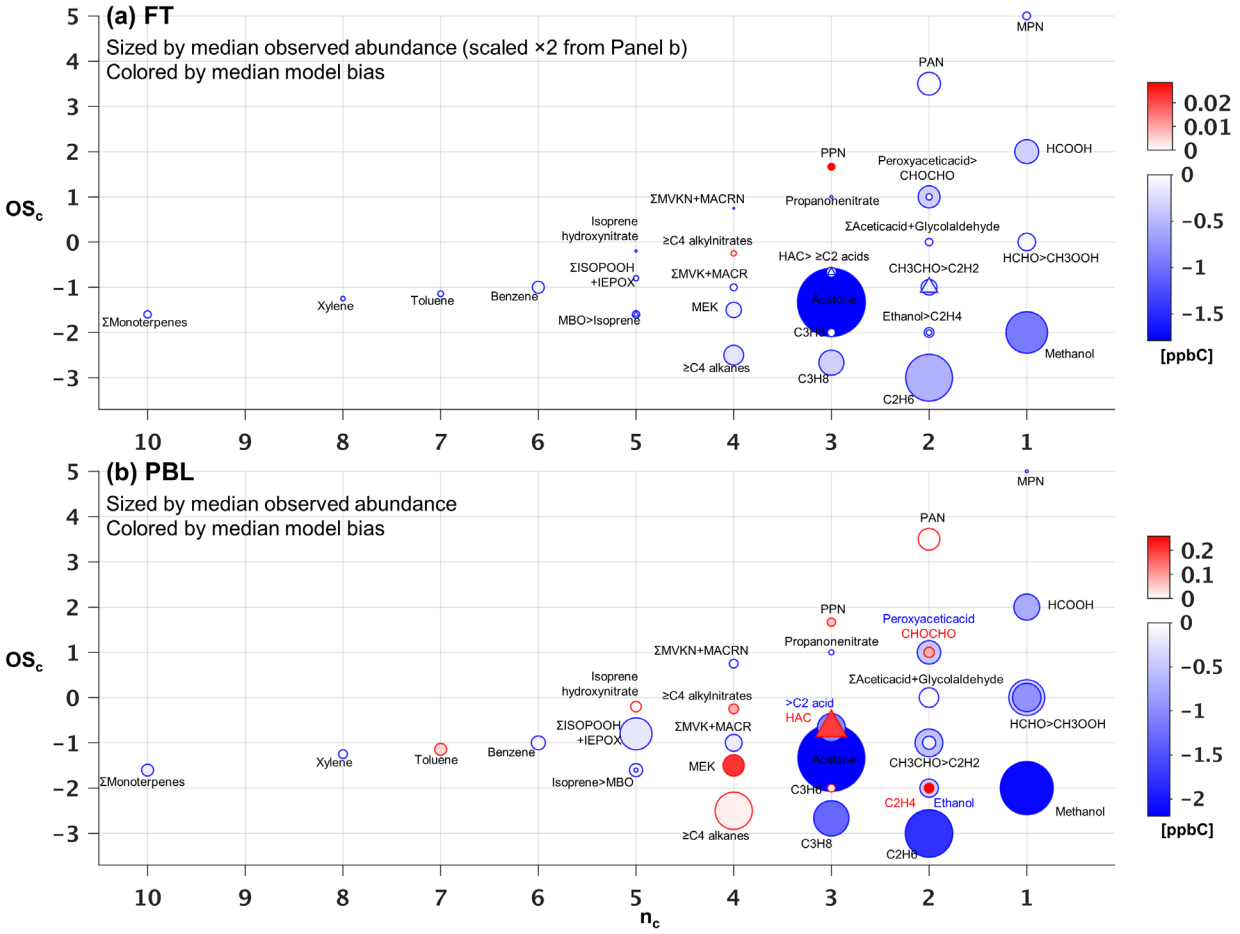

Figure 7. Observed versus predicted VOC-carbon as a function of carbon oxidation state (OS_c) and number of carbon atoms (n_c). Each circle indicates a single VOC (or lumped category for those that are measured or modeled collectively). Symbols are sized according to the observed median abundance (ppbC) of each species in the FT (panel a) and in the PBL (panel b, note altered size scaling from Panel a). Triangles are used when co-located circles are too close in size to distinguish, and symbols are colored according to the median absolute model bias in each case. For overlapping species, the more abundant of the two is indicated with ">".

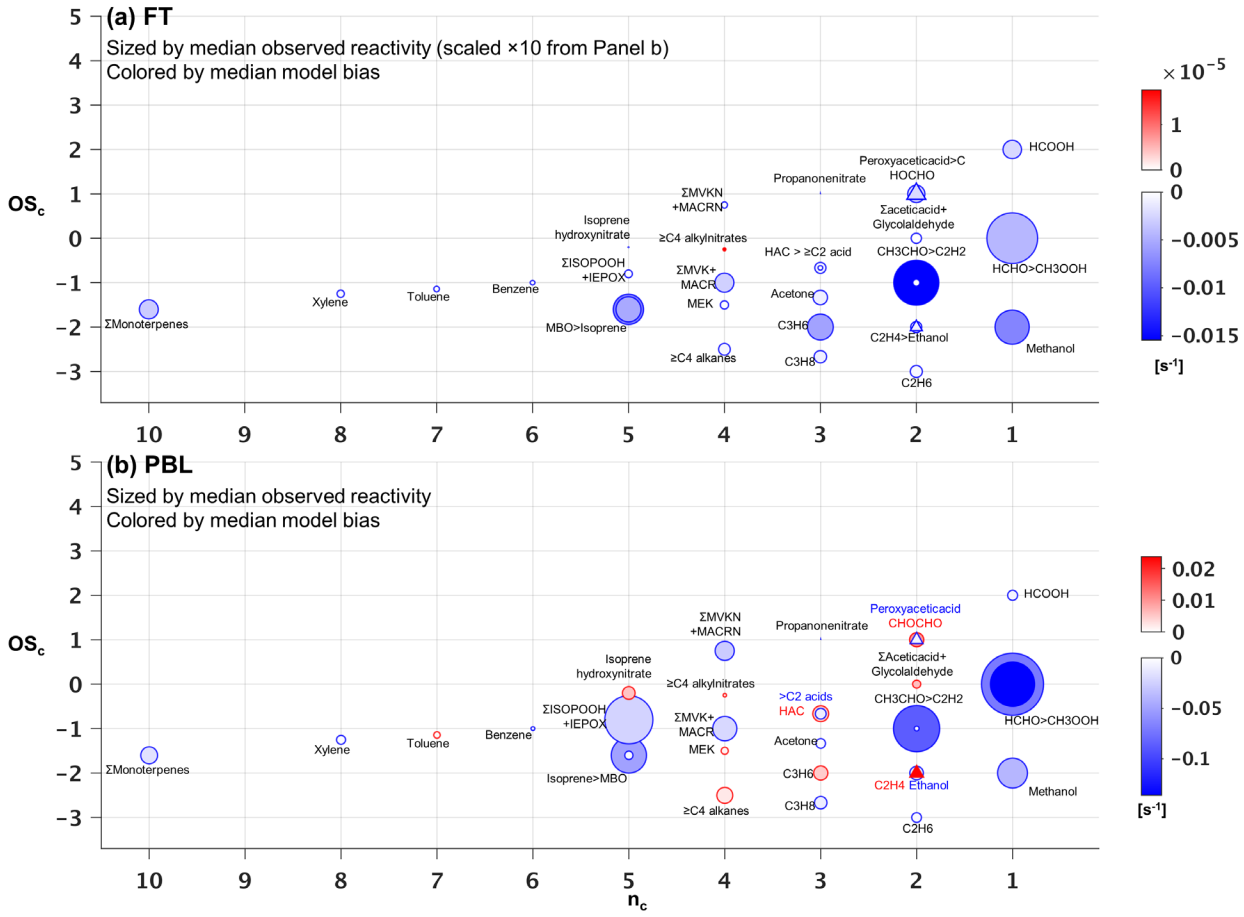

Figure 8. Observed versus predicted VOC reactivity as a function of carbon oxidation state (OS_c) and number of carbon atoms (n_c). Each circle indicates a single VOC (or lumped category for those that are measured or modeled collectively). Symbols are sized according to the observed median reactivity (s^{-1}) of each species in the FT (Panel a) and in the PBL (Panel b, note altered size scaling from Panel a). Triangles are used when co-located circles are too close in size to distinguish, and symbols are colored according to the median absolute model bias in each case. For overlapping species, the more abundant of the two is indicated with ">".

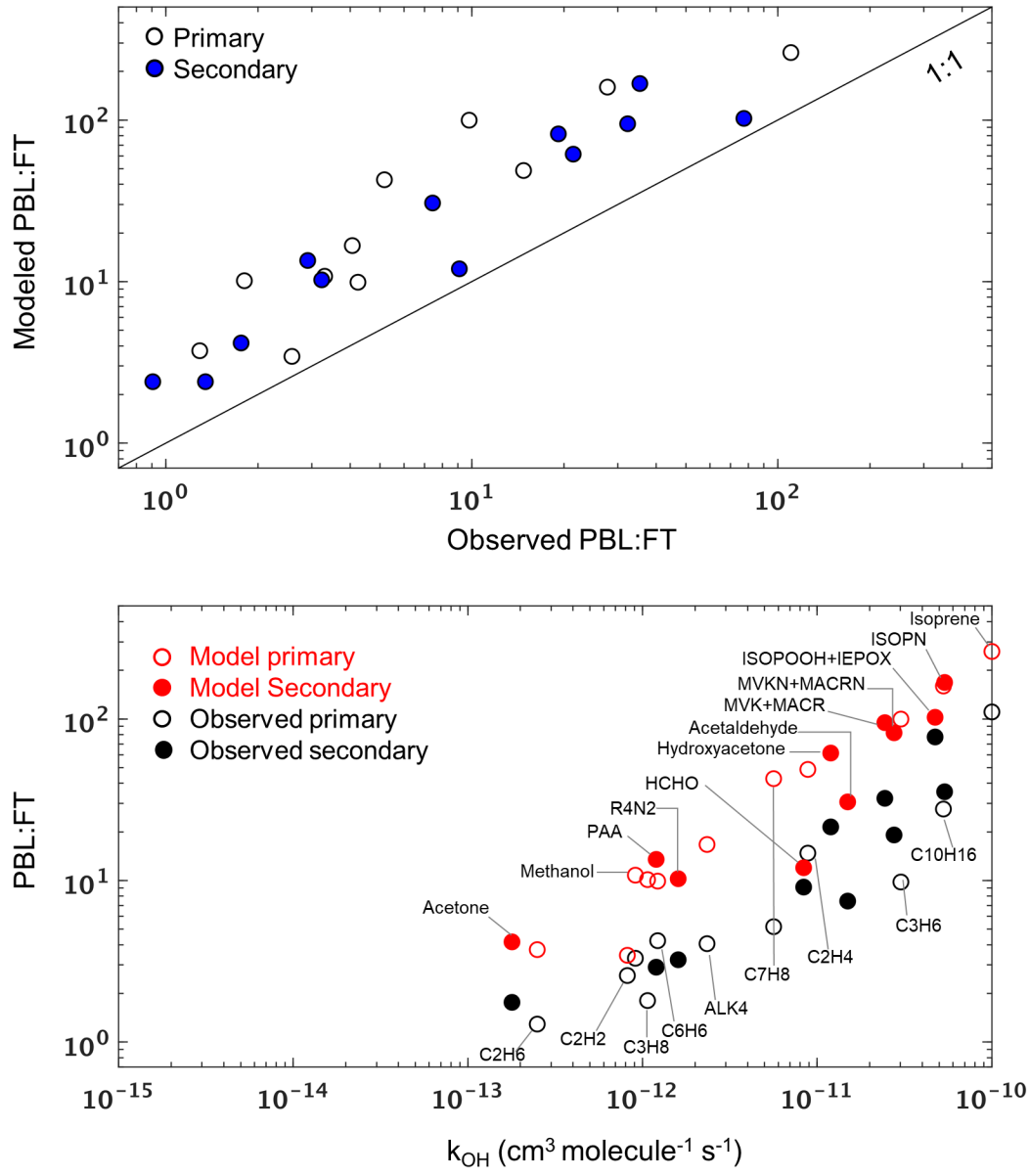

Figure 9. Top panel: Modeled versus observed mean PBL:FT ratio (mixing ratio units) for each VOC during the SEAC[4]RS campaign. Each datapoint represents a single VOC, and the 1:1 line is also shown. Bottom panel: Modeled and observed mean PBL:FT ratio for VOCs during SEAC[4]RS as a function of their OH reaction rate coefficient at 298K. In both panels, unfilled and filled symbols indicate species with predominantly primary and secondary sources, respectively.

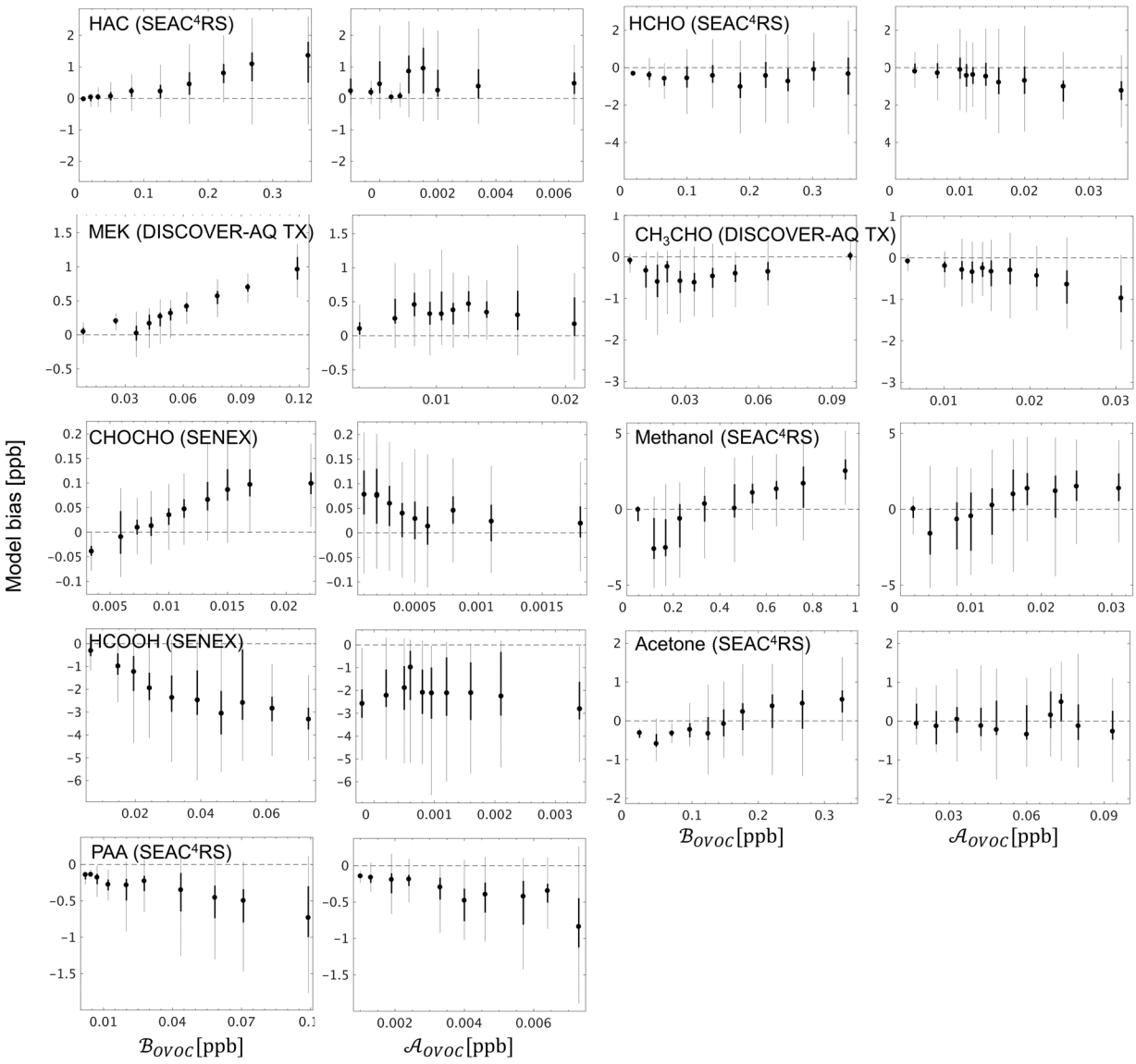

Figure 10. GEOS-Chem model bias for select OVOCs in the boundary layer (<1 km here), binned according to the contribution from biogenic ($\mathcal{B}_{OVOC}$) and anthropogenic ($\mathcal{A}_{OVOC}$) sources to the overall abundance. $\mathcal{B}_{OVOC}$ and $\mathcal{A}_{OVOC}$ represent the integrated influence of primary + secondary biogenic and anthropogenic sources (respectively) for a given OVOC along the aircraft flight track based on the model simulation, as described in-text. The 10 plotted bins each represent an equal number of datapoints for a given OVOC, with the box plots indicating the corresponding median (filled circle), interquartile range (thick line), and 99% confidence interval (thin line).

Supplement of

On the sources and sinks of atmospheric VOCs: An integrated analysis of recent aircraft campaigns over North America

Xin Chen, Dylan B. Millet et al.

Correspondence to: Dylan B. Millet (dbm@umn.edu)

Table S1. Gas-phase species and instrumentation used here.

Campaign	Species involved in this work	Measurement technique	Measurement reference
CalNex	isoprene, monoterpenes, benzene, toluene, C8 aromatics methanol, acetone, methyl ethyl ketone, formaldehyde, acetaldehyde, MVK+MACR acetonitrile	PTR-MS	de Gouw and Warneke (2007)
	2-$BuONO_2$, 3-$PenONO_2$, 2-$PenONO_2$, 3-methyl-2-$BuONO_2$ C_2H_6, C_3H_8, i-butane, n-butane, i-pentane, n-pentane, n-hexane, n-heptane, n-octane, 2,3-dimethylbutane, 2-methylpentane, 3-methylpentane, C_2H_4, propene, 1-butene, trans-2-butene, cis-2-butene, C_2H_2	WAS	Colman et al. (2001), Schauffler et al. (2003)
	PAN	CIMS	Zheng et al. (2011), Osthoff et al. (2008)
	NO, NO_2, NO_y	Gas-phase chemiluminescence	Pollack et al. (2010), Ryerson et al. (1999), Ryerson et al. (1998)
DC3 DC-8	isoprene, monoterpenes, benzene, toluene, xylene methanol, acetone, acetaldehyde, MVK+MACR acetonitrile	PTR-MS	Wisthaler et al. (2002)
	formaldehyde	DFGAS (base)	Richter et al. (2015), Weibring et al. (2010)
	formaldehyde	ISAF-LIF (sens)	Cazorla et al. (2015), DiGangi et al. (2011), Hottle et al. (2009)
	ISOPOOH+IEPOX, glycolaldehyde, hydroxyacetic acid, CH_3OOH ISOPN, PROPNN	CIT-CIMS (CF_3O^-)	Crounse et al. (2006), St Clair et al. (2010)
	2-$BuONO_2$, 3-methyl-2-$BuONO_2$, 3-$PenONO_2$, 2-$PenONO_2$ C_2H_6, C_3H_8, i-butane, n-butane, i-pentane, n-pentane, 2,3-dimethylbutane, 2-methylpentane, 3-methylpentane, n-hexane, n-heptane, 2,4-dimethylpentane, 2-methylhexane, 2,3-dimethylpentane, 3-methylhexane, 2,2,4-trimethylpentane, C_2H_4, propene, trans-2-butene, cis-2-butene, cyclopentane, methylcyclopentane, cyclohexane, methylcyclohexane, C_2H_2	WAS	Blake et al. (2003)
	PAN, PPN	CIMS	Huey (2007), Kim et al. (2007), Slusher et al. (2004)
	MPN	TD-LIF	Wooldridge et al. (2010)
	NO, NO_2, NO_y	Gas-phase chemiluminescence	Pollack et al. (2010), Ryerson et al. (1999), Ryerson et al. (1998)
DC3 GV	i-butane, n-butane, i-pentane, n-pentane, n-hexane, n-heptane, benzene, toluene, ethylbenzene+m,p-xylene, o-xylene, isoprene, alpha-pinene, camphene, beta-pinene, limonene methanol, ethanol, methyl butenol, acetone, MEK, propanal, butanal, acetaldehyde, MVK, MACR acetonitrile	TOGA	Apel et al. (2010)
	formaldehyde	CAMS	Fried et al. (2011)
	CH_3OOH	PCIMS	O'Sullivan et al. (2018)
	NO, NO_2	Gas-phase chemiluminescence	Weinheimer et al. (1994)
SENEX	isoprene, monoterpenes, benzene, toluene, xylene methanol, acetone, methyl ethyl ketone, acetaldehyde, MVK+MACR acetonitrile	PTR-MS	de Gouw and Warneke (2007)
	C_2H_6, C_3H_8, i-butane, n-butane, i-pentane, n-pentane, n-hexane, C_2H_4, propene, C_2H_2	WAS	Lerner et al. (2017), Gilman et al. (2009)
	formaldehyde	ISAF-LIF	Cazorla et al. (2015), DiGangi et al. (2011), Hottle et al. (2009)
	ISOPOOH+IEPOX ISOPN, MVKN+MACRN HCOOH, $C_2H_4O_3$, $C_3H_4O_3$, $C_3H_4O_4$, $C_5H_8O_4$, $C_9H_{14}O_4$, $C_{10}H_{16}O_3$	UW CIMS (sens)	Lee et al. (2014)
	HCOOH	NOAA CIMS (base)	
	glyoxal	ACES	Min et al. (2016)

	PAN, PPN	CIMS	_ENREF_28, Zheng et al. (2011), Osthoff et al. (2008), Slusher et al. (2004)
	NO, NO_2, NO_y	Gas-phase chemiluminescence	Pollack et al. (2010), Ryerson et al. (1999), Ryerson et al. (1998)
SEAC^{4}RS	isoprene, monoterpenes, benzene, toluene methanol, acetone, acetaldehyde, MVK+MACR acetonitrile	PTR-MS	Wisthaler et al. (2002)
	formaldehyde	CAMS (base)	Fried et al. (2011)
	formaldehyde	ISAF-LIF (sens)	Cazorla et al. (2015), DiGangi et al. (2011), Hottle et al. (2009)
	ISOPOOH+IEPOX, hydroxyacetone, peroxyacetic acid ISOPN, PROPNN, MVKN+MACRN $C_4O_4H_7N$, $C_5O_5H_9N$, BUTENE_HN	CIT-CIMS (CF_3O^-)	Crounse et al. (2006), St Clair et al. (2010)
	2-$BuONO_2$, 3-methyl-2-$BuONO_2$, 3-$PenONO_2$, 2-$PenONO_2$ C_2H_6, C_3H_8, i-butane, n-butane, i-pentane, n-pentane, neopentane, n-hexane, 2,3-dimethylbutane, 2-methylpentane, 3-methylpentane, n-heptane, C_2H_4, propene, trans-2-butene, cis-2-butene, 1-butene, i-butene, 1-pentene, C_2H_2	WAS	Blake et al. (2003)
	PAN, PPN	PAN-CIMS	Huey (2007), Kim et al. (2007), Slusher et al. (2004)
	MPN	TD-LIF	Wooldridge et al. (2010)
	NO, NO_2, NO_y	Gas-phase chemiluminescence	Pollack et al. (2010), Ryerson et al. (1999), Ryerson et al. (1998)
DISCOVER-AQ	formaldehyde	DFGAS	Richter et al. (2015), Weibring et al. (2010)
	non-methane VOCs	PTR(-ToF-)MS	Müller et al. (2016), Müller et al. (2014)
	ethane (DISCOVER-AQ CO)	TILDAS	Yacovitch et al. (2014)
	NO, NO_2, NO_y	Gas-phase chemiluminescence	Weinheimer et al. (1994)
FRAPPÉ	formaldehyde, ethane	CAMS	Fried et al. (2011)
	monoterpenes, acetonitrile methanol, acetaldehyde, acetone, isoprene, MVK+MACR, methyl ethyl ketone, benzene, toluene, C8 aromatics	PTR-MS (sens)	Kaser et al. (2013)
	methanol, acetaldehyde, acetone, isoprene, MVK, MACR, methyl ethyl ketone, benzene, toluene, ethylbenzene-m-p-xylene+o-xylene ethanol, propanal, butanal, methyl butenol C_3H_8, i-butane, n-butane, i-pentane, n-pentane, n-hexane,2-methylpentane, 3-methylpentane, n-heptane tert-butylnitrate, 2-butylnitrate-n-butylnitrate, 2-pentylnitrate-3-pentylnitrate	TOGA (base)	Apel et al. (2010)
	CH_3OOH, HCOOH, Acetic acid	PCIMS	Treadaway et al. (2018)
	C_2H_4, propene, cyclopentane, methylcyclopentane, cyclohexane, methylcyclohexane, C_2H_2	WAS	Blake et al. (2003)
	PAN, PPN	PAN-CIMS	Zheng et al. (2011)
	NO, NO_2	Gas-phase chemiluminescence	(Weinheimer et al. (1994))

7

Table S2. Sensitivity of spatially aggregated model performance for total VOC-carbon to the use of data from alternate instruments for co-measured VOCs.

	Base case[a]	DC3 LIF HCHO	SEAC4RS LIF HCHO	SENEX UW CIMS HCOOH	FRAPPÉ PTRMS VOCs	All
NMB						
FT (>3km)	-63.7%	-62.0%	-63.8%	-63.7%	-63.7%	-62.1%
PBL (<2km)	-37.2%	-36.3%	-37.3%	-37.2%	-37.3%	-36.3%
R^2						
FT (>3km)	0.066	0.097	0.067	0.065	0.066	0.098
PBL (<2km)	0.361	0.445	0.362	0.369	0.360	0.449

[a]Base case uses DC3 DFGAS HCHO, SEAC4RS CAMS HCHO, SENEX NOAA CIMS HCOOH, FRAPPÉ TOGA methanol, acetaldehyde, acetone, isoprene, MVK, MACR, MEK, benzene, toluene, C8 aromatics.

Table S3. Sensitivity of spatially aggregated model performance for total VOC reactivity to the use of data from alternate instruments for co-measured VOCs.

	Base case[a]	DC3 LIF HCHO	SEAC4RS LIF HCHO	SENEX UW CIMS HCOOH	FRAPPÉ PTRMS VOCs	All
NMB						
FT (>3km)	-62.6%	-61.9%	-63.2%	-62.6%	-62.6%	-62.5%
PBL (<2km)	-33.9%	-32.7%	-34.0%	-33.7%	-33.9%	-32.8%
R^2						
FT (>3km)	0.043	0.045	0.046	0.043	0.043	0.048
PBL (<2km)	0.542	0.629	0.542	0.547	0.542	0.631

[a]Base case uses DC3 DFGAS HCHO, SEAC4RS CAMS HCHO, SENEX NOAA CIMS HCOOH, FRAPPÉ TOGA methanol, acetaldehyde, acetone, isoprene, MVK, MACR, MEK, benzene, toluene, C8 aromatics.

Table S4. Sensitivity of campaign-aggregated mixing ratio and model bias to the use of data from alternate instruments for co-measured VOCs

		PBL			FT		
		Mixing ratio (ppbC)	Model bias (ppbC)	Model bias (%)	Mixing ratio (ppbC)	Model bias (ppbC)	Model bias (%)
Formaldehyde	base	1.930	-0.401	-22.6	0.230	-0.048	-27.8
	sens	1.944	-0.424	-23.3	0.250	-0.072	-36.9
Formic acid	base	1.006	-0.721	-76.4	0.430	-0.330	-86.3
	sens	0.972	-0.709	-75.8	0.244	-0.153	-73.5
Methanol	base	4.238	-2.135	-59.9	1.299	-0.924	-77.7
	sens	4.191	-2.062	-58.8	1.303	-0.927	-77.7
Acetaldehyde	base	1.162	-0.545	-57.3	0.185	-0.156	-91.0
	sens	1.212	-0.580	-59.3	0.186	-0.159	-91.1
Acetone	base	6.671	-2.150	-34.7	3.459	-1.761	-52.3
	sens	6.803	-2.272	-36.0	3.466	-1.776	-52.4
Isoprene	base	0.259	-0.116	-74.1	0.019	-0.018	-100.0
	sens	0.309	-0.155	-78.1	0.020	-0.019	-100.0
MVK+MACR	base	0.424	-0.165	-58.5	0.035	-0.031	-99.7
	sens	0.450	-0.177	-58.5	0.035	-0.031	-99.7
MEK	base	0.636	0.240	43.4	0.167	-0.077	-75.5
	sens	0.697	0.187	34.9	0.168	-0.078	-76.4
Benzene	base	0.291	-0.095	-38.9	0.108	-0.073	-72.9
	sens	0.298	-0.105	-40.6	0.108	-0.074	-73.0
Toluene	base	0.210	0.041	13.6	0.026	-0.021	-97.8
	sens	0.221	0.039	8.6	0.026	-0.021	-97.8
Xylene	base	0.112	-0.039	-59.5	0.014	-0.013	-100.0
	sens	0.126	-0.052	-62.9	0.015	-0.015	-100.0

Table S5. Sensitivity of campaign-aggregated reactivity and model bias to the use of data from alternate instruments for co-measured VOCs

		PBL			FT		
		Reactivity (s^{-1})	Model bias (s^{-1})	Model bias (%)	Reactivity (s^{-1})	Model bias (s^{-1})	Model bias (%)
Formaldehyde	base	0.343	-0.071	-22.6	0.023	-0.004	-26.7
	sens	0.346	-0.076	-23.3	0.026	-0.007	-35.8
Formic acid	base	0.009	-0.006	-76.4	0.003	-0.002	-86.3
	sens	0.009	-0.006	-75.8	0.002	-0.001	-73.5
Methanol	base	0.080	-0.039	-59.2	0.010	-0.008	-77.2
	sens	0.080	-0.038	-58.2	0.010	-0.008	-77.2
Acetaldehyde	base	0.191	-0.087	-57.4	0.018	-0.015	-90.7
	sens	0.198	-0.093	-59.3	0.018	-0.016	-90.8
Acetone	base	0.008	-0.003	-34.6	0.002	-0.001	-52.1
	sens	0.008	-0.003	-36.0	0.002	-0.001	-52.3
Isoprene	base	0.111	-0.050	-74.1	0.006	-0.005	-100.0
	sens	0.130	-0.066	-78.1	0.006	-0.005	-100.0
MVK+MACR	base	0.052	-0.021	-58.5	0.003	-0.003	-99.7
	sens	0.055	-0.022	-58.2	0.003	-0.003	-99.7
MEK	base	0.004	0.001	40.6	0.001	-0.000	-72.3
	sens	0.005	0.001	34.7	0.001	-0.000	-73.2
Benzene	base	0.001	-0.000	-38.1	0.000	-0.000	-73.3
	sens	0.001	-0.000	-40.6	0.000	-0.000	-73.4
Toluene	base	0.004	0.001	13.7	0.000	-0.000	-97.7
	sens	0.004	0.001	8.6	0.000	-0.000	-97.8
Xylene	base	0.007	-0.002	-59.5	0.001	-0.000	-100.0
	sens	0.008	-0.003	-62.9	0.001	-0.001	-100.0

Table S6. Correlation between observed OVOCs and model-derived biogenic ($\mathcal{B}_{OVOC}$) and anthropogenic ($\mathcal{A}_{OVOC}$) contributions.

	SEAC^{4}RS	SENEX	DISCOVER-AQ TX	Other campaigns
Acetaldehyde	0.71	0.62	0.65	
Formaldehyde	0.71	0.71	0.63	
Acetone	0.87	0.70	0.68	
MEK	n/a	0.68	0.62	
PAA	0.85	n/a	n/a	
Methanol	0.55	0.73	0.53	
MVK	0.74	0.75	0.82	<0.50
MACR	0.75	0.75	0.78	
HCOOH	n/a	0.79	n/a	
Acetic acid	n/a	n/a	0.44	
Glyoxal	n/a	0.79	n/a	
Glycolaldehyde	n/a	n/a	0.63	
Hydroxyacetone	0.80	n/a	n/a	

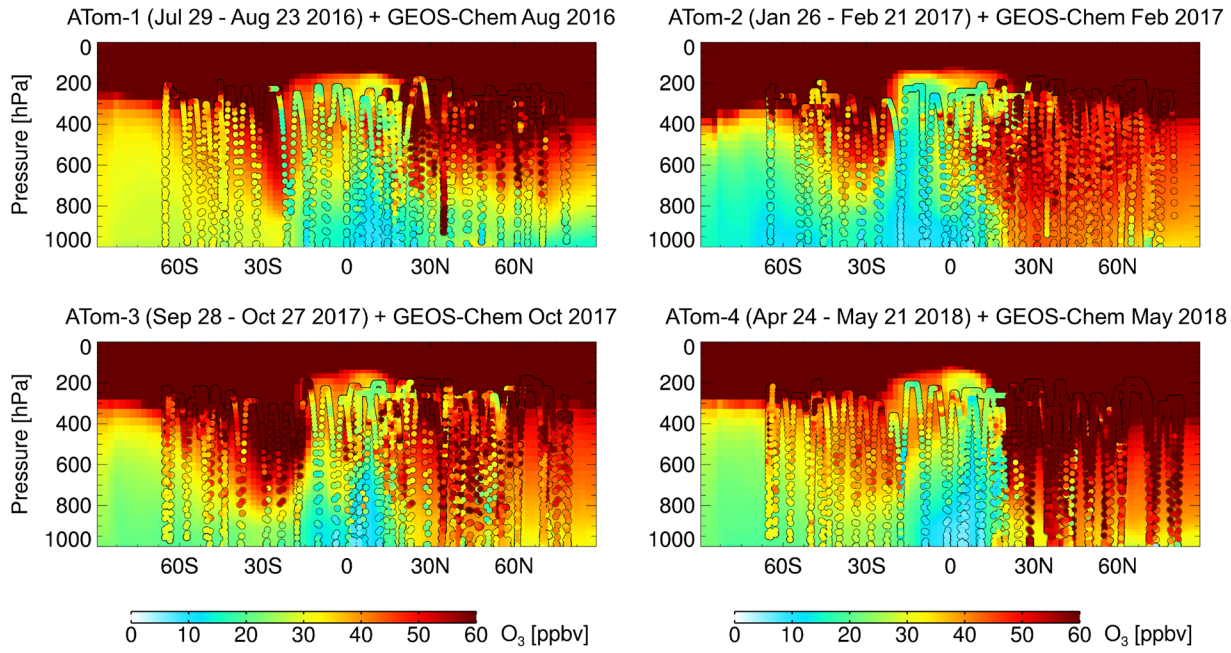

Figure S1. Ozone over the Pacific Ocean. Colored circles show airborne observations from the Atmospheric Tomography Mission (ATom) (Wofsy et al., 2018) within 100°W-170°E. Plotted in the background is the monthly mean ozone curtain simulated by GEOS-Chem (global simulation at 2°×2.5°) at ~177.5°W for the corresponding month.

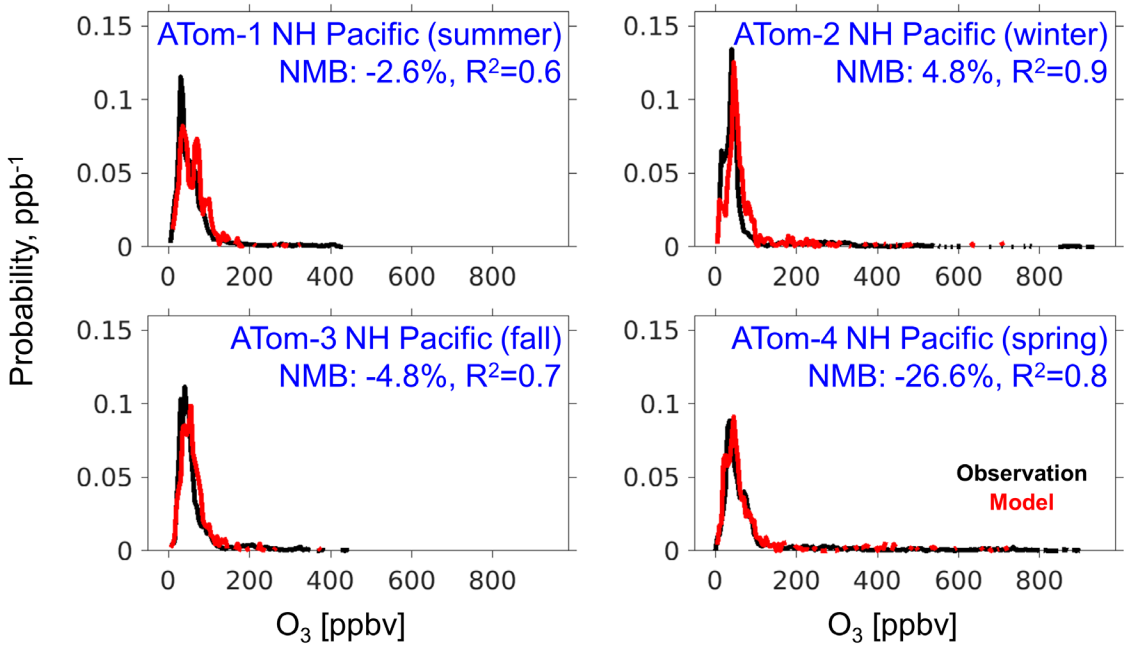

Figure S2. Ozone probability density functions over the northern Pacific (100°W-170°E, 0°-90°N). Plotted are ATom observations (black) and co-located GEOS-Chem model predictions (red), with correlations and normalized mean biases given inset.

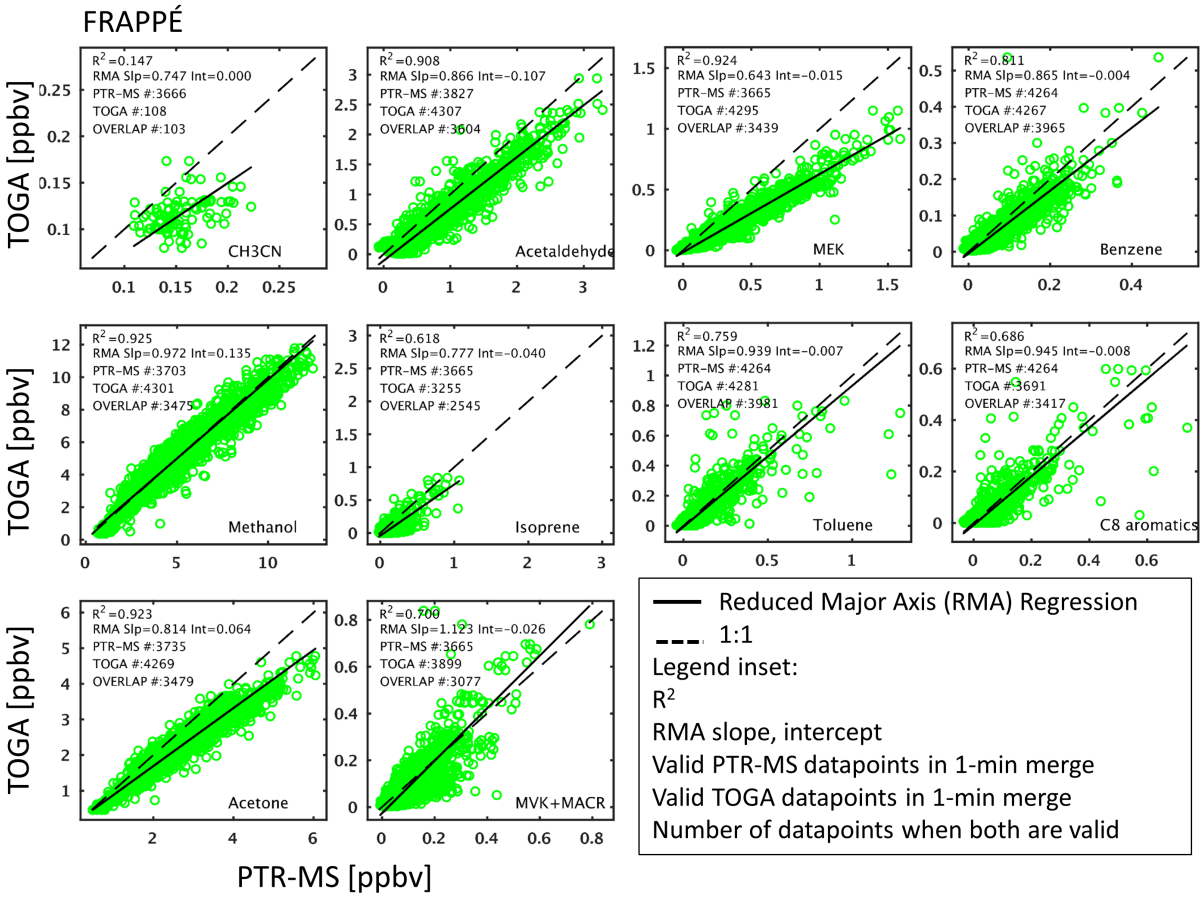

Figure S~~18~~. Inter-comparison of co-measured VOCs from FRAPPÉ.

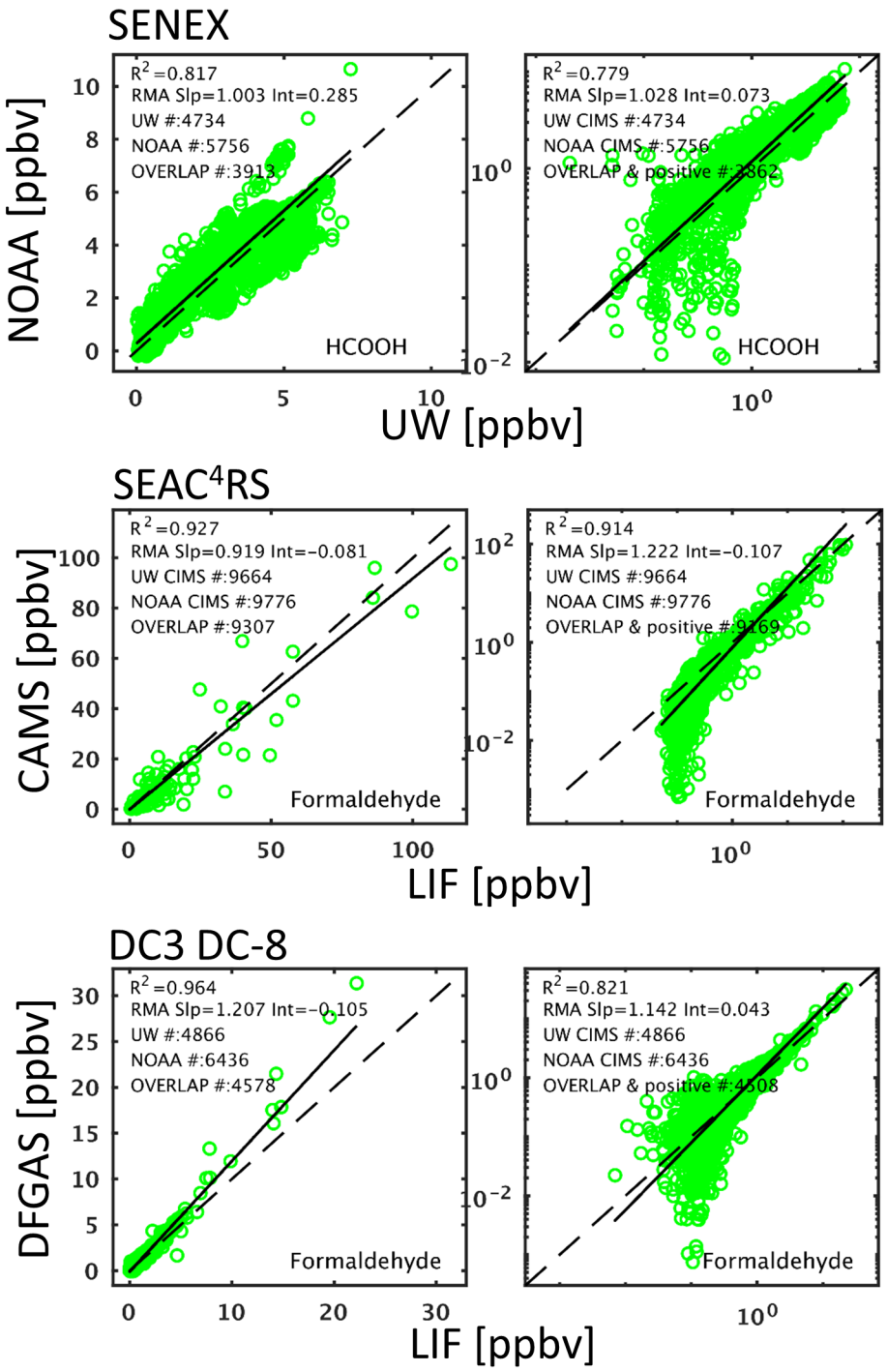

Figure S~~19~~. Inter-comparison of concurrent HCOOH measurements during SENEX and of concurrent formaldehyde measurements during DC3 DC-8 and SEAC^{4}RS. See legends in Figure S18.

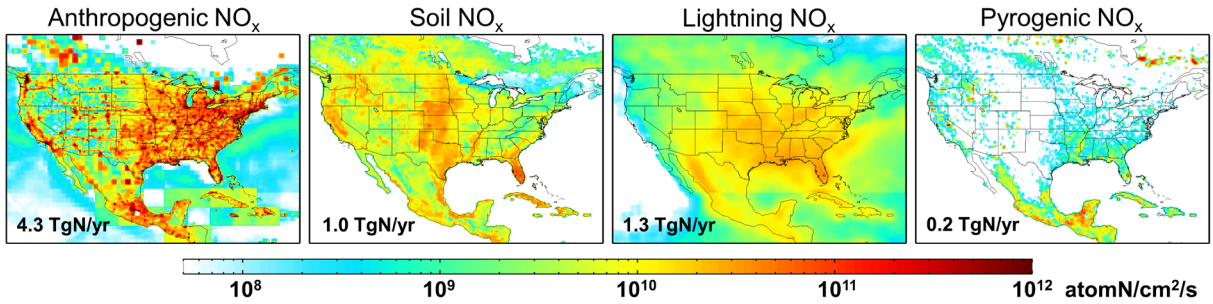

Figure S5. Annual NO_x emissions fluxes over North America as simulated by GEOS-Chem for 2013.

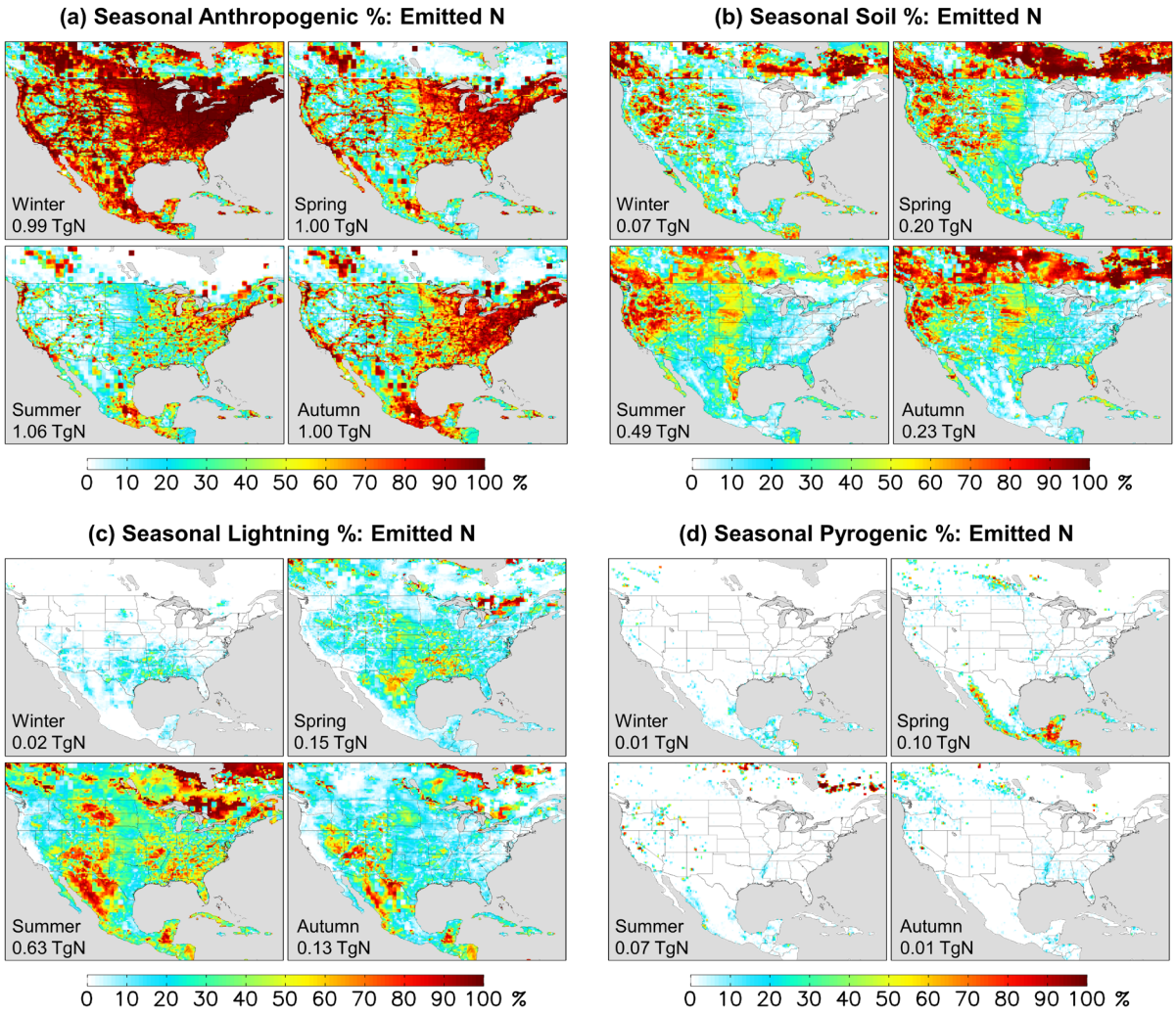

Figure S6. Seasonal contribution of each emission sector to total modeled NO_x emissions.

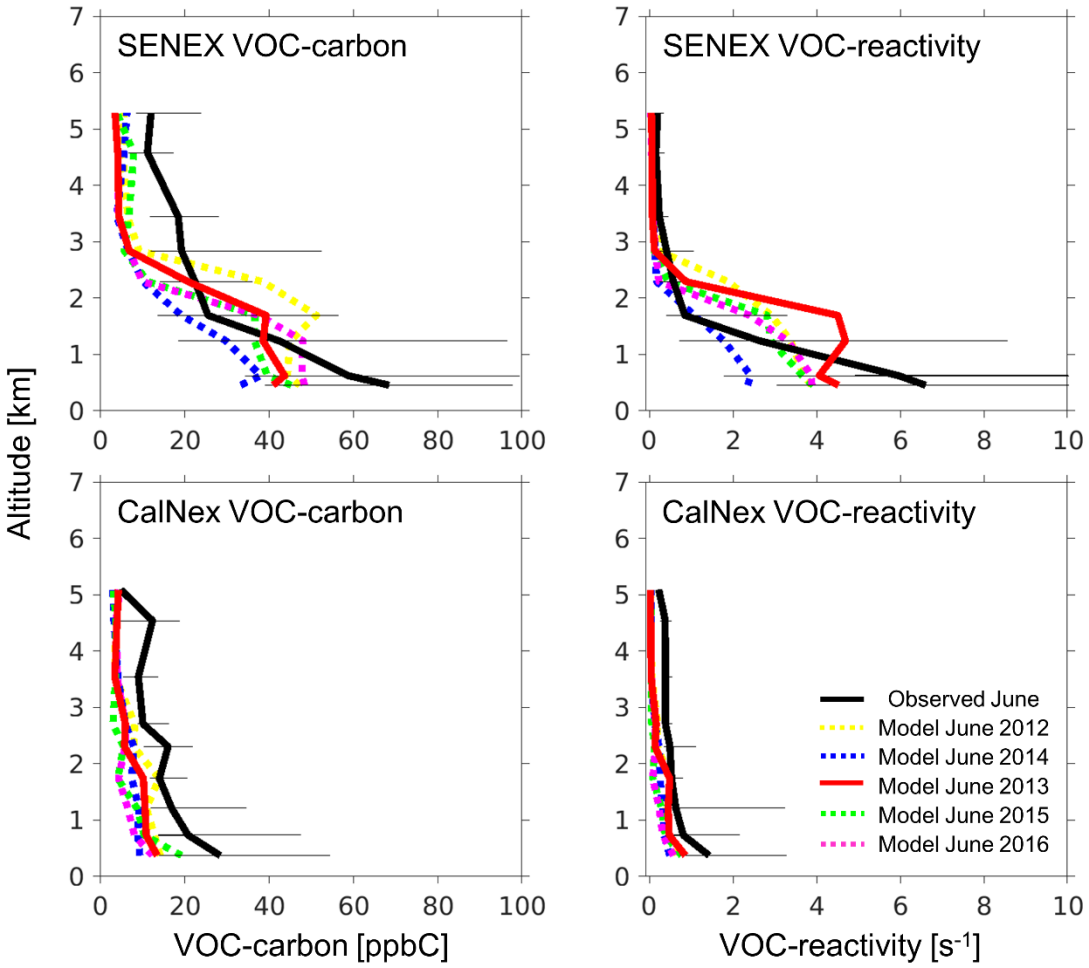

Figure S7. Vertical VOC-carbon and reactivity profiles as measured in 2013 and simulated by GEOS-Chem for June of 2012-2016 along the SENEX and CalNex aircraft flight tracks. Plotted are the observed (solid black lines) and predicted (2013: solid red lines; other years: dashed lines) median profiles, with horizontal bars indicating the 5th-95th percentiles measured for each vertical bin. Bin resolution is 0.5km below 3km and 1km above 3km. VOCs included in the profile correspond to the species shown in Fig. S17 (CalNex) and S18 (SENEX).

Given the range in measurement years spanned by the aircraft measurements, we performed a set of one-month simulations spanning 5 different years (June for 2012-2016) to assess the potential impact of interannual variability on these findings. Results are shown in Fig. S1 for the CalNex and SENEX flight tracks. In both cases the model-measurement VOC-C differences are highly consistent across years. We see a higher degree of interannual variability for VOC-reactivity over the SENEX domain, reflecting year-to-year differences in biogenic VOC emissions over this region. However, the key features of the comparison (a model underestimate near-surface, overly-flat vertical profile within the PBL, and strong FT underestimate) are consistent between our simulation year (2013) and the other four years.

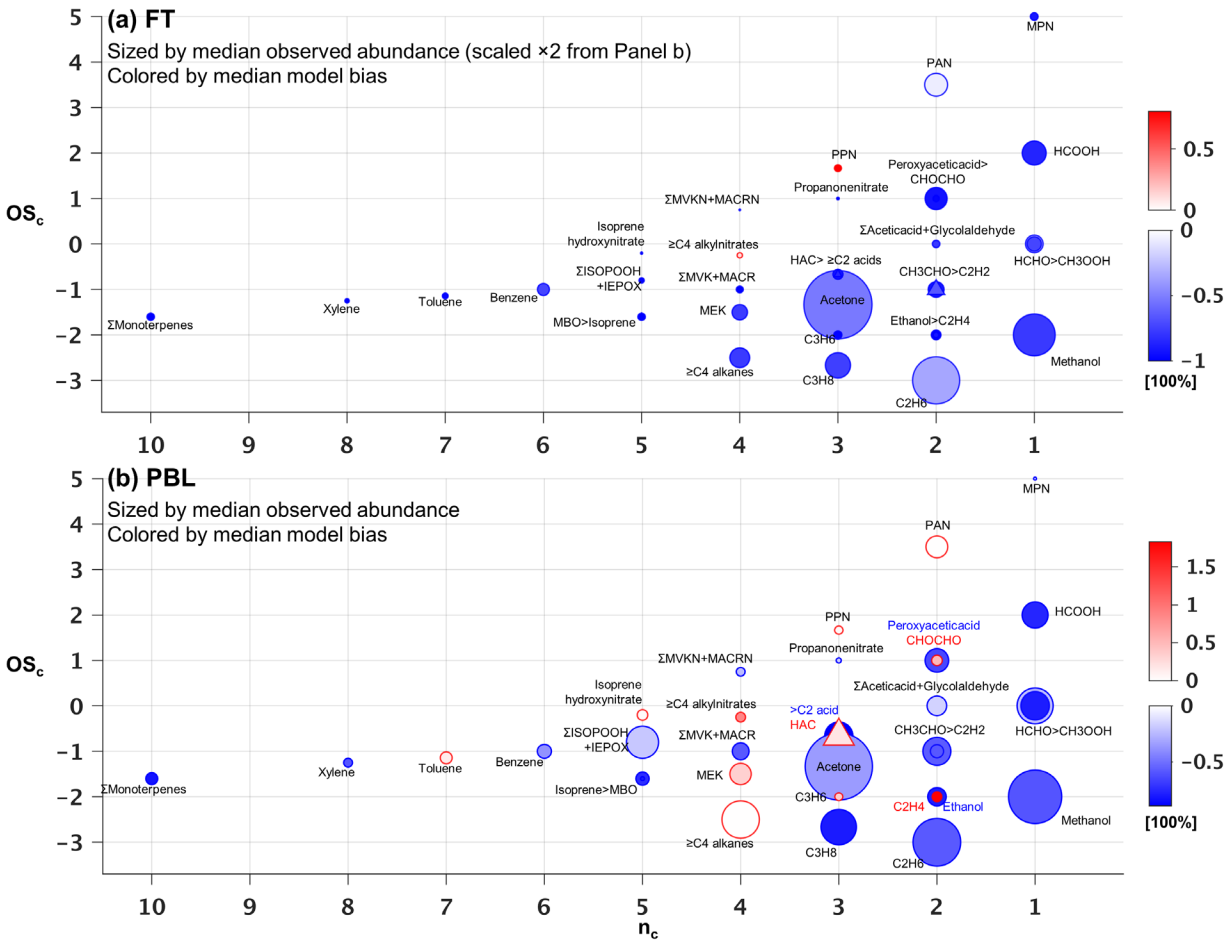

Figure S81. Same as Figure 5, but with the color shaded indicating the median relative model bias.

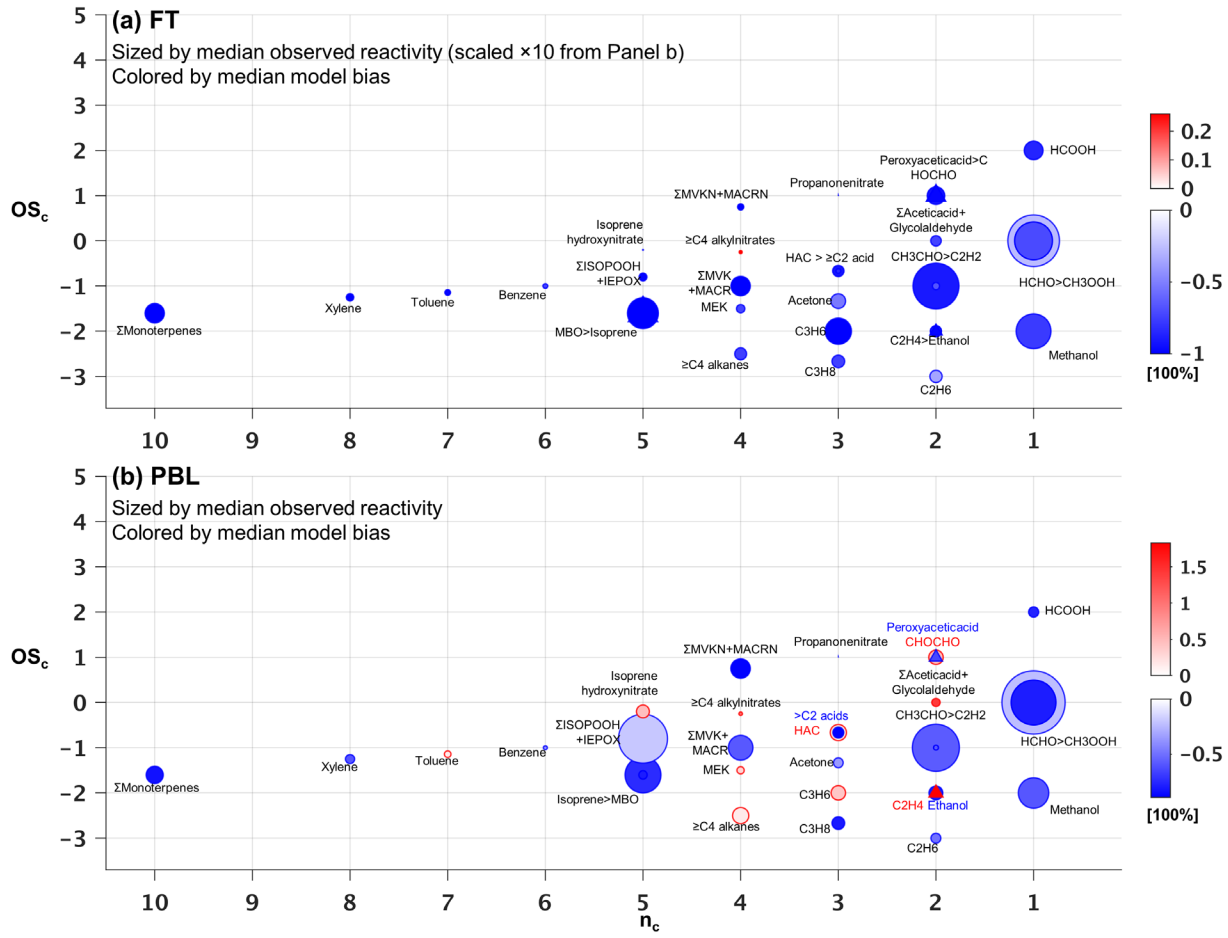

Figure S92. Same as Figure 6, but with the color shaded indicating the median relative model bias. Note that the relative model bias in VOC-carbon for a given species is identical to that for OH reactivity, except in the case of lumped or co-measured species.

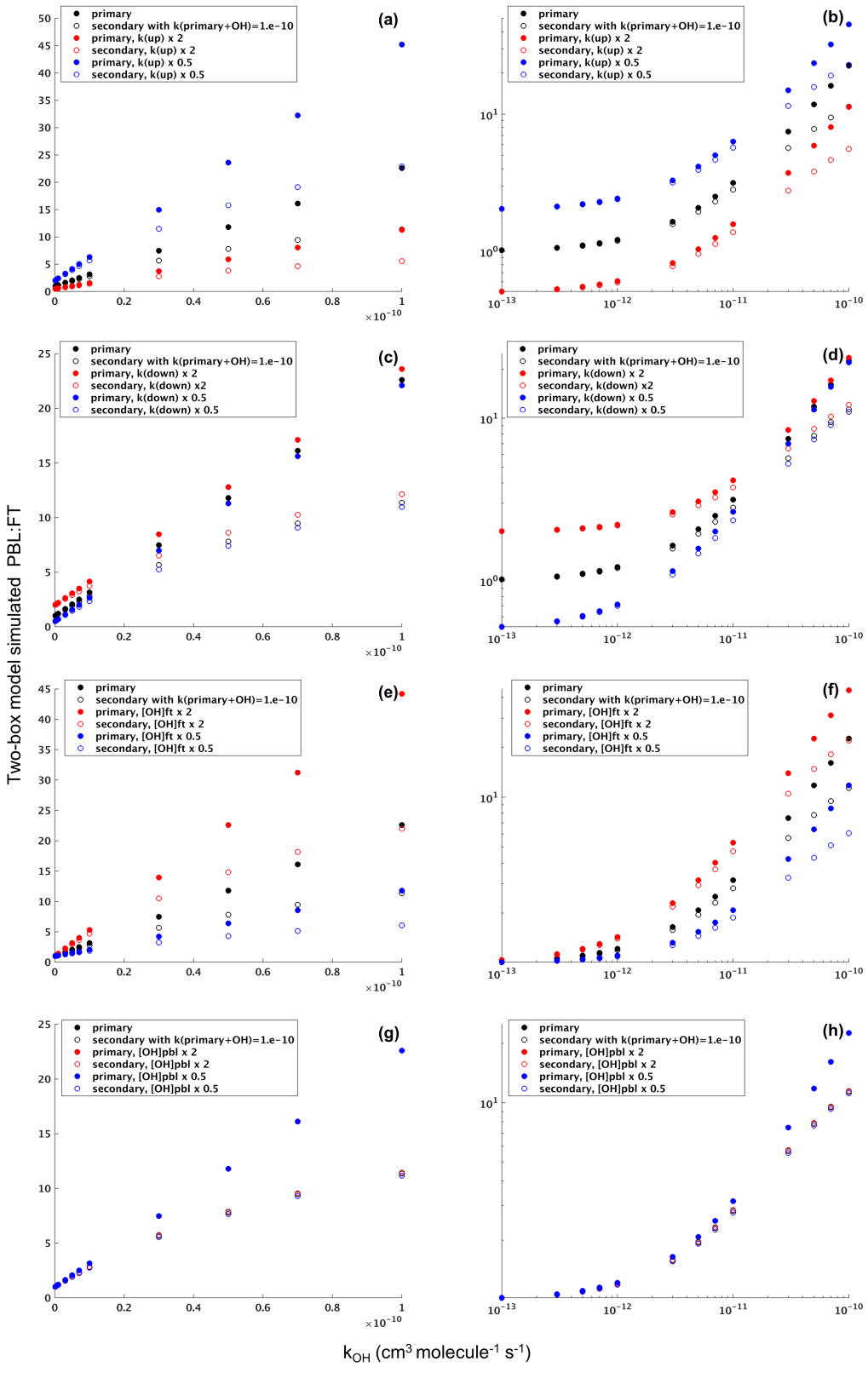

Figure S103. Sensitivity of the PBL:FT concentration ratio for primary and secondary VOCs to PBL-FT exchange rates, OH, and reactivity, based on a simple two-box model. See main text.

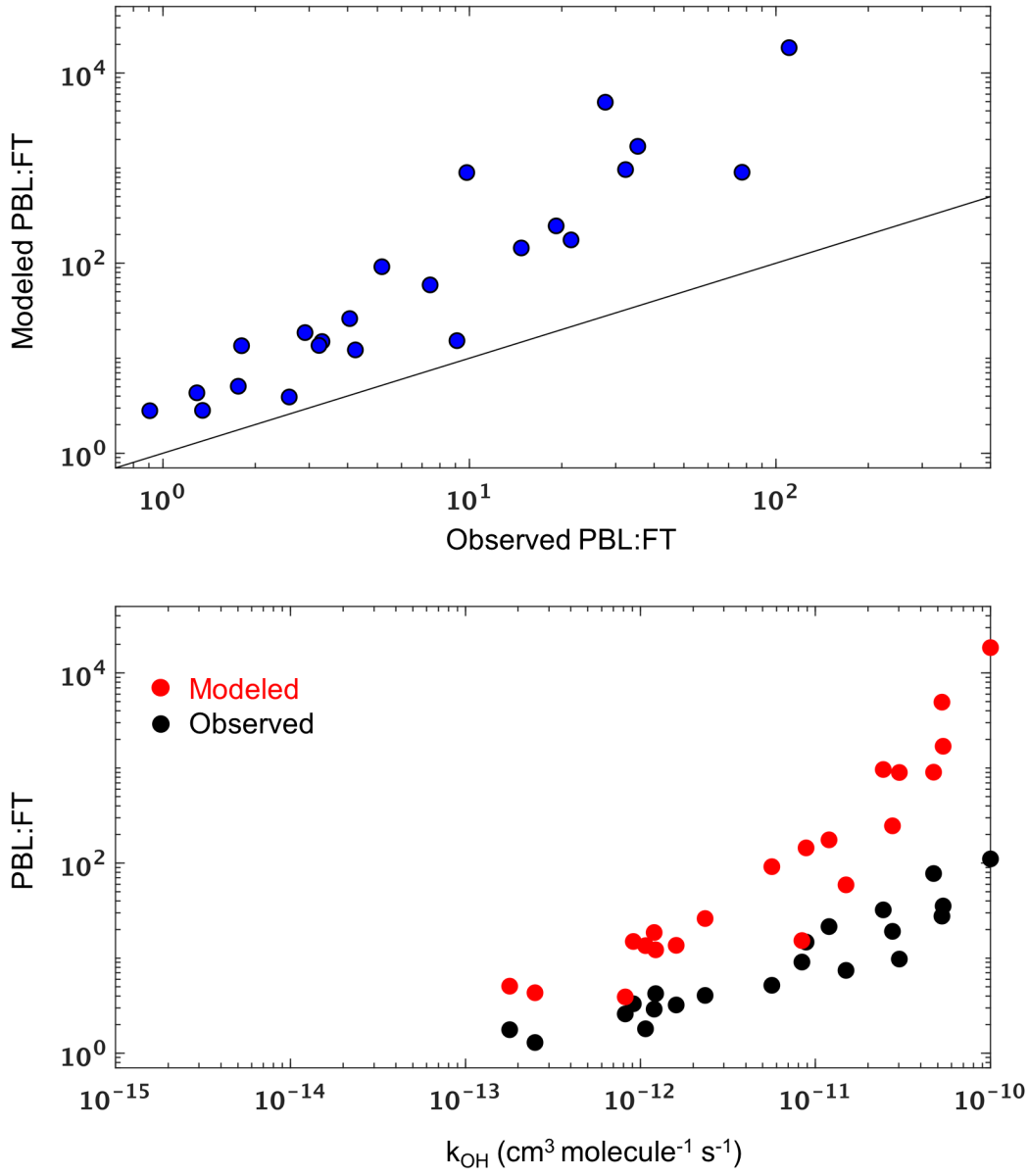

Figure S114. Same as Figure 9, but with model results from a sensitivity simulation with 40% reduced PBL depths.

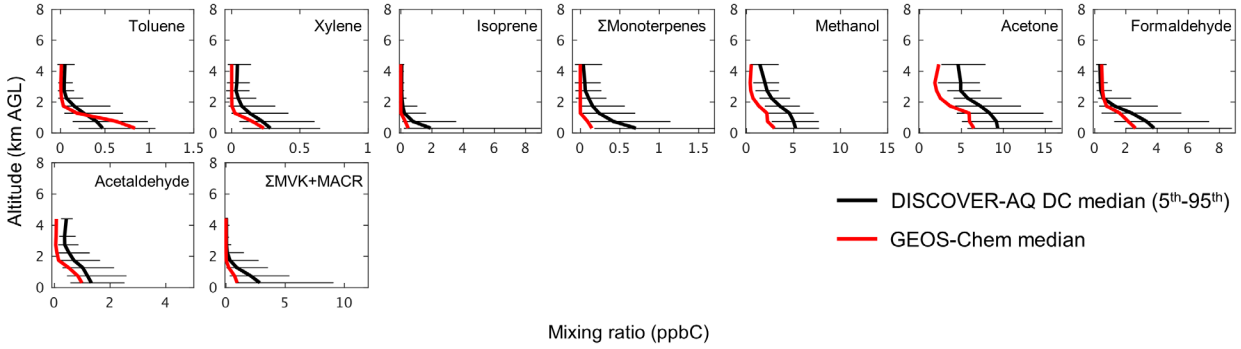

Figure S125. Vertical VOC profiles as measured and simulated by GEOS-Chem during the DISCOVER-AQ DC aircraft campaign. Plotted are the observed (black) and predicted (red) median profiles (in ppbC), with horizontal bars indicating the 5th - 95th percentiles measured for each bin. The vertical bin resolution is 0.5km below 3km and 1km above 3km. Fresh biomass burning and pollution plumes have been filtered out as described in-text.

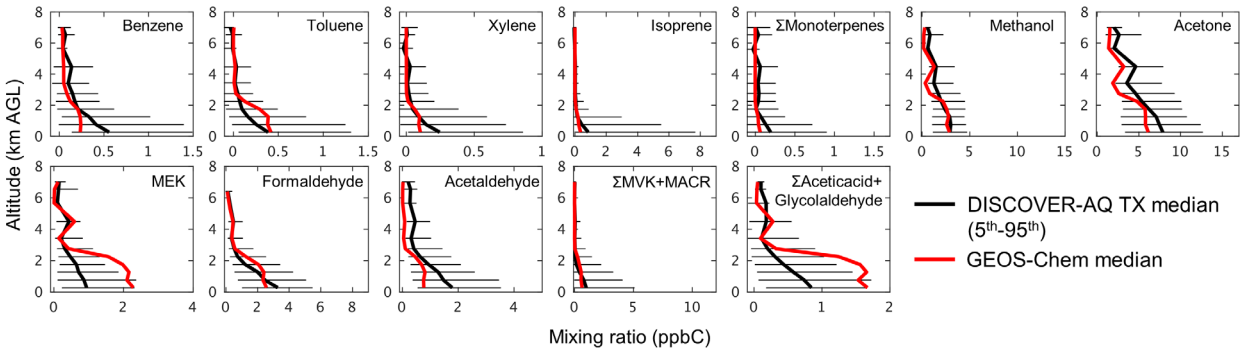

Figure S136. Same as Figure S5 but for the DISCOVER-AQ TX aircraft campaign.

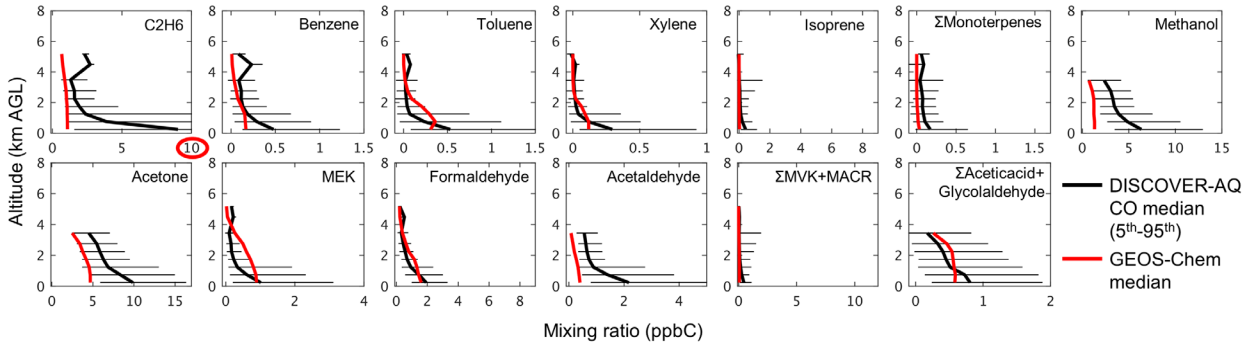

Figure S147. Same as Figure S5 but for the DISCOVER-AQ CO aircraft campaign. Red circles indicate axis scales that differ from others for the same compound in Fig. S5, 6, 9, 10.

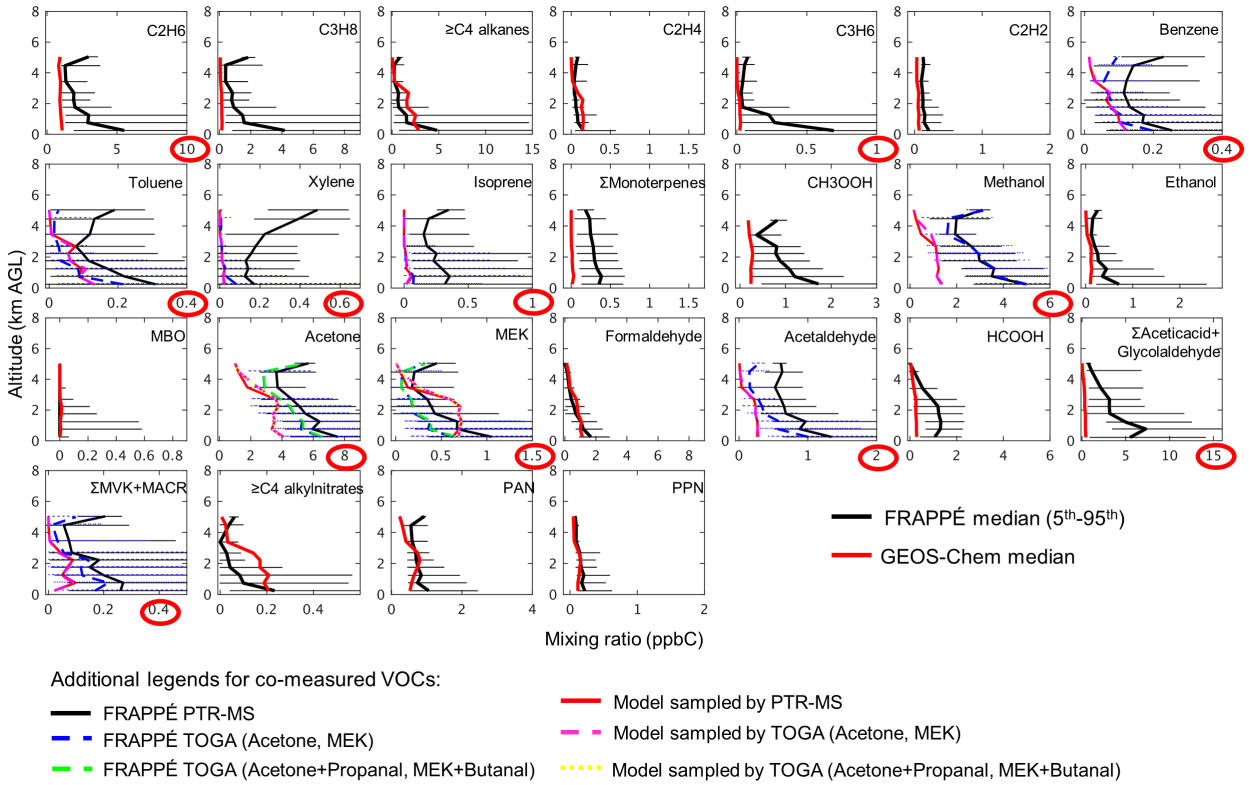

92

93 **Figure S158. Same as Figure S5 but for the FRAPPÉ aircraft campaign. Red circles indicate axis scales that**
94 **differ from others for the same compound in Fig. S5, 6, 9, 10.**

95

96

97

98

99

100

101

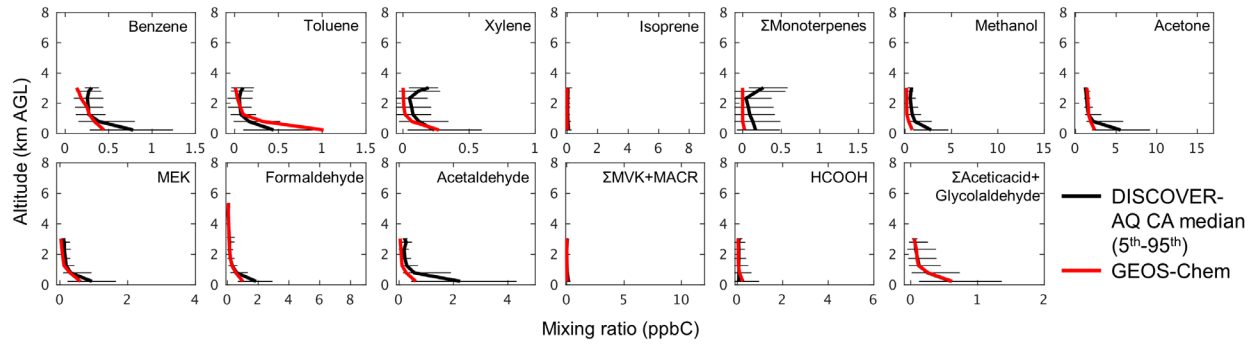

102

103 **Figure S169. Same as Figure S5 but for the DISCOVER-AQ CA aircraft campaign.**

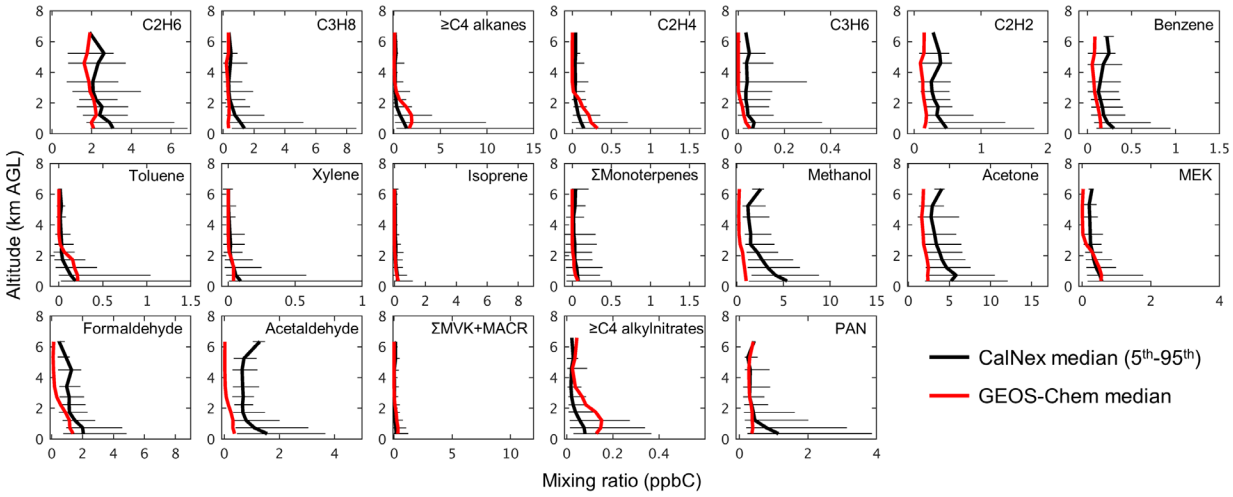

Figure S17. Same as Figure S5 but for the CalNex aircraft campaign.

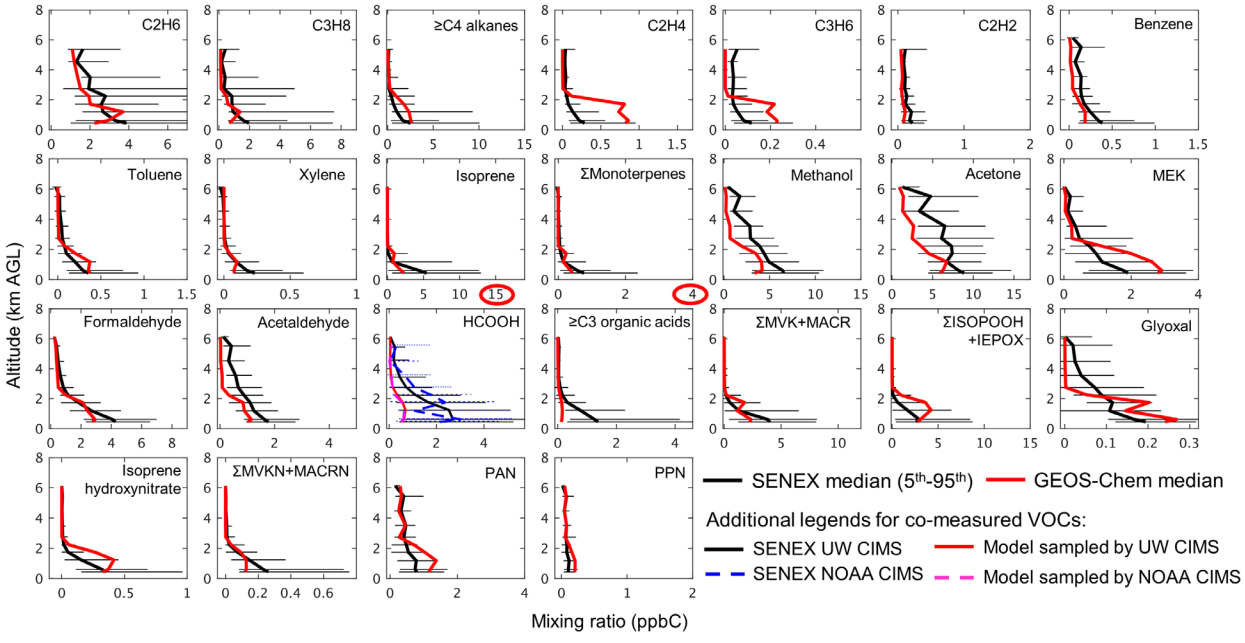

Figure S18. Same as Figure S5 but for the SENEX aircraft campaign. Red circles indicate axis scales that differ from others for the same compound in Figures S5, 6, 9, 10.

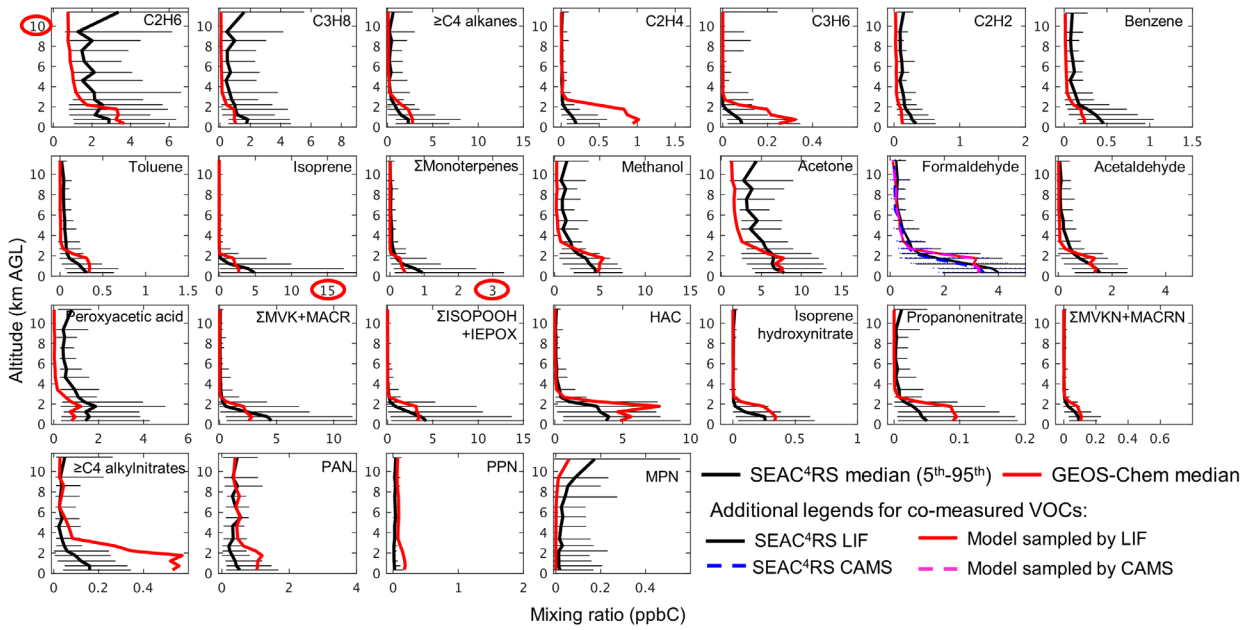

Figure S192. Same as Figure S5 but for the SEAC⁴RS aircraft campaign. Red circles indicate axis scales that differ from others for the same compound in Figures S5, 6, 9, 10.

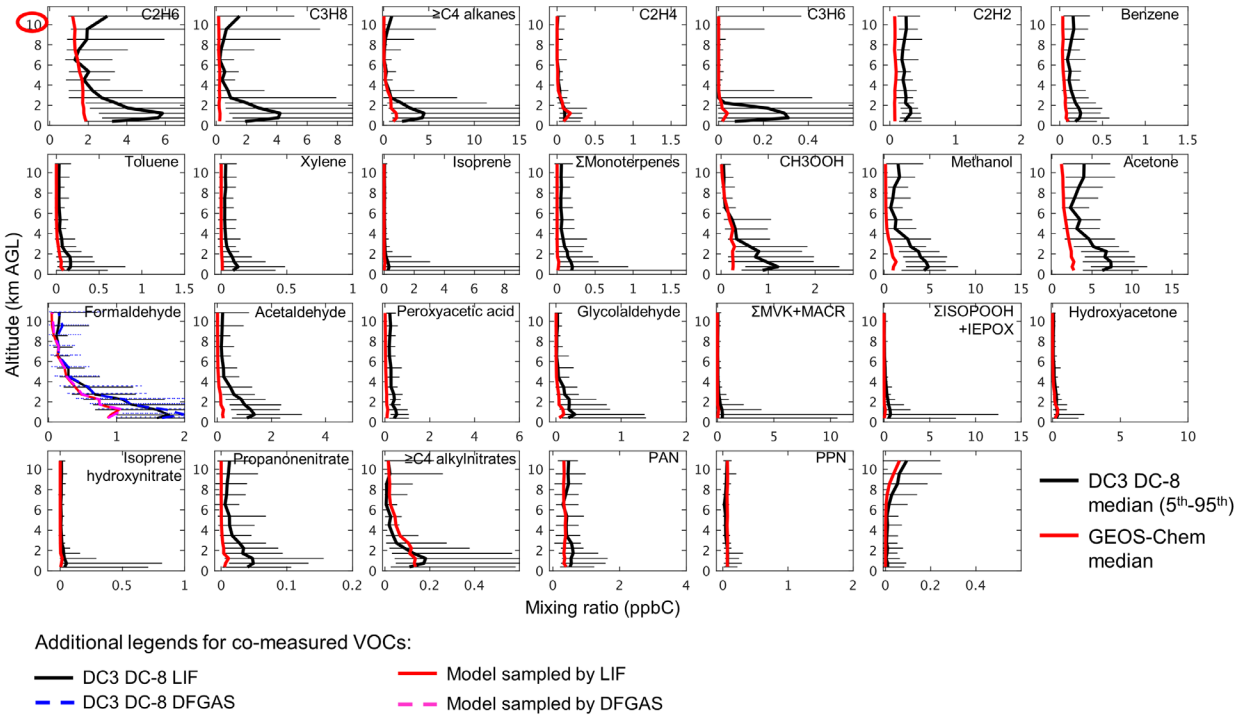

Figure S2013. Same as figure S5 but for the DC3 DC-8 aircraft observation. Red circles indicate axis scales that differ from others for the same compound in Figures S5, 6, 9, 10.

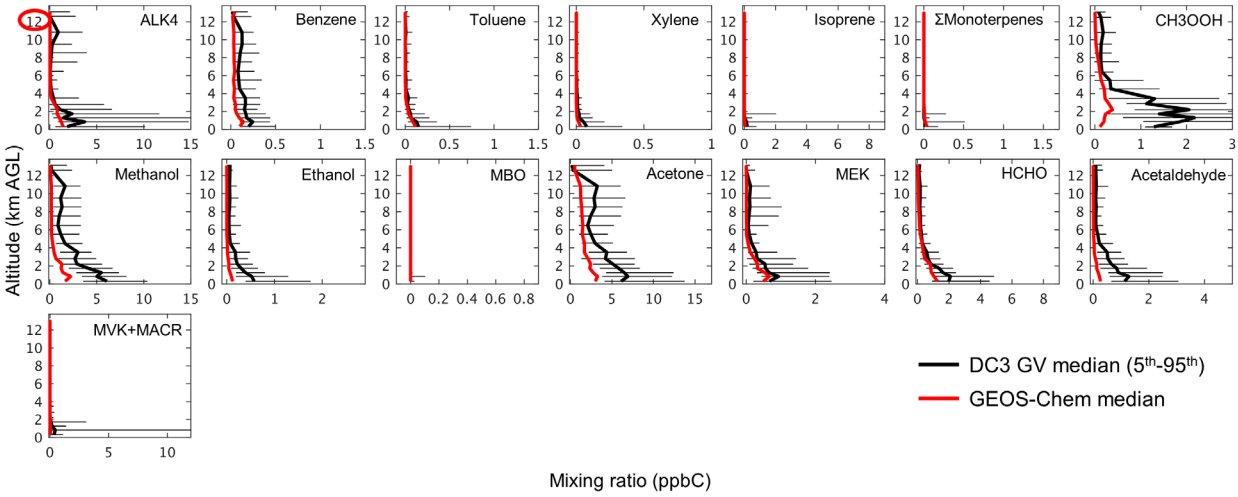

Figure S2114. Same as figure S5 but for the DC3 GV aircraft observation. Red circles indicate axis scales that differ from others for the same compound in Figures S5, 6, 9, 10.

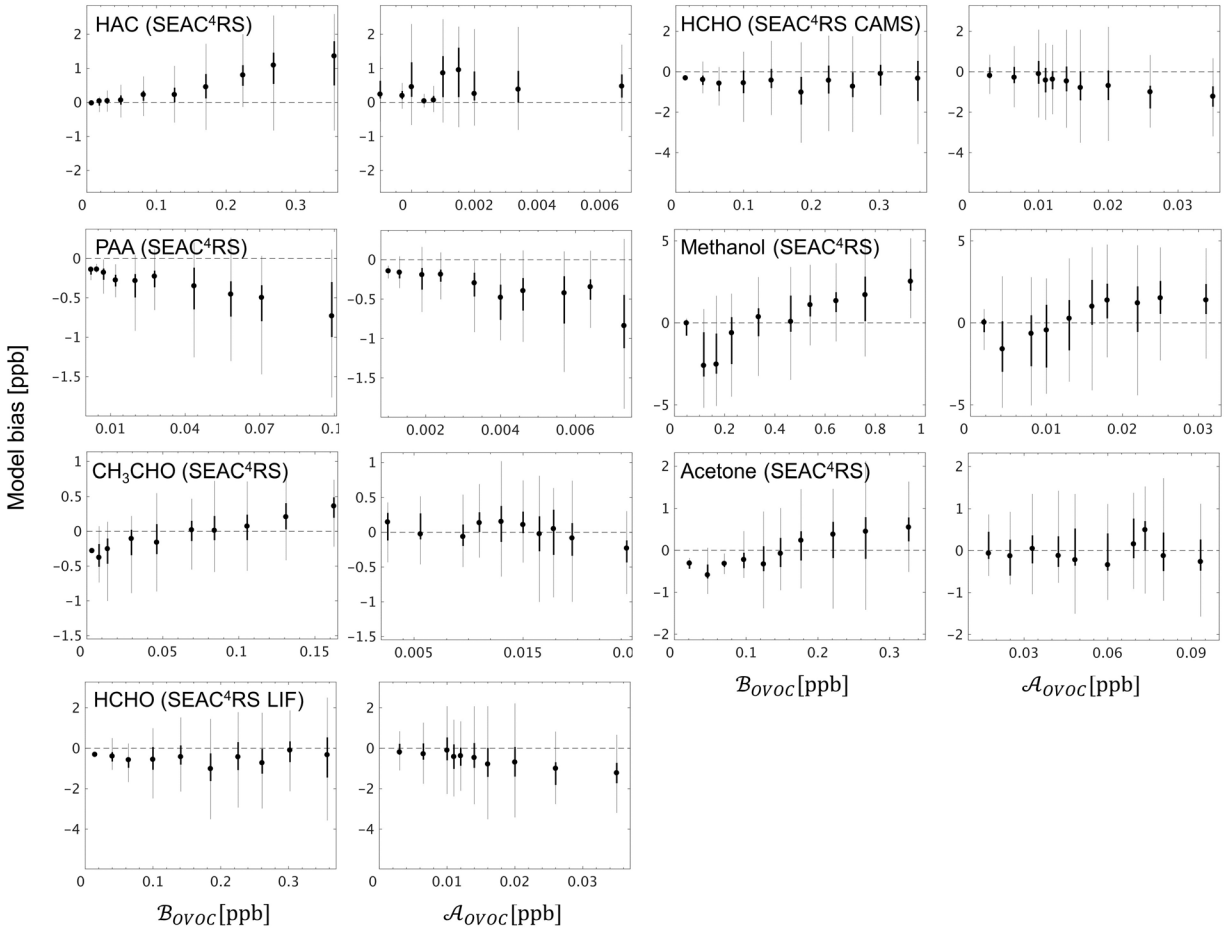

~~**Figure S15. Same as Figure 10 but for the SEAC⁴RS campaign.**~~

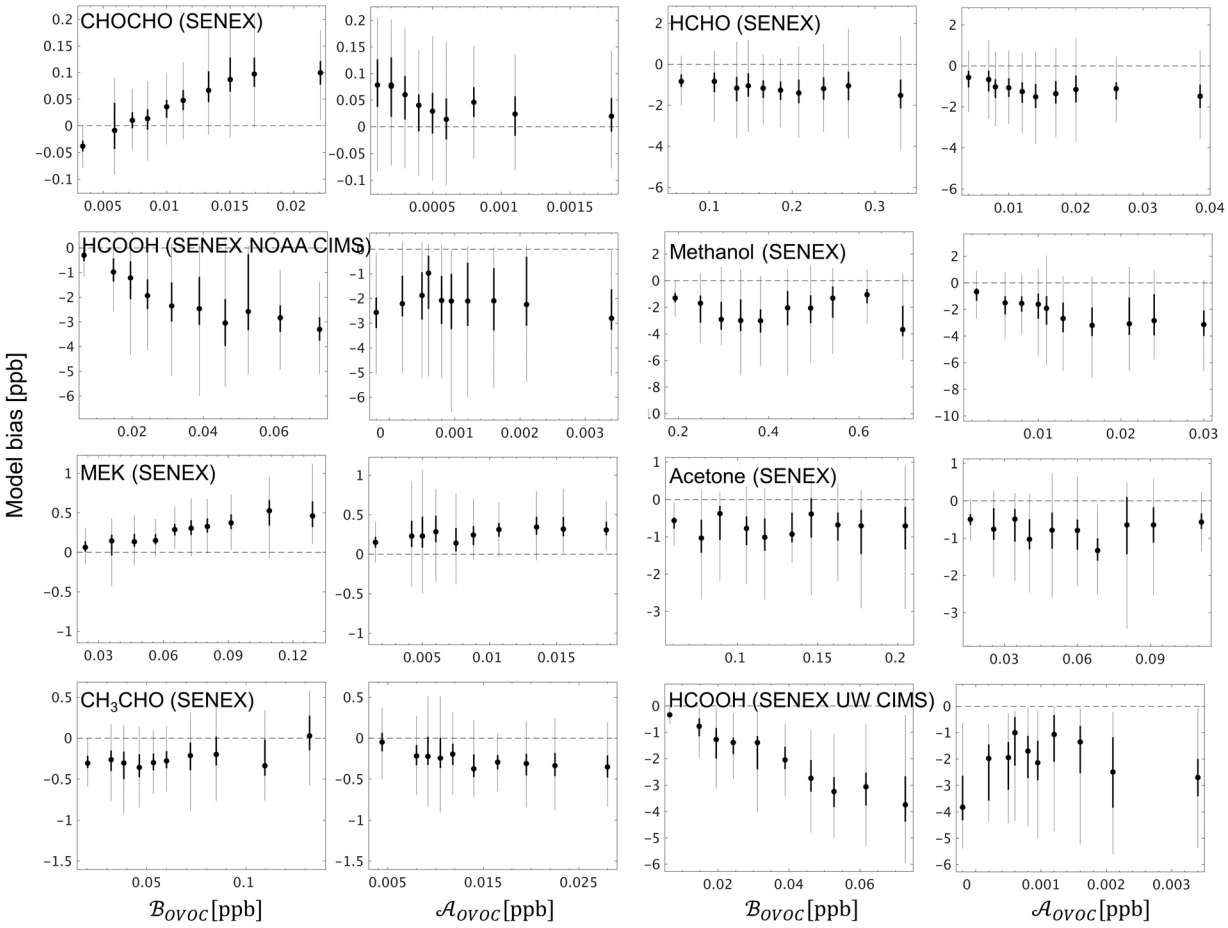

131

132 **Figure S22~~16~~. Same as Figure 10 but for the SENEX campaign.**

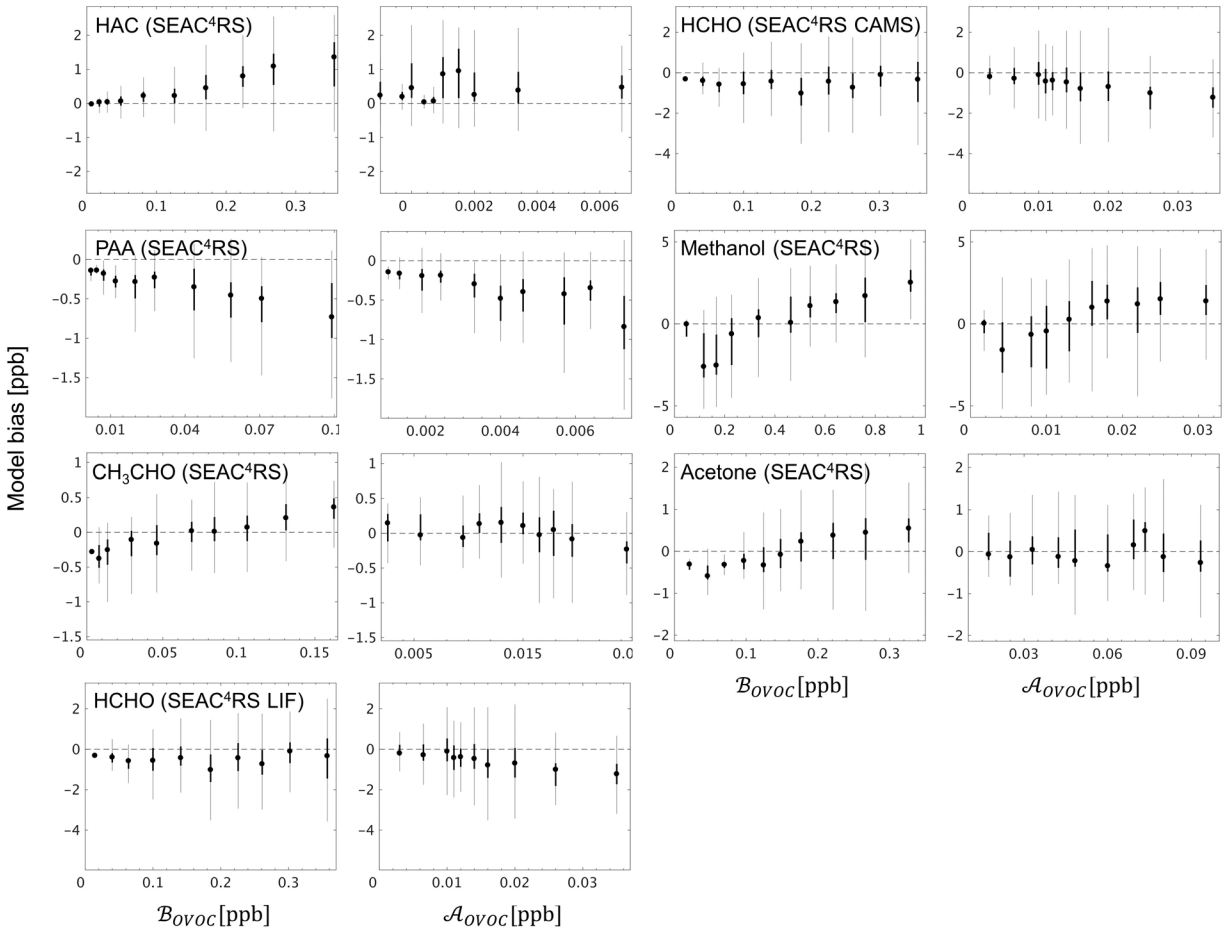

Figure S23. Same as Figure 10 but for the SEAC⁴RS campaign.

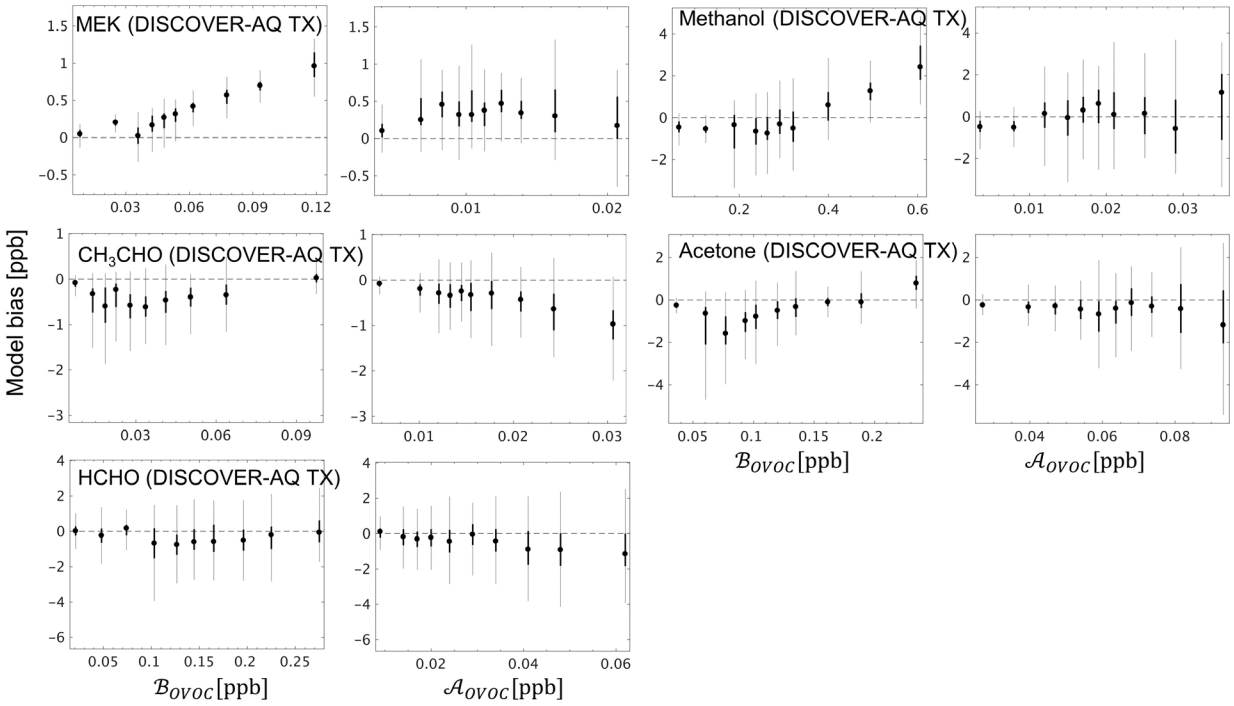

Figure S2417. Same as Figure 10 but for the DISCOVER-AQ TX campaign.

References

Apel, E. C., Emmons, L. K., Karl, T., Flocke, F., Hills, A. J., Madronich, S., Lee-Taylor, J., Fried, A., Weibring, P., Walega, J., Richter, D., Tie, X., Mauldin, L., Campos, T., Weinheimer, A., Knapp, D., Sive, B., Kleinman, L., Springston, S., Zaveri, R., Ortega, J., Voss, P., Blake, D., Baker, A., Warneke, C., Welsh-Bon, D., de Gouw, J., Zheng, J., Zhang, R., Rudolph, J., Junkermann, W., and Riemer, D. D.: Chemical evolution of volatile organic compounds in the outflow of the Mexico City Metropolitan area, Atmos. Chem. Phys., 10, 2353-2375, https://doi.org/10.5194/acp-10-2353-2010, 2010.

Blake, N. J., Blake, D. R., Swanson, A. L., Atlas, E., Flocke, F., and Rowland, F. S.: Latitudinal, vertical, and seasonal variations of C1-C4 alkyl nitrates in the troposphere over the Pacific Ocean during PEM-Tropics A and B: Oceanic and continental sources, J. Geophys. Res. Atmos., 108, https://doi.org/10.1029/2001jd001444, 2003.

Cazorla, M., Wolfe, G. M., Bailey, S. A., Swanson, A. K., Arkinson, H. L., and Hanisco, T. F.: A new airborne laser-induced fluorescence instrument for in situ detection of formaldehyde throughout the troposphere and lower stratosphere, Atmos. Meas. Tech., 8, 541-552, https://doi.org/10.5194/amt-8-541-2015, 2015.

Colman, J. J., Swanson, A. L., Meinardi, S., Sive, B. C., Blake, D. R., and Rowland, F. S.: Description of the analysis of a wide range of volatile organic compounds in whole air samples collected during PEM-tropics A and B, Anal. Chem., 73, 3723-3731, https://doi.org/10.1021/ac010027g, 2001.

Crounse, J. D., McKinney, K. A., Kwan, A. J., and Wennberg, P. O.: Measurement of gas-phase hydroperoxides by chemical ionization mass spectrometry, Anal. Chem., 78, 6726-6732, https://doi.org/10.1021/ac0604235, 2006.

de Gouw, J., and Warneke, C.: Measurements of volatile organic compounds in the earth's atmosphere using proton-transfer-reaction mass spectrometry, Mass Spectrom. Rev., 26, 223-257, https://doi.org/10.1002/mas.20119, 2007.

DiGangi, J. P., Boyle, E. S., Karl, T., Harley, P., Turnipseed, A., Kim, S., Cantrell, C., Maudlin, R. L., Zheng, W., Flocke, F., Hall, S. R., Ullmann, K., Nakashima, Y., Paul, J. B., Wolfe, G. M., Desai, A. R., Kajii, Y., Guenther, A., and Keutsch, F. N.: First direct measurements of formaldehyde flux via eddy covariance: implications for missing in-canopy formaldehyde sources, Atmos. Chem. Phys., 11, 10565-10578, https://doi.org/10.5194/acp-11-10565-2011, 2011.

Fried, A., Cantrell, C., Olson, J., Crawford, J. H., Weibring, P., Walega, J., Richter, D., Junkermann, W., Volkamer, R., Sinreich, R., Heikes, B. G., O'Sullivan, D., Blake, D. R., Blake, N., Meinardi, S., Apel, E., Weinheimer, A., Knapp, D., Perring, A., Cohen, R. C., Fuelberg, H., Shetter, R. E., Hall, S. R., Ullmann, K., Brune, W. H., Mao, J., Ren, X., Huey, L. G., Singh, H. B., Hair, J. W., Riemer, D., Diskin, G., and Sachse, G.: Detailed comparisons of airborne formaldehyde measurements with box models during the 2006 INTEX-B and MILAGRO campaigns: potential evidence for significant impacts of unmeasured and multi-generation volatile organic carbon compounds, Atmos. Chem. Phys., 11, 11867-11894, https://doi.org/10.5194/acp-11-11867-2011, 2011.

Gilman, J. B., Kuster, W. C., Goldan, P. D., Herndon, S. C., Zahniser, M. S., Tucker, S. C., Brewer, W. A., Lerner, B. M., Williams, E. J., Harley, R. A., Fehsenfeld, F. C., Warneke, C., and de Gouw, J. A.: Measurements of volatile organic compounds during the 2006 TexAQS/GoMACCS campaign: Industrial influences, regional characteristics, and diurnal dependencies of the OH reactivity, J. Geophys. Res. Atmos., 114, https://doi.org/10.1029/2008jd011525, 2009.

Hottle, J. R., Huisman, A. J., DiGangi, J. P., Kammrath, A., Galloway, M. M., Coens, K. L., and Keutsch, F. N.: A laser induced fluorescence-based instrument for in-situ measurements of atmospheric formaldehyde, Environ. Sci. Technol., 43, 790-795, https://doi.org/10.1021/es801621f, 2009.

Huey, L. G.: Measurement of trace atmospheric species by chemical ionization mass spectrometry: speciation of reactive nitrogen and future directions, Mass Spectrom. Rev., 26, 166-184, https://doi.org/10.1002/mas.20118, 2007.

Kaser, L., Karl, T., Schnitzhofer, R., Graus, M., Herdlinger-Blatt, I. S., DiGangi, J. P., Sive, B., Turnipseed, A., Hornbrook, R. S., Zheng, W., Flocke, F. M., Guenther, A., Keutsch, F. N., Apel, E., and Hansel, A.: Comparison of different real time VOC measurement techniques in a ponderosa pine forest, Atmos. Chem. Phys., 13, 2893-2906, https://doi.org/10.5194/acp-13-2893-2013, 2013.

Kim, S., Huey, L. G., Stickel, R. E., Tanner, D. J., Crawford, J. H., Olson, J. R., Chen, G., Brune, W. H., Ren, X., Lesher, R., Wooldridge, P. J., Bertram, T. H., Perring, A., Cohen, R. C., Lefer, B. L., Shetter, R. E., Avery, M., Diskin, G., and Sokolik, I.: Measurement of HO2NO2 in the free troposphere during the intercontinental chemical transport experiment - North America 2004, J. Geophys. Res. Atmos., 112, https://doi.org/10.1029/2006jd007676, 2007.

Lee, B. H., Lopez-Hilfiker, F. D., Mohr, C., Kurten, T., Worsnop, D. R., and Thornton, J. A.: An iodide-adduct high-resolution time-of-flight chemical-ionization mass spectrometer: application to atmospheric inorganic and organic compounds, Environ. Sci. Technol., 48, 6309-6317, https://doi.org/10.1021/es500362a, 2014.

Lerner, B. M., Gilman, J. B., Aikin, K. C., Atlas, E. L., Goldan, P. D., Graus, M., Hendershot, R., Isaacman-VanWertz, G. A., Koss, A., Kuster, W. C., Lueb, R. A., McLaughlin, R. J., Peischl, J., Sueper, D., Ryerson, T. B., Tokarek, T. W., Warneke, C., Yuan, B., and de Gouw, J. A.: An improved, automated whole air sampler and gas chromatography mass spectrometry analysis system for volatile organic compounds in the atmosphere, Atmos. Meas. Tech., 10, 291-313, https://doi.org/10.5194/amt-10-291-2017, 2017.

Min, K. E., Washenfelder, R. A., Dube, W. P., Langford, A. O., Edwards, P. M., Zarzana, K. J., Stutz, J., Lu, K., Rohrer, F., Zhang, Y., and Brown, S. S.: A broadband cavity enhanced absorption spectrometer for aircraft measurements of glyoxal, methylglyoxal, nitrous acid, nitrogen dioxide, and water vapor, Atmos. Meas. Tech., 9, 423-440, https://doi.org/10.5194/amt-9-423-2016, 2016.

Müller, M., Mikoviny, T., Feil, S., Haidacher, S., Hanel, G., Hartungen, E., Jordan, A., Mark, L., Mutschlechner, P., Schottkowsky, R., Sulzer, P., Crawford, J. H., and Wisthaler, A.: A compact PTR-ToF-MS instrument for airborne measurements of volatile organic compounds at high spatiotemporal resolution, Atmos. Meas. Tech., 7, 3763-3772, https://doi.org/10.5194/amt-7-3763-2014, 2014.

Müller, M., Anderson, B. E., Beyersdorf, A. J., Crawford, J. H., Diskin, G. S., Eichler, P., Fried, A., Keutsch, F. N., Mikoviny, T., Thornhill, K. L., Walega, J. G., Weinheimer, A. J., Yang, M., Yokelson, R. J., and Wisthaler, A.: In situ measurements and modeling of reactive trace gases in a small biomass burning plume, Atmos. Chem. Phys., 16, 3813-3824, https://doi.org/10.5194/acp-16-3813-2016, 2016.

O'Sullivan, D. W., Silwal, I. K. C., McNeill, A. S., Treadaway, V., and Heikes, B. G.: Quantification of gas phase hydrogen peroxide and methyl peroxide in ambient air: Using atmospheric pressure chemical ionization mass spectrometry with O2−, and O2−(CO2) reagent ions, Int. J. Mass Spectrom., 424, 16-26, https://doi.org/10.1016/j.ijms.2017.11.015, 2018.

Osthoff, H. D., Roberts, J. M., Ravishankara, A. R., Williams, E. J., Lerner, B. M., Sommariva, R., Bates, T. S., Coffman, D., Quinn, P. K., Dibb, J. E., Stark, H., Burkholder, J. B., Talukdar, R. K., Meagher, J., Fehsenfeld, F. C., and Brown, S. S.: High levels of nitryl chloride in the polluted subtropical marine boundary layer, Nat Geosci, 1, 324-328, https://doi.org/10.1038/ngeo177, 2008.

Pollack, I. B., Lerner, B. M., and Ryerson, T. B.: Evaluation of ultraviolet light-emitting diodes for detection of atmospheric NO2 by photolysis - chemiluminescence, J. Atmos. Chem., 65, 111-125, https://doi.org/10.1007/s10874-011-9184-3, 2010.

Richter, D., Weibring, P., Walega, J. G., Fried, A., Spuler, S. M., and Taubman, M. S.: Compact highly sensitive multi-species airborne mid-IR spectrometer, Appl. Phys. B: Lasers Opt., 119, 119-131, https://doi.org/10.1007/s00340-015-6038-8, 2015.

Ryerson, T. B., Buhr, M. P., Frost, G. J., Goldan, P. D., Holloway, J. S., Hubler, G., Jobson, B. T., Kuster, W. C., McKeen, S. A., Parrish, D. D., Roberts, J. M., Sueper, D. T., Trainer, M., Williams, J., and Fehsenfeld, F. C.: Emissions lifetimes and ozone formation in power plant plumes, J. Geophys. Res. Atmos., 103, 22569-22583, https://doi.org/10.1029/98jd01620, 1998.

Ryerson, T. B., Huey, L. G., Knapp, K., Neuman, J. A., Parrish, D. D., Sueper, D. T., and Fehsenfeld, F. C.: Design and initial characterization of an inlet for gas-phase NOy measurements from aircraft, J. Geophys. Res. Atmos., 104, 5483-5492, https://doi.org/10.1029/1998jd100087, 1999.

Schauffler, S. M., Atlas, E. L., Donnelly, S. G., Andrews, A., Montzka, S. A., Elkins, J. W., Hurst, D. F., Romashkin, P. A., Dutton, G. S., and Stroud, V.: Chlorine budget and partitioning during the Stratospheric Aerosol and Gas Experiment (SAGE) III Ozone Loss and Validation Experiment (SOLVE), J. Geophys. Res. Atmos., 108, https://doi.org/10.1029/2001jd002040, 2003.

Slusher, D. L., Huey, L. G., Tanner, D. J., Flocke, F. M., and Roberts, J. M.: A thermal dissociation-chemical ionization mass spectrometry (TD-CIMS) technique for the simultaneous measurement of peroxyacyl nitrates and dinitrogen pentoxide, J. Geophys. Res. Atmos., 109, https://doi.org/10.1029/2004jd004670, 2004.

St Clair, J. M., McCabe, D. C., Crounse, J. D., Steiner, U., and Wennberg, P. O.: Chemical ionization tandem mass spectrometer for the in situ measurement of methyl hydrogen peroxide, Rev. Sci. Instrum., 81, 094102, https://doi.org/10.1063/1.3480552, 2010.

Treadaway, V., Heikes, B. G., McNeill, A. S., Silwal, I. K. C., and O'Sullivan, D. W.: Measurement of formic acid, acetic acid and hydroxyacetaldehyde, hydrogen peroxide, and methyl peroxide in air by chemical ionization mass spectrometry: airborne method development, Atmos. Meas. Tech., 11, 1901-1920, https://doi.org/10.5194/amt-11-1901-2018, 2018.

Weibring, P., Richter, D., Walega, J. G., Rippe, L., and Fried, A.: Difference frequency generation spectrometer for simultaneous multispecies detection, Opt. Express, 18, 27670-27681, https://doi.org/10.1364/OE.18.027670, 2010.

Weinheimer, A. J., Walega, J. G., Ridley, B. A., Gary, B. L., Blake, D. R., Blake, N. J., Rowland, F. S., Sachse, G. W., Anderson, B. E., and Collins, J. E.: Meridional distributions of NOx, NOy and other species in the lower stratosphere and upper troposphere during AASE II, Geophys Res Lett, 21, 2583-2586, https://doi.org/10.1029/94gl01897, 1994.

Wisthaler, A., Hansel, A., Dickerson, R. R., and Crutzen, P. J.: Organic trace gas measurements by PTR-MS during INDOEX 1999, J. Geophys. Res. Atmos., 107, https://doi.org/10.1029/2001jd000576, 2002.

Wofsy, S. C., Afshar, S., Allen, H. M., Apel, E., Asher, E. C., Barletta, B., Bent, J., Bian, H., Biggs, B. C., Blake, D. R., Blake, N., Bourgeois, I., Brock, C. A., Brune, W. H., Budney, J. W., Bui, T. P., Butler, A., Campuzano-Jost, P., Chang, C. S., Chin, M., Commane, R., Correa, G., Crounse, J. D., Cullis, P. D., Daube, B. C., Day, D. A., Dean-Day, J. M., Dibb, J. E., DiGangi, J. P., Diskin, G. S., Dollner, M., Elkins, J. W., Erdesz, F., Fiore, A. M., Flynn, C. M., Froyd, K., Gesler, D. W., Hall, S. R., Hanisco, T. F., Hannun, R. A., Hills, A. J., Hintsa, E. J., Hoffman, A., Hornbrook, R. S., Huey, L. G., Hughes, S., Jimenez, J. L., Johnson, B. J., Katich, J. M., Keeling, R. F., Kim, M. J., Kupc, A., Lait, L. R., Lamarque, J.-F., Liu, J., McKain, K., Mclaughlin, R. J., Meinardi, S., Miller, D. O., Montzka, S. A., Moore, F. L., Morgan, E. J., Murphy, D. M., Murray, L. T., Nault, B. A., Neuman, J. A., Newman, P. A., Nicely, J. M., Pan, X., Paplawsky, W., Peischl, J., Prather, M. J., Price, D. J., Ray, E., Reeves, J. M., Richardson, M., Rollins, A. W., Rosenlof, K. H., Ryerson, T. B., Scheuer, E., Schill, G. P., Schroder, J. C., Schwarz, J. P., St.Clair, J. M., Steenrod, S. D., Stephens, B. B., Strode, S. A., Sweeney, C., Tanner, D., Teng, A. P., Thames, A. B., Thompson, C. R., Ullmann, K., Veres, P. R., Vieznor, N., Wagner, N. L., Watt, A., Weber, R., Weinzierl, B., Wennberg, P., Williamson, C. J., Wilson, J. C., Wolfe, G. M., Woods, C. T., and Zeng, L. H.: ATom: Merged Atmospheric Chemistry, Trace Gases, and Aerosols. ORNL DAAC, Oak Ridge, Tennessee, USA, https://doi.org/10.3334/ornldaac/1581, 2018.

Wooldridge, P. J., Perring, A. E., Bertram, T. H., Flocke, F. M., Roberts, J. M., Singh, H. B., Huey, L. G., Thornton, J. A., Wolfe, G. M., Murphy, J. G., Fry, J. L., Rollins, A. W., LaFranchi, B. W., and Cohen, R. C.: Total Peroxy Nitrates (ΣPNs) in the atmosphere: the Thermal Dissociation-Laser Induced Fluorescence (TD-LIF) technique and comparisons to speciated PAN measurements, Atmos. Meas. Tech., 3, 593-607, https://doi.org/10.5194/amt-3-593-2010, 2010.

Yacovitch, T. I., Herndon, S. C., Roscioli, J. R., Floerchinger, C., McGovern, R. M., Agnese, M., Petron, G., Kofler, J., Sweeney, C., Karion, A., Conley, S. A., Kort, E. A., Nahle, L., Fischer, M., Hildebrandt, L., Koeth, J., McManus, J. B., Nelson, D. D., Zahniser, M. S., and Kolb, C. E.: Demonstration of an ethane spectrometer for methane source identification, Environ. Sci. Technol., 48, 8028-8034, http://doi.org/10.1021/es501475q, 2014.

Zheng, W., Flocke, F. M., Tyndall, G. S., Swanson, A., Orlando, J. J., Roberts, J. M., Huey, L. G., and Tanner, D. J.: Characterization of a thermal decomposition chemical ionization mass spectrometer for the measurement of peroxy acyl nitrates (PANs) in the atmosphere, Atmos. Chem. Phys., 11, 6529-6547, https://doi.org/10.5194/acp-11-6529-2011, 2011.